To the Graduate Council:

I am submitting herewith a thesis written by Satyashayee Misra entitled "Mathematical Modeling Investigation of the Spunbonding Process and Role of Molecular Weight Distribution in Fiber Spinning". I have examined the final copy of this thesis for form and content and recommend that it be accepted in partial fulfillment of the requirements for the degree of Master of Science, with a major in Polymer Engineering.

Joseph E. Spruiell, Major Professor

We have read this thesis and
recommend its acceptance:

Accepted for the council:

Associate Vice Chancellor and
Dean of the Graduate School

MATHEMATICAL MODELING INVESTIGATION OF THE SPUNBONDING PROCESS AND ROLE OF MOLECULAR WEIGHT DISTRIBUTION IN FIBER SPINNING

A Thesis

Presented for the

Master of Science Degree

The University of Tennessee, Knoxville

SATYASHAYEE MISRA

May 1994

To my elder brother

Sambit Mishra

ACKNOWLEDGMENTS

The author wishes to express his sincere thanks to his advisor, Professor Joseph E. Spruiell, for his guidance, suggestions and patience during the course of this work. The author also thanks his committee, Professors J. E. Spruiell, D. C. Bogue and R. S. Benson for their effort in making this work possible.

Special thanks are extended to the Exxon Chemical Company for the financial support provided during the present work, the preparation of the resins and the measurement of MFR, dynamic viscosity and GPC data on each resin .

The author thanks Mr. F. M. Lu for his help in the experiments of melt spinning and valuable discussions during this work. The author appreciates the help of Dr. Nejib Hajji for his help in computer simulation work. The author also acknowledges the technical support provided by the machine and electronic shops.

Finally, the author wishes to express his deepest gratitude to his parents for their moral support and patience.

ABSTRACT

The present research consisted of two parts: i) Investigation of the Spunbonding process through mathematical modeling and ii) Experimental investigation of the role of molecular weight and its distribution in structure development during melt spinning of polypropylene. A mathematical model for the Reicofil Spunbonding process, developed earlier at the University of Tennessee, was applied to investigate the effects of various process and material variables on the resulting filament structure and properties. The material parameters studied were the polymer elongational viscosity and the kinetics of "Stress induced crystallization". The process parameters varied included the extrusion temperature and the temperature and flow rate of the cooling air. Some changes in the process itself, such as the length of the spinline and the shape of the drawdown venturi were also considered. A combination of more than one of the effects was tried in order to examine the possibility of producing a thinner fiber with higher final birefringence.

The model indicated that the elongational viscosity is a key factor in controlling the amount of drawdown, the temperature of onset of crystallization and the level of molecular orientation developed in the spunbonded filament. The kinetics of stress induced crystallization also has a major influence on the extent of undercooling before the crystallization begins but it has relatively little effect on the drawdown of the filament. Among the process parameters, the cooling air temperature and the air flow rate appear to be the most significant variables. Changes in the process, such as the

shape of the drawdown venturi can also lead to significant changes in the resulting filament diameter and properties.

Melt spinning experiments were conducted on polypropylenes of various molecular weight and molecular weight distributions to study the structure development in the filament and also to obtain the respective apparent elongational viscosities. Three sets of polypropylene samples, each consisting of three samples with similar melt flow index but different polydispersities were examined. The on-line profiles of the spinline and the characteristics of the as-spun filaments give an indication of how the molecular weight and its distribution affect the structure and properties of the spun filaments. Filaments spun from samples of broad molecular weight distribution are found to develop higher crystallinity but lower birefringence and tensile strength than those spun from the samples of narrow molecular weight distribution(MWD). From the birefringence profiles it can be suggested that the crystallization takes place closer to the spinneret as the molecular weight distribution widens. The higher crystallinity of the broad MWD samples is attributed to stress induced crystallization due to the presence of long chain molecules in those samples. It was speculated that the long chain molecules are entangled, and, when elongated in the spinning process produce substantial molecular orientation and "row-nuclei" which cause crystallization to occur at higher temperatures and proceed to greater levels of crystallinity and crystalline perfection. The apparent elongational viscosities were obtained by the "inversion procedure". It was observed that the samples with narrow molecular weight distribution showed an Arrhenius type Newtonian behavior whereas the samples with higher polydispersities seemed to deviate from the Arrhenius type formulation. This may indicate that viscoelasticity plays an important role in those samples.

TABLE OF CONTENTS

CHAPTER		PAGE
1.	INTRODUCTION	1
2.	BACKGROUND	5
	2.1 Dynamics of Single Filament Spinline	6
	2.2 Energy Balance	10
	2.3 Correlations For Heat Transfer Coefficient	11
	2.4 Melt Rheology and Constitutive Equations	15
	2.5 Inversion Procedure	24
	2.6 Crystallization Kinetics	29
	2.7 Orientation and Birefringence	39
	2.8 Structure Development in Fiber Formation	40
	2.9 Development of Mathematical Model for the "Reicofil" Spunbonding Process	44
3.	EXPERIMENTAL MATERIALS, EQUIPMENT AND METHODS	47
	3.1 Materials	47
	3.2 Melt Spinning	53
	3.3 On-line Measurements	55
4.	MELT SPINNING STUDY OF POLYPROPYLENE	59
	4.1 Preliminary studies of Spinnability	59
	4.2 Structure and Properties of As-spun Filaments	66

4.3 On-line Profiles During Melt Spinning 76

4.4 Analysis and Discussion of Role of Molecular Weight and its Distribution in the Melt Spinning of Polypropylene 91

4.5 Application of 'Inversion Procedure' for Measurement of Apparent Elongational Viscosity 99

5. INVESTIGATION OF 'REICOFIL' SPUNBONDING PROCESS VIA MATHEMATICAL MODELING 110

5.1 Predicted Effects of Changes in Material Parameters 112

5.2 Predicted Effects of Changes in Process Variables 123

5.3 Predicted Effects of Some Major Process Changes 132

5.4 Use of the Model to Guide Experimentation 139

6. SUMMARY AND CONCLUSIONS 143

REFERENCES 148

VITA 159

LIST OF FIGURES

FIGURE		PAGE
2.1	Schematic diagram for steps of calculation in the 'Inversion Procedure'...	28
2.2	Schematic diagram of the 'Reicofil' Spunbonding process	45
3.1	Dynamic viscosity for the 16-18 MFR resins as a function of angular frequency	50
3.2	Dynamic viscosity for the 35-42 MFR resins as a function of angular frequency	51
3.3	Dynamic viscosity for the 74-78 MFR resins as a function of angular frequency	52
3.4	Schematic diagram of the melt spinning setup	54
3.5	Schematic arrangement for birefringence measurement	57
4.1	Diameter distribution of running filaments of 16-18 MFR at 220 cm below the spinneret under low air pressure of 5 psi(g)	63
4.2	Diameter distribution of running filaments of 35-42 MFR at 220 cm below the spinneret under low air pressure of 5 psi(g)	64
4.3	Diameter distribution of running filaments of 74-78 MFR at 220 cm below the spinneret under low air pressure of 5 psi(g)	65
4.4	Graphical representation of density versus spinning speed of as-spun fibers	74
4.5	Graphical representation of birefringence versus spinning speed of as-spun fibers	75
4.6	On-line diameter profiles for the 16-18 MFR resins spun under low air pressure of 5 psi(g)	77
4.7	On-line diameter profiles for the 35-42 MFR resins spun under low air pressure of 5 psi(g)	78

4.8 On-line diameter profiles for the 74-78 MFR resins spun under low air pressure of 5 psi(g) 79

4.9 Comparison of on-line diameter profiles spun under different air pressures 80

4.10 Comparison of the temperature profiles of the resins of the 74-78 MFR range at 5 psi(g) air pressure 81

4.11 On-line birefringence profiles for the 16-18 MFR resins spun under low air pressure of 5 psi(g) 82

4.12 On-line birefringence profiles for the 35-42 MFR resins spun under low air pressure of 5 psi(g) 83

4.13 On-line birefringence profiles for the 74-78 MFR resins spun under low air pressure of 5 psi(g) 84

4.14 Comparison of On-line birefringence profiles of the resins of 35-42 MFR and 74-78 MFR 85

4.15 On-line birefringence profiles for the 16-18 MFR resins spun under high air pressure 86

4.16 On-line birefringence profiles for the 35-42 MFR resins spun under high air pressure 87

4.17 On-line birefringence profiles for the 74-78 MFR resins spun under high air pressure 88

4.18 Drag force versus fiber diameter for different air pressures in the suction venturi 101

4.19 Apparent elongational viscosities for the narrow MWD samples 104

4.20 Apparent elongational viscosities for the medium MWD samples 105

4.21 Apparent elongational viscosities for the broad MWD samples 106

4.22 Profile of reciprocal of absolute temperature 107

5.1 Comparison of diameter profiles for resins of three different MFRs 115

5.2 Comparison of temperature profiles for resins of three different MFRs ... 116

5.3 Comparison of development of crystallinity for resins of three different MFRs 117

5.4 The effect of changes in crystallization kinetics on the temperature profiles 120

5.5 The effect of changes in crystallization kinetics on the development of crystallinity along the spinline 121

5.6 The effect of extrusion temperature on the diameter profile 124

5.7 The effect of extrusion temperature on the development of total birefringence 125

5.8 The effect of cool air temperature on the diameter profile 128

5.9 The effect of cool air temperature on the development of crystallinity ... 129

5.10 Illustration of potential changes in the venturi angle 134

5.11 Illustration of some possible changes in the venturi design which include an extended minimum section 137

5.12 Comparison of stress versus temperature profile for the original base case and the fine denier case 142

LIST OF TABLES

TABLE		PAGE
3.1	Classification of experimental polypropylene samples	48
3.2	GPC data of the experimental polypropylene samples	49
4.1	Spinnability test for 'difficult-to-spin polypropylene samples	61
4.2	Processing conditions of polypropylene samples at low air pressure	67
4.3	Processing conditions of polypropylene samples at high air pressure	68
4.4	Comparison of on-line and off-line data for fibers spun using 5 psi(g) air pressure	70
4.5	Comparison of on-line and off-line data for fibers spun using higher air pressure	71
4.6	Characteristics of as-spun fibers spun using 5 psi(g) air pressure	72
4.7	Characteristics of as-spun fibers spun using higher air pressures	73
5.1	Processing conditions used for examining the effects of resin variables on the structure and properties of spunbonded polypropylene webs	113
5.2	Predictions of the model for different viscosity resins	114
5.3	Predictions for different crystallization kinetics	122
5.4	Predictions for different extrusion temperatures	126
5.5	Predictions for different cooling air temperatures	130
5.6	Predictions for different air velocity profiles	131
5.7	Predictions for different venturi lengths	133
5.8	Effect of venturi angles and positions	136
5.9	Effect of increasing length of reduced section in the venturi	138

CHAPTER 1

INTRODUCTION

Formation of fibers from polymeric melts and solutions has revolutionized the textile industries because of the technological and economic advantages of synthetic fibers over naturally occurring fibers such as cotton, silk and wool fibers. The fiber spinning industry can be broadly classified into three categories: melt spinning, dry spinning and wet spinning. Among these processes melt spinning is the process most commonly used to produce synthetic fibers from polymeric materials. The first commercial melt spun fiber was produced from polyvinyl chloride by I.G. Farbenindustrie in the early 1930's but did not prove very successful (1). Based on the research of Carothers (2,3), E.I. duPont de Nemours developed the first commercially successful process to produce Nylon-66 filaments in 1939. This was followed by the commercialization of Nylon-6 fiber in 1942 and polyethylene terepthalate (PET) fiber of in 1946 by I.G. Farbenindustrie and Imperial Chemicals Limited, respectively. Isotactic polypropylene was melt spun and commercialized by Montecatine in 1954. This was followed by rapid development of melt spinning of various other thermoplastic polymers including polyolefins, polyesters and polyamides. Meltspun fibers have found major applications such as ropes, cords and filtration fabrics made from low, high and linear low density polyethylenes, high temperature gas filtration

fabrics made from modified Nylons and snap back fibers made from modified thermoplastic elastomer type polyesters (4).

Spunbonding is one of the most commonly used processes in Nonwovens fabric technology. A primary factor in the production of spunbonded fabrics is control of four simultaneous integrated operations: filament extrusion, drawing, lay down and bonding. The first three operations are directly adapted from the conventional multifilament melt spinning process and constitute the "spun" or web formation phase of the process, while the last operation is the consolidation or the "bond" phase of the process- hence the generic term spunbond (5). The concept of the spunbond process was developed simultaneously in Europe and United States in the late 1950's, but the first commercial product available in the United States was manufactured of polyester under the trade name Reemay^{R}, in 1965, by Dupont. This was followed by polypropylene Typar^{R} and polyethylene Tyvek^{R} (6). In Europe several companies have introduced their own spunbonding processes since the early 1960's. In 1984, Reifenhauser GmbH of Germany introduced their first spunbonding process called Reicofil^{R} for producing webs primarily from polypropylene. A generalized definition of the spunbonding process is as follows (7): *Spunbonding is a process in which usually a thermoplastic fiber forming polymer is extruded through a linear or circular spinneret. The extruded polymer streams are rapidly cooled and attenuated by air to form desired diameter filaments. The filaments are then laid down to a conveyor belt to form a web. This web is then bonded to form a spunbonded web.* The various spunbonding processes differ in the way the fiber is attenuated and is bonded. Nonwoven fabrics play key role in hundreds of everyday products , from luxury automobiles to familiar tea bags (8).

Primary fiber formation in the spunbonding process is very important for the quality of the product. The strength of the final spunbonded web depends upon the strength of individual fibers. Of course, the uniformity of web formation is important too. In spite of the industrial importance of the spunbonding process, little effort has been expended to simulate it mathematically. In view of the dependence of the product on interaction of multiple parameters such as extrusion temperature, mass throughput rate, air flow rate and temperature, viscosity and crystallizability of the polymer being spun etc., it is necessary to model the process to see the effect of individual as well as multiple parameters. A mathematical model for the Reicofil spunbonding process has been developed for the first time by Hajji, Spruiell, Lu and Malkan (9). The model has been tested for a range of operating conditions in the pilot-line of the process, located at the University of Tennessee Textiles and Nonwovens Development Center (TANDEC).

It is the purpose of the present research to investigate the effects of several process and material parameters on the fiber produced in the spunbonding process through the application of the mathematical model developed by Hajji et al. Investigation via mathematical modeling is useful in the sense that it can eliminate costly experimental procedure and guide the direction in order to achieve the desired fiber properties. Changes in the process itself may also lead to significant change in the fiber properties (10). Such changes in the process can be considered by varying the mathematical model appropriately.

It is also the aim of the present research to find the effect of molecular weight and its distribution in the melt spinning of polypropylene. Previous research has shown that there is a significant change in fiber properties with change in molecular weight of

polypropylene, but a systematic study that emphasizes the effect of molecular weight distribution has not yet been reported. The apparent elongational viscosity of different polypropylene samples with different melt indexes and polydispersities are measured by applying the "Inversion Procedure" developed earlier at the University of Tennessee. Emphasis is also given on correct measurement of the tension at the bottom of the spinline which affects the apparent elongational viscosity.

Reading this thesis, one might wonder why the results obtained from the melt spinning studies on the different polypropylene samples were not used in the simulation of the spunbonding process. The answer to this question is that the simulation work of the spunbonding process was conducted before the melt spinning studies of the polypropylene samples. The research findings relating the melt spinning studies of the polypropylene samples is presented before the results of the 'investigation of the spunbonding process via mathematical modeling' in order to maintain continuity from Chapter-3 of this thesis, i.e., the materials and methods described in Chapter-3 were used in the melt spinning of the polypropylene samples, the results of which are presented in Chapter-4.

CHAPTER 2

BACKGROUND

Melt spinning, dry spinning and wet spinning constitute three major processes for the formation of synthetic fibers(12). Among these three processes, the melt spinning process has been under extensive investigation to be simulated mathematically because of its conceptual simplicity. The material, in this process, undergoes extensional deformation accompanied by heat transfer during the deformation. The process does not involve chemical reaction or mass transfer during the deformation of the material. To produce the fiber of desired properties, it is necessary to understand the effect of various process parameters and resin characteristics on the fiber properties. This can be done by varying the various parameters during melt spinning experiment. This can also be understood through a mathematical model that accurately describes the process. Some other processes for fiber formation such as the Reicofil Spunbonding process that bear similarity with the melt spinning process with key differences in the boundary and draw down conditions of the fiber, can also be modeled with the help of the model for melt spinning(9). The correlations obtained from on-line measurement of different parameters during the melt spinning experiment are the key inputs to the model. The on-line measurement of diameter and temperature during processing along with the tension at the bottom of the spinline give rise to an important processing parameter known as the apparent

elongational viscosity. Similarly, the on-line birefringence measurement along with the stress in the spinline and the quiescent crystallization kinetics with description of the effect of stress on crystallization can be the key inputs for the prediction of the crystallinity and birefringence of the fiber. Parameters such as crystallinity and birefringence give an insight to measurable properties like tensile strength and elongation to break, etc. which are directly related to the end-use of the fiber.

2.1. Dynamics of Single Filament Spinline:

A model for single filament spinline was first developed by Kase and Matsuo(13,14,15). This model assumed constant rheological force along the spinline and it was intended for low-speed spinning. The present day model recognizes the change in rheological force along the spinline(16) as well as the effect of crystallization(17-20). The present research work is based on the models developed for melt spinning and spunbonding at the University of Tennessee, Knoxville(9,20,21).

The single filament melt spinning model is based on the simultaneous solution of a system of four equations which represent the momentum balance, energy balance, rheological constitutive equation and the crystallization kinetics respectively.

Force Balance of the Fiber Spinning Process:

The overall force balance for fiber spinning at any point along the spinline can be written as follows(12):

$$F_{rheo} = F_o + F_{drag} + F_{inert} + F_{grav} \qquad [2.1.1]$$

where F_{rheo} is the rheological force in the fiber at any point along the spinline, F_o is the rheological force at the beginning of the spinline, F_{drag} is the drag force on the fiber due to the relative velocity between the moving fiber and the surrounding air, F_{inert} is the inertial force as the fiber is accelerated, F_{grav} is the gravitational force on the fiber and F_{surf} is the surface tension force at the fiber-air interface. The surface tension force can be ignored because it is negligible in magnitude compared to the other forces acting on the fiber. These forces can be expressed in terms of measurable quantities such as diameter, velocity, density etc. as follows(12):

$$F_{drag} = \int_0^z \pi D \sigma_f dz \qquad [2.1.2(i)]$$

$$F_{inert} = W(v - v_o) \qquad [2.1.2(ii)]$$

$$F_{grav} = \int_0^z \rho g \left(\frac{\pi D^2}{4} \right) dz \qquad [2.1.2(iii)]$$

$$F_{surf} = \int_0^z \frac{\pi \sigma}{2} (D_o - D) dz \qquad [2.1.2(iv)]$$

where D_o and v_o are the diameter of the die and the average velocity of the melt in the die respectively, σ_f is the shear stress at the fiber-surrounding interface due to aerodynamic drag and σ is the surface tension of the polymer melt with respect to the surrounding. The surrounding medium is almost always air unless the fiber is spun through a liquid. W is the mass flow rate of the melt. The continuity equation relates the mass flow rate of the material to other variables at any point on the spinline such as the diameter, the density and the velocity of the fiber through the equation

$$W = \rho\pi\left(\frac{D}{2}\right)^2 v \qquad [2.1.3]$$

At this point it necessary to discuss the radial variations of axial velocity and temperature of the fiber. The radial variation of the fiber velocity was investigated by Kase(22). The velocity field within a molten spinning thread line was studied. A series solution for the velocity as a function of the radial component in the cylindrical coordinate system was determined from the equation of continuity and momentum balance. Kase concluded from the result that the velocity profile could be considered flat across the cross section of the fiber without any appreciable error. However the same is not true for the temperature profile across the fiber cross section(23-29). The maximum temperature difference across the radius of the spinline has been observed to be more than 15 ^{o}C(28) under certain conditions. Since the density is a function of melt temperature, it has a variation across the cross section of the fiber. However, it is complicated to write a force balance that will incorporate such a variation. Neglecting this radial variation and the force due to surface tension, an equation can be obtained for the gradient of the rheological force along the spinning axis by differentiating equation [2.1.1] and replacing the various components of force from equations [2.1.2(i-iii)]:

$$\frac{dF_{rheo}}{dz} = W\frac{dv}{dz} + \frac{1}{2}\rho_a C_d v^2 \pi D - W\frac{g}{v} \qquad [2.1.4]$$

where v, D and g are the fiber velocity, fiber diameter and the acceleration due to gravity respectively at any point, z, along the spinline. C_d is the drag coefficient used in the equation for shear stress at the fiber-surrounding interface due to the aerodynamic drag. If the surrounding medium is air, then the shear stress is given by

$\sigma_f = \frac{1}{2}\rho_a v^2 C_d$, where ρ_a is the density of the surrounding air. Many correlations are available for the estimation of the drag coefficient, both empirically and using the boundary layer analysis. Using the latter approach, Sakiadis has given the following correlation for the estimation of drag coefficient at any point on the spinline(30):

$$\xi^2 = \frac{64Re.z}{D} \qquad [2.1.5]$$

$$\xi^2 = \int_0^{\beta} \frac{(z - 1)\exp(2z) + z^2 + 1}{z^2} dz \qquad [2.1.6]$$

Thus β can be obtained implicitly from the above two equations for any velocity and diameter of the fiber. The drag coefficient is then calculated by

$$C_d = \frac{4}{(\beta Re)} \qquad [2.1.7]$$

In this approach the Reynolds number is based on the surrounding air properties, i.e., $Re = \rho_a v D/\mu_a$. For high speed spinning, a common case in present day fiber industry, the Reynolds number based on the air properties shows a turbulent regime. Under this condition, the correlation often adopted is given by Matsui(31) which is of the form $C_d = K \cdot Re^{-n}$ where K=0.37 and n=0.61. The axial stress along the spinline, σ_{zz} or σ_{11}, is obtained from the rheological force in the fiber through the relation $\sigma_{11} = F_{rheo}/A$ where A is the area of cross section of the fiber. Thus, at any point of interest, the axial stress is given by:

$$\sigma_{11} = \frac{4F_{rheo}}{\pi D^2} \qquad [2.1.8]$$

The rheological properties of the melt and the stress-elongation behavior during spinning will be discussed separately later in this chapter.

2.2 Energy Balance :

Non isothermal melt spinning is associated with a variation of temperature of the fiber along the spinline. The variation of temperature is represented by energy balance which is as follows(32):

$$\frac{dT}{dz} = \frac{-\pi Dh}{WC_p}(T - T_a) + \frac{\Delta H}{C_p}.\frac{dx}{dz} \qquad [2.2.1]$$

where T is the fiber temperature at the point z, T_a is the bulk temperature of the surrounding, h is the heat transfer coefficient between the fiber and the surrounding, C_p is the specific heat of the polymer, ΔH_f is the heat of fusion of the polymer and X is the crystalline fraction in the fiber. It should be noted that the heat transfer coefficient, h, used in the above equation is based on the average temperature of the fiber and the bulk temperature of the surrounding air. The effect of radiation is neglected in the evaluation of h. The first term in the right hand side of equation [2.2.1] represents the decrease in temperature due to loss of heat from the fiber to the surroundings whereas the second term gives the increase in temperature due to the increase in the crystalline fraction in the fiber. Crystallization releases the latent heat of fusion and hence may lead to an increase in temperature. When the two opposing effects have the same order of magnitude, a plateau may be observed in the temperature profile of the fiber along the spinline which indicates that crystallization is taking place in that section of the spinline.

2.3 Correlations for Heat Transfer Coefficient:

The key parameter in the equation for energy balance for obtaining the temperature profile is the heat transfer coefficient, h. There have been many attempts to derive theoretical and empirical correlations for the heat transfer coefficient in fiber spinning. Theoretical analyses of cooling of fibers have been done by mainly the use of boundary layer theory(11,32-41). The empirical correlations derived for the heat transfer coefficient are numerous and are based on heated wire experiments(11,13), direct evaluation through the "Inversion Procedure" from the diameter and temperature profiles(31,42) or from the correlations for drag coefficient using the momentum-heat transfer analogy(43).

Boundary Layer Approach:

This approach is based on the analysis of a flow field in the boundary layer regime solving the Navier-Stokes equations for momentum transfer and heat transfer. Since the original problem is three dimensional and difficult to solve, an assumption that the boundary layer is axially symmetric would reduce the problem to two dimensions by eliminating the dependence of heat transfer(or momentum transfer) on the "θ" of the cylindrical coordinate system. However, such assumption is not valid when the spinline has transverse vibrations.

The boundary layer approach was first used for laminar regimes only(11). Among different authors investigating fluid flow over a cylindrical surface parallel to the axis of the fiber, Glauert and Lighthill(44) studied momentum transfer on the boundary layer around thin cylindrical surfaces of finite length. Later, Bourne and Davis(36) adopted an approach similar to that of Glauert and Lighthill to solve the

energy balance equation. Both the drag coefficient and the heat transfer coefficient obtained from the momentum balance and the energy balance equations respectively were found to be functions of a parameter, ε, given by:

$$\varepsilon = 8\frac{\sqrt{Re_x}}{Re_D} \qquad [2.3.1]$$

where Re_D is the Reynolds number based on the diameter of the cylinder and Re_x is the same based on the distance to the leading edge. Sakiadis(45) extended the work of Glauert and Lighthills which was for cylinders of finite length to continuous cylindrical surface. He assumed that the boundary layer started from the point where the cylinder originated. An approach similar to Sakiadis was adopted by Bourne and Elliston(45) to solve the energy balance equation for moving continuous cylindrical surfaces. However, the boundary layer approach using the integral method of solution was limited to the laminar regime only because it was difficult to choose a consistent velocity profile in the turbulent zone(11). Later, studies on the boundary layer theory used what is known as "exact solution" for the boundary layer equation and employed numerical techniques for the solution. This method eliminates the necessity for the assumption of a velocity profile but it can not produce analytical expressions for the heat transfer coefficient unlike the integral method. These studies assumed a constant cylinder diameter and a constant surface temperature. however, fiber spinning is associated with attenuation in diameter and large changes in temperature along the spinline. Investigations on diameter attenuation in the boundary layer equations, conducted by Sayles(41), indicated an increase in local Nusselt number with the attenuation of diameter. Moutsoglou(34), in his studies, assumed an exponential decrease in fiber diameter with distance. An exponential decay form of the variation of the diameter is not valid in non isothermal melt spinning. An analytical expression for

the heat transfer coefficient using the concept of "sublayer" has been derived by Bos(46). A sublayer can be defined as the layer immediately in contact with the fiber surface where the flow is determined by viscous forces only. The expression derived by Bos relates the Nusselt number based on the fiber radius, R, with other dimensionless numbers as follows:

$$Nu_R = \frac{P}{\ln\left(1+(1.29Re_x^{1/3})/Re_R\right)}Pr^{1/3} \qquad [2.3.2]$$

where Re_x and Re_R are the Reynolds numbers based on the distance from the spinneret and the local radius of the fiber respectively. Pr is the Prandtl number, Nu_R is the Nusselt number based on the radius of the fiber and P is the local velocity drop across the sublayer. This provides a local heat transfer coefficient that is dependent on the radius of the fiber.

Empirical Correlations:

Numerous empirical correlations have been derived for the heat transfer coefficient and only the important ones are discussed here. Three main approaches are the heated wire experiment, momentum-heat transfer analogy and inversion procedure.

The heated wire experiment to derive the heat transfer coefficient is relatively easy. A wire is directly heated by an electric current and is subjected to a cooling air stream. At steady state condition, the amount of heat lost by the wire is equivalent to the electrical heat dissipation. If the effect of heat loss due to radiation is neglected then Newton's law of cooling can be applied to calculate the heat transfer coefficient. Various expressions relating the heat transfer coefficient to processing variables in

fiber spinning has been summarized by Ziabicki(12). Experiments conducted by Kase and Matsuo(13) give the following expression:

$$Nu_D = \frac{hD}{K_a} = 0.42\left(\frac{\rho_a v D}{\mu_a}\right)^{0.334} \qquad [2.3.3]$$

where K_a, ρ_a and μ_a are the thermal conductivity, density and viscosity of the cooling medium respectively. The effect of cross air flow normal to fiber axis has also been examined by Kase and Matsuo(14) and it assumes the following form:

$$Nu_D = 0.42\left(\frac{\rho_a v D}{\mu_a}\right)^{0.334}\left[1 + 8\left(\frac{v_c}{v}\right)^2\right] \qquad [2.3.4]$$

where v_c is the velocity of cross air. In processes such as spunbonding, where the draw down of the fiber is achieved by high velocity parallel air flow, v is the relative velocity between the air and the moving fiber(9). Presently, the Kase-Matsuo correlation is commonly used for the modeling of melt spinning and related processes(17,47-55). However, many other investigators have proposed different correlations for the heat transfer coefficcients for gases flowing around cylinders which may be applicable for fiber spinning(11,56-59). The correlation derived by Muller(57) gave the following equation:

$$Nu_D = 0.51 Pr^{0.3} Re_D^{0.43} \qquad [2.3.5]$$

Several other formulations have been reported in the literature.

Reynolds analogy gives the relationship between the rate of momentum transfer and the rate of heat transfer(60). It is described as follows:

$$\left(\frac{Nu}{Re_x Pr}\right) = \frac{f}{2} \qquad [2.3.6]$$

where Nu, Re and Pr are the Nusselt number, the Reynolds number and the Prandtl number respectively. "f" is the friction factor of the surface of interest. Taking this approach, Glicksman(43) derived the following correlation for the turbulent regime:

$$Nu_D = 0.4Re^{0.3} \qquad [2.3.7]$$

where Re_R is the Reynolds number based on the radius of the fiber.

The heat transfer coefficient can also be obtained from on-line measurements of temperature and diameter during melt spinning through the "inversion procedure". The inversion procedure will be discussed separately due to its importance and applicability in the present research work.

2.4 Melt Rheology and Constitutive Equations:

The axial stress and hence the rheological force are related to the kinematics of the spinline such as the deformation and the deformation rate, etc. through the rheological constitutive equations. In melt spinning, the spinline flow is not spatially homogeneous, i.e., the stress and the strain rate vary along the spinline(61). The spinline flow can be interpreted in two ways. At any point of the spinline, the velocity of the fluid is constant with respect to time. Hence the flow is steady in a Eularian sense. However, the flow is unsteady from a Lagrangian point of view, i.e., any fluid particle experiences a change in velocity as it moves along the spinline. The rheological response of viscoelastic melts depends not only on the temperature but also on the instantaneous as well as the prior history of the deformation rate. For incompressible materials such as polymeric melts, the stress tensor can not be uniquely

determined from deformation of the material because any isotropic pressure can be added without actually affecting the deformation. Hence the total stress tensor has two components, viz., an isotropic stress tensor $P\delta_{ij}$(the isotropic stress tensor can be viewed as the hydrostatic pressure in a stationary fluid) and the deviatoric stress tensor T_{ij}. Thus,

$$\sigma_{ij} = -P\delta_{ij} + T_{ij} \qquad [2.4.1]$$

where δ_{ij} is the Kroneker delta which is unity i and j are equal and zero when i and j are unequal. Since the isotropic component of the total stress does not affect deformation, therefore the kinematics of the melt is related to the deviatoric stress tensor through the rheological constitutive equations. The simplest form of rheological constitutive equation is defined by Newton's law of viscosity which states that the rate of deformation of a viscous fluid is directly proportional to the applied stress. In terms of tensor notation, it can be written as(62):

$$T_{ij} = \mu d_{ij} \qquad [2.4.2]$$

where,

T_{ij} = deviatoric stress tensor

d_{ij} = deformation rate tensor $= \left(\frac{\partial u_i}{\partial x_j} + \frac{\partial u_j}{\partial x_i} \right)$

and μ = viscosity, independent of the rate of deformation.

For simple shear flow, Newton's law of viscosity can be treated as $T_{xy}=T_{yx}=\mu\gamma$ where γ is the rate of shear and μ is the shear viscosity. During various polymer processing operations, such as melt spinning and film blowing, the polymeric melt experiences

elongational flow. For this reason, it is often necessary to define an uniaxial elongational viscosity, η_e, as

$$\eta_e = \sigma_{11}/E \qquad [2.4.3]$$

where E is the rate of elongation. It is important to note that the elongational viscosity is determined by the total stress σ_{11} rather than the deviatoric stress, T_{11}, even though the deviatoric stress is the fundamental parameter for the correlations describing the rheological response of the melt. Also the elongational viscosity so defined depends only on the instantaneous rate of elongation and not on its prior history. Therefore it is called the "apparent elongational viscosity". However, it is a convinient parameter to represent the spinline data. For a Newtonian fluid, the elongational viscosity is three times the shear viscosity(63). This result is mathematically similar to the relationship between the young's modulus and the shear modulus of an incompressible isotropic Hookean solid. Temperature has a large effect on viscosity. The temperature dependence of viscosity for Newtonian fluids and polymeric melts far above the glass transition temperature can be expressed in terms of an Arhenius type equation(64):

$$\eta = Ae^{B/RT} \qquad [2.4.4]$$

where A is a constant, B is the activation energy, R is the universal gas constant and T is the absolute temperature in Kelvins. For polymeric materials, A and B are characteristics of the polymer. The activation energy for the flow process generally varies between 5 and 50 KCal/mole(64). The Arrhenius type of equation can be expressed in terms of several molecular theories. The explanation of Eyring(65) is based on a lattice structure of the liquid, containing some unoccupied sites or holes. These sites move at random throughout the liquid as they are filled and created anew

by molecules jumping from one site to another. Under an applied stress, the probability of such jumps is higher in the direction that relieves the stress. Each jump is made by overcoming an energy barrier of level B, the theory leads to the equation (2.4.4). As the molecular weight is increased in a homologous series of liquids up to the polymer range, the activation energy of flow, B, should not increase proportionally but should level off at a value independent of the molecular weight. This arises from the argument that in long chains, the unit of flow is considerably smaller than the entire molecule. However, a variation of A and B is observed when the melt flow rate and hence the average molecular weight is varied. B increases as the size of the side group increases and as the chain becomes more rigid. This can be qualitatively explained from a physical point of view that the flow becomes increasingly more difficult with increase in the size of side group and with increase in rigidity of the chain. For polymers, as the temperature is decreased, the Arrhenius type of equation starts deviating from the experimental data for temperatures less than 100 °C above their T_g. A better representation of the viscosity data can be obtained, using the free volume approach, by the Williams-Landel-Ferry(WLF) equation(64):

$$\mathbf{Log_{10}}\left(\frac{\eta}{\eta_g}\right)=\frac{-c_1(T-T_g)}{c_2+(T-T_g)}-\mathbf{Log_{10}}\left(\frac{T_g\rho_g}{T\rho}\right) \qquad [2.4.5]$$

for $T_g<T<(T_g+100)$

where c_1 and c_2 are universal constants with $c_1=17.44$ and $c_2=51.6$, η_g and ρ_g are respectively the viscosity and density of the melt at glass transition temperature, T_g, of the polymer. η and ρ are respectively the viscosity and density at temperature, T. Temperatures are on the absolute scale. The term $(T_g\rho_g/T\rho)$ is close to unity and hence

'$Log_{10}(T_g\rho_g/T\rho)$' is often neglected in practice. The use of T_g is not universal and it is sometimes replaced by some other reference temperature.

The basic rheological response of polymeric melt can be separated from the temperature dependence of its behavior by isothermal melt spinning process. The isothermal elongational behavior of low molecular weight polypropylenes using the gravity spinning method was extensively studied by Patel and Bogue(66,67). A convected Maxwell model in the differential form was used for the analysis of the viscoelastic response of the polymeric melts. They found out that under isothermal gravity spinning conditions, where the take-up force at the end of the spinline could be neglected, the elongational viscosity of low molecular weight polypropylenes was close to three times the zero shear viscosity. As the molecular weight was increased, non-Newtonian thinning was observed. The elastic modulus, G, was found out to be nearly independent of molecular weight within the range of investigation and therefore the time constant was found out to be proportional to zero shear viscosity. Since the experiments were conducted under isothermal conditions, they suggested that the time constant could be correlated with temperature through an Arrhenius type of shift factor. In their study, they found out that the apparent elongational viscosity was close to that of a Newtonian fluid in the upper part of the spinline for the lower molecular weight polypropylenes. They concluded that , since the stress and the strain rate changed along the spinline, a viscoelastic analysis, using a convected Maxwell model that incorporated a deformation dependent time constant should be done. however, the work of Patel and Bogue was in the low stress region. Little investigation has been done for realistic cases, where the take-up forces dominate, to show how the time constant varies with molecular weight and temperature. Evident from the work of Patel

and Bogue is the fact that transient viscoelastic effects in molten polypropylenes are typical for elongational flows, particularly for higher spinning speeds.

The Newtonian constitutive equation has been assumed to describe adequately the rheological response of polymeric melts in fiber spinning by most researchers, perhaps, due to the lack of a better model to describe the experimental data in nonisothermal high speed melt spinning. The apparent elongational viscosity is independent of the rate of elongation and is constant at a particular temperature under the Newtonian assumption. Since the spinline temperature varies greatly, except in isothermal melt spinning, the apparent elongational viscosity is then taken as a function of temperature only. Normally, the effect of temperature on the viscosity is quite strong and the rate of change of temperature on the spinline is of the order of several hundred degrees per minute. Hence, for relatively inelastic melts such as polyesters or nylons, it is appropriate to describe the rheological response of the melt during spinning by an Arrhenius type temperature dependent Newtonian viscosity. However, for melts that show deformation rate thinning and elastic effects, such as polyethylenes, a purely viscous constitutive equation may not be sufficient(68).

The constitutive equations that describe the rheological behavior of polymeric melt fall into two principal categories: differential type and integral type. The on-line data obtained from the melt spinning experiments can be fitted into any of the models based on either type of constitutive equation but the result should be interpreted in terms of the model that describes the spinline data appropriately. Application of the integral type constitutive equation requires the knowledge of the kinematics of flow at the beginning, i.e., at the spinneret. Since the kinematics of flow at the spinneret is not known, it can only be approximated(69,70). On the other hand, the derivative type

constitutive equation is easy to apply because it relates the instantaneous values at any point of time, i.e., the material history is formulated to be dependent on the instantaneous quantities. Thus, the problem of spinneret kinematics can be overcome by using the derivative type constitutive equations. The traditional derivative type constitutive equation comes from the classical "Maxwell model". This model is formed by a series combination of spring and dashpot describing the elastic and the viscous elements of the fluid respectively. In terms of tensor notation, the convected Maxwell model of the derivative type can be represented by the following equation:

$$T_{ij} + \tau\left(\delta T_{ij} / \delta t\right) = G\tau d_{ij} \qquad [2.4.6]$$

where d_{ij} is the deformation rate tensor ($d_{ij} = \frac{\partial u_i}{\partial x_j} + \frac{\partial u_j}{\partial x_i}$), G is the modulus and t is the relaxation time. $\delta T_{ij}/\delta t$ is the convected time derivative that moves and deforms with the fluid element. Three convected time derivatives that satisfy the requirement are the contravariant and covariant Oldroyd derivatives(71) and the Juamann derivative(72,73). The contravariant Oldroyd derivative predicts finite first normal stress difference, N_1, and zero second normal stress difference, N_2, in shear flow. Experimental studies by White et al(74) showed a negative N_2 of magnitude of the order 0.1 to 0.3 times the magnitude of N_1 for shear flow using a cone and plate viscometer. However, the approximation of a zero second normal stress difference is often used for simplicity in simulation. Using the contravariant Oldroyd derivative, the convected Maxwell model predicts the following relationship for one dimensional shear flow:

$$T_{12} = G\gamma\tau$$
$$N_1 = T_{11} - T_{22} = 2G\gamma^2\tau^2 \qquad [2.4.7]$$
$$N_2 = T_{22} - T_{33} = 0$$

The above set of equations shows that the viscosity is a product of the shear modulus and the relaxation time and is independent of the shear rate, γ. It is well known from experiments that both the viscosity and the shear rates are functions of shear rate. To account for this effect, a variation of the convected Maxwell model was suggested by Bogue and White(75,76) in which the relaxation time was taken to be deformation rate dependent and was given by:

$$\tau_{eff} = \frac{\tau_n}{1+\left(a\tau_n\left\langle\Pi_d^{1/2}\right\rangle\right)^b} \qquad [2.4.8]$$

where τ_{eff} is an effective deformation rate dependent relaxation time, Π_d is the second invariant of the deformation rate tensor d_{ij}, a is a thinning parameter and b is an adjustable parameter. "b" is used to obtain the correct asymptotic slope of the viscosity-shear rate curve at large shear rate. a = 0 corresponds to the original convected Maxwell model. The value of b has been found to vary between 0.75 and 0.8(66, 67). In the case of simple shear, "$\Pi_d^{1/2}$" is nothing but the shear rate, γ, and for uniaxial elongational flow, it is $\sqrt{3}\dot{E}$.

During processing, polymers almost always undergo temperature change and deformation simultaneously. An excellent example is conventional melt spinning where both the change in temperature and the change in rate of deformation (elongation in this case) along the spinline are quite large. Thus, it leads to the requirement of having a constitutive equation that can handle change in deformation rate and temperature change simultaneously, in other words, non-isothermal constitutive

equation. It is important to note that BKZ constitutive equation is valid only for isothermal rheology. The constitutive equations derived under isothermal conditions have been extended to account for the variation of temperature by using "thermorheological simplicity" which relates the rheological response of a polymeric melt at different temperatures. The concept of thermorheological simplicity was first suggested by Morland and Lee(77). They represented the temperature influence on viscoelasticity on a logarithmic time scale that equated temperature change to a translation on the logarithmic time scale for all viscoelastic functions. Later, this became to be known by the "Principle of time-temperature superposition". The concept of thermorheological simplicity has been introduced for melt spinning and idealized elongational flow by Matsui and Bogue(69). They modified the integral BKZ constitutive equation by using reduced time:

$$\sigma_{ij} = -p\delta_{ij} \int_{-\infty}^{t} \Sigma G_n \frac{\exp\left(-\int_{t}^{t'} \frac{dt''}{\tau_n(t'')}\right)}{\tau_n(t')} C_{ij}^{-1} dt' \qquad [2.4.9]$$

where $\tau_n( ) = a_T\{T( )\}\tau_n^o$ and a_T is a temperature shift factor and C_{ij}^{-1} is the finger strain tensor. This, when applied to the melt spinning data by Dees and Spruiell(78), gave fairly good agreement(69). The Maxwell model of the derivative type was modified for non isothermal conditions by Marruci(79) as:

$$T_{ij}\left\{1 - \frac{\tau D(\ln T)}{Dt}\right\} + {}^{\tau\delta T_{ij}}\!/_{\delta t} = G\tau d_{ij} \qquad [2.4.10]$$

where d_{ij} is the deformation rate tensor, $\delta/\delta t$ is the Oldryd contravariant time derivative, D/Dt is the material time derivative, T_{ij} is the deviatoric stress, T is the absolute temperature and τ is the relaxation time. The relaxation time is both a

function of temperature and deformation rate. The deformation rate dependence is incorporated by using the Bogue-White model whereas the temperature dependence is introduced by the thermorheological simplicity. This theory does not however predict the rheological behavior of polymer melts near their glass transition temperature.

2.5 Inversion Procedure:

Once the background of various correlations such as the heat transfer coefficient and the rheological constitutive equation etc. are known from a theoretical point of view, it is important to discuss how these material and process parameters can be obtained, in the context of present research, from the "Inversion Procedure". The experimentally measured diameter and temperature profiles and a single tension measurement at the bottom of the spinline are used to calculate the apparent elongational viscosity and the heat transfer coefficient relations over the region where the temperature and diameter are measured. The inversion procedure has both limitations and advantages. The advantage lies in the fact that there are no restrictions on the process conditions, especially the spinning speed, in which the logic of the inversion procedure is not applicable. However, processing of semicrystalline polymers does pose a problem. Due to crystallization on the spinline, a temperature plateau may sometimes be observed or the temperature of the region of the spinline where the polymer crystallizes may be higher than that of a non crystalline polymer because of evolution of heat of fusion. The temperature plateau is prominent in low speed spinning of polyolefins such as polyethylenes and isotactic polypropylenes. Also crystallization has a stiffening effect on the fiber in the sense that the viscosity of the polymer increases with crystallization. Sometimes necking of the fiber is observed

with crystallization. This limits the applicability of the inversion procedure to smooth regions of the measured temperature and diameter profiles because the velocity and temperature gradient are calculated through the derivatives of the diameter and the temperature profiles respectively. Hence, necking of the fiber or a temperature plateau may give rise to zero derivative values which lead to singularities in the computation(31).

Different authors have used different methods to fit the diameter and the temperature profiles. Two regression models for fitting the profiles were first suggested by George and Deeg(80) in which they calculated velocity profile from the diameter data and used a polynomial fitting of log(v) versus log(z). The models were as follows:

$$\log(v - v_o) = \sum_{i=1}^{N} A_i \{\log(z)\}^i + A_{N+1} \qquad [2.5.1]$$

$$T = \sum_{i=1}^{N} B_i \{\log(z)\}^i + B_{N+1} \qquad [2.5.2]$$

where,

v_O = initial velocity of the fiber

N = order of fitting

and A_i, B_i are the regression coefficients.

Bheda(31) and Zhou(81) used direct polynomial fitting for the diameter to obtain the elongation rate. Patel(68) used a polynomial fitting of reciprocal of the diameter instead of the diameter. He argued that the nature of the diameter profile did not allow a smooth polynomial fitting without vibrations in the fit towards the end of the

spinline. A fitting of 1/D gave considerably smoother results. Once the rate of elongation is determined, the apparent elongational viscosity can be calculated using equation (2.4.3). The stress appearing in this equation is given by the equation (2.1.8). Calculation of the rheological force, F_{rheo}, involves the integration of the differential force balance as shown in equation (2.1.4). The correlations for the drag coefficient used in this equation were discussed in the previous sections. The integration of the equation (2.1.4) involves the evaluation of the constant of integration which is nothing but the initial rheological force, F_0, as shown in equation (2.1.1). Since it is impossible to determine the rheological force in the fiber as it comes out from the extruder by direct measurement, it is evaluated indirectly from the rheological force of the fiber at the bottom of the spinline. The rheological force at the bottom of the spinline is nothing but the tension in the spinline that can be experimentally measured. The initial rheologial force is guessed in the inversion procedure till the final rheological force matches the tension measured at the bottom of the spinline.

The heat transfer correlation is calculated using the equation (2.2.1) but neglecting the heat of crystallization term:

$$\frac{dT}{dz} = \frac{-\pi Dh}{WC_p}(T - T_a) + \frac{\Delta H}{C_p}\cdot\frac{dx}{dz} \qquad [2.5.3]$$

Thus the inversion procedure, as described earlier in the current section, is limited to the region of the spinline where crystallization does not occur. The temperature gradient is calculated from a direct polynomial fitting of the temperature profile.

The apparent elongational viscosity obtained by using the inversion procedure is correlated with the measured temperature profile using an Arrhenius type relation:

$$\mu = \mu_o \exp^{E/RT} \qquad [2.5.4]$$

where μ_o and E are constants, R is the universal gas constant and T is the absolute temperature in Kelvin. This equation assumes that, at a particular temperature, the apparent elongational viscosity is independent of any function of the rate of elongation and consequently it can be expressed as a function of only temperature for nonisothermal fiber spinning. The heat transfer coefficient is usually correlated using a relation of the form:

$$h = a\left[\frac{v}{A}\right]^b \qquad [2.5.5]$$

where v and A are the velocity and the area of cross section of the fiber respectively at the point of interest along the spinline and a and b are constants obtained from the fitting of the log(h) versus log(v/A).

A schematic diagram of the steps of calculation in the inversion procedure is given in Figure 2.2. As shown in the figure, the rheo-optical coefficient can be calculated from the stress and the birefringence profile. The inversion procedure is used in the present work to obtain the apparent elongational viscosities of various polypropylene resins of varying molecular weight and molecular weight distribution. The diameter and temperature measurement techniques are fairly well established and are discussed in detail by previous researchers(11,31,68,81). Nevertheless, a brief description of these techniques used in the present research work will be given in Chapter-3. However, the measurement of tension at the bottom of the spinline still needs improvement when the force at the bottom of the spinline is provided by an airjet. This will be presented in Chapter-4.

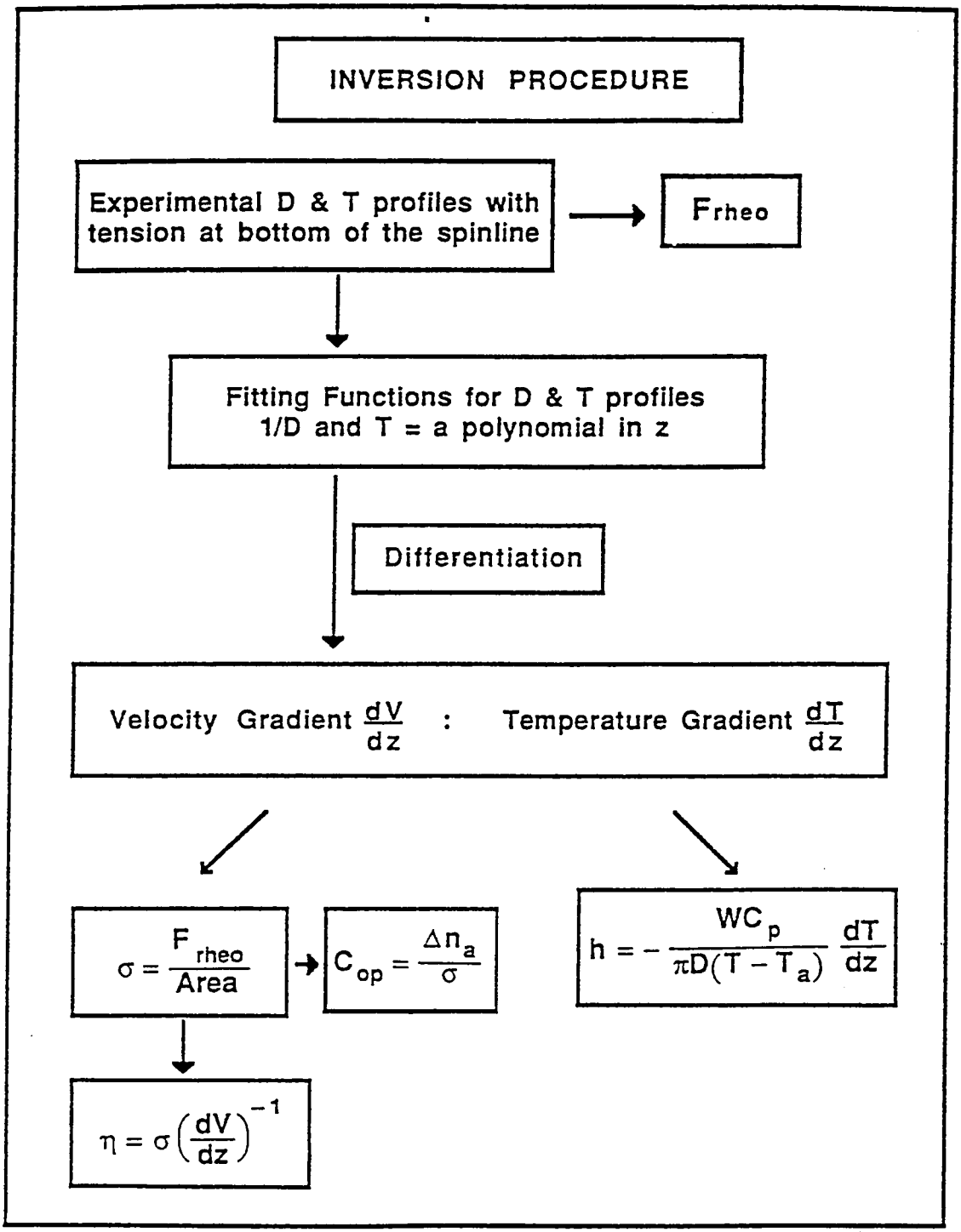


Figure 2.1 Schematic diagram for steps of calculation in the "Inversion Procedure".

2.6 Crystallization Kinetics:

In the processing of semicrystalline polymers, crystallization is an important phase transition where an ordered structure is formed from a disordered phase. In meltspinning, the degree of crystallinity along with other variables affect the final properties of the fiber such as the tensile strength, density of the fiber, shrinkage on annealing etc. The development of crystallinity along the spinline influences the rheological properties of the polymer, the heat transfer and consequently the dynamics of the process. The morphological structure of the fiber is also dependent on the degree of crystallinity. Polymer processing operations are almost always associated with nonisothermal conditions and the presence of molecular orientation of the polymer chains due to the applied stresses. Thus crystallization, during polymer processing, occurs almost always under nonisothermal conditions and often in the presence of molecular orientation. This is particularly true in the case of fiber spinning. The description of crystallization for such processes requires an understanding of its dependence on temperature and molecular orientation. The difficulty in applying the crystallization kinetics, obtained through experiments, to practical processing comes from the fact that the variables in experiments and those in processing do not lie in the same range. Experiments on isothermal crystallization kinetics are accessible only over a narrow temperature range at low undercoolings. On the other hand, crystallization in polymer processing takes place in a temperature range that is well below the that of experimental studies. Experimental study of crystallization kinetics under nonisothermal conditions is limited to a maximum cooling rate that is well below practical cooling rates during processing. Also the experiments are done under quiescent conditions whereas, as mentioned above, the crystallization during processing is associated with stress and hence molecular

orientation of the melt. However, it is necessary to understand quiescent isothermal and nonisothermal crystallization kinetics in order to investigate the possibility of applying and extrapolating it for practical polymer processing conditions.

Isothermal Crystallization Kinetics:

It is well known that when a polymer sample is crystallized at a constant temperature, a characteristic sigmoidal shaped isotherms are obtained. The half time, $t_{1/2}$, is a strong function of the temperature of crystallization. The half time also serves as a measure of the rate of crystallization. As the temperature of crystallization is decreased, starting from the melting temperature T_m, the rate passes through a maximum at a certain temperature below T_m. For the case of a solid nucleating from a liquid under quiescent isothermal conditions, Turnbull and Fisher(82) obtained the following correlation for the rate of nucleation in condensed systems(i.e., liquid-solid or solid-solid):

$$N = N_o \exp\left[-\frac{(\Delta\Phi + \Delta G_i)}{kT}\right] \qquad [2.6.1]$$

where N_O is a constant dependent on molecular parameters, $\Delta\Phi$ is the activation energy of viscous flow of a molecule across the phase boundary, ΔG_i is the critical free energy required to form the critical nucleus, k is the Boltzmann constant and T is the absolute temperature. Hence, the overall nucleation rate described by the above equation is attributed to the rate of transport of molecules to the nucleation site and the rate of formation of the nuclei. Since the two rates have opposite temperature dependence, the rate of nucleation passes through a maximum at an intermediate temperature between the melting temperature T_m(at which the rate of formation of nuclei is zero) and the glass transition temperature T_g(at which rate of molecular transport to the nucleus site

is zero)(83). Under quiescent isothermal conditions, the crystallization takes the shape of spherulites. Experimental evidence for a number of polymers shows a linear relationship between the time and the radii of the growing spherulites under isothermal conditions(83). The temperature dependence of the growth rate, G, of polymer crystals is given by(84):

$$G = G_o \exp\left(\frac{-E_{act}}{RT}\right)\exp\left(\frac{-\Delta W^*}{kT}\right) \qquad [2.6.2]$$

where E_{act} is the activation energy for the transport process at the interface and ΔW^* is the work needed to form a crystal nucleus of critical size, R is the universal gas constant and K is the Boltzmann constant. Based on a secondary nucleation theory, the following has been proposed by Hoffman for the growth rate(85-87):

$$\frac{E_{act}}{RT} = \frac{U^*}{R(T - T_\infty)} \qquad [2.6.3]$$

$$\frac{\Delta W^*}{kT} = \frac{K_g}{T(T_m^o - T)f} \qquad [2.6.4]$$

where " $U^* / R(T - T_\infty)$ " represents the temperature dependence of the segmental jump rate of the polymers. T_∞ is a hypothetical temperature where all motion associated with viscous flow ceases. Usually T_∞ is taken to be within 5 - 10 ^oK of being 50 ^oK below T_g. K_g is a parameter related to the crystallization regime, interfacial free energy parallel and perpendicular to the chain and the latent heat of fusion. T_m^o is the equilibrium melting temperature and f is a correction term that accounts for the latent heat of fusion with change in temperature, usually $f=2T/(T_m^o+T)$.

The above describes the crystallization theory from a molecular point of view. However, macroscopic determination of crystallinity as a function of time is useful for the application in processing. Examples include the determination of crystallinity using DSC, dilatometry and light depolarization microscopy etc. Avrami has proposed the following equation for the degree of phase transformation with respect to time at constant temperature(88):

$$X(t) = 1 - \exp(kt^n) \qquad [2.6.5]$$

where X(t) is the degree of crystallinity at time t, k is the crystallization rate constant incorporating Nucleation and growth rates and n is the Avrami index which depends on the mode of nucleation and the geometry of crystal growth. There has been considerable research and discussion on the Avrami formulation, especially by Wunderlich(89) and Khanna et al.(90). It is important to note that Avrami analysis neglects the slow secondary crystallization process during isothermal crystallization. Dietz(91) modified the differential form of the Avrami equation to account for the secondary crystallization with an additional term:

$$\frac{d\theta}{dt} = nkt^{n-1}(1-\theta)\exp\left(\frac{-a\theta}{1-\theta}\right); \; a \geq 0 \qquad [2.6.6]$$

where $\theta = X(t) / X_\infty$ and a is a parameter accounting for secondary crystallization and is evaluated by fitting the data towards the end of crystallization. "a=0" leads to the original Avrami equation in its differential form. The evaluation of crystallization rate constant, k, in the Avrami equation can be done by data fitting. Frequently, the rate constant is evaluated from the half time of crystallization, i.e., $k = \ln(2)/(t_{1/2})^n$ where n is the Avrami index. It is well known that the rate of crystallization is strongly dependent on crystallization temperature. Consequently, as the temperature is lowered

below the melting point, the half time for crystallization, $t_{1/2}$, decreases to a minimum at a certain undercooling below which it increases with further decrease in temperature. Since crystallization occurs at lower temperatures at higher cooling rates which is a common case in polymer processing, the measured values of $t_{1/2}$ need to be extrapolated to lower temperatures. Several correlations are available for temperature dependence of $t_{1/2}$(12,92,93). A frequently adopted correlation is the one proposed by Archmbault and Prud'homme(93). It uses the Laurizen-Hoffman theory and can be written as follows:

$$\frac{1}{t_{1/2}} = \frac{1}{(t_{1/2})_o} \exp\left[-\frac{U^*}{R(T - T_\infty)}\right] \exp\left[-\frac{C_3}{T\Delta Tf}\right] \qquad [2.6.7]$$

where $T_\infty = T_g - 30\ ^oK$, U^* is the activation energy of segmental jump of polymer and f is the correction factor accounting for the change in latent heat of fusion with temperature.

Non-Isothermal Crystallization Kinetics:

The Avrami analysis for isothermal crystallization was extended for the non-isothermal case by Nakamura et al(94,95). In their analysis they assumed isokinetic condition and independence of ultimate crystallinity of the cooling process. The following equation was derived with these assumptions:

$$\frac{X(t)}{X_\infty} = 1 - \exp\left\{-\left(\int_o^t K(T)d\tau\right)^n\right\} \qquad [2.6.8]$$

where X(t) is the degree of phase transformation at time t, n is the Avrami index determined in the isothermal experiment and K(T) is related to the crystallization rate

constant for isothermal crystallization, k(T), through the equation $K(t)=\{k(t)\}^{1/n}$. Experiments of non isothermal crystallization of HDPE, carried out under various cooling conditions, to verify the above formulation matched the equation for primary crystallization only(95). Using temperature as the independent variable, equation (2.6.8) can be written as(68):

$$\frac{X(T)}{X_\infty} = 1 - \exp\left[-\left(\int_{T_\bullet}^{T} K(T)\frac{dT}{R}\right)^n\right] \qquad [2.6.9]$$

where X(T) is the degree of phase transformation at temperature T, R is the cooling rate and other variables are the same as before. Kamal and Chu(96) have suggested, for non isothermal crystallization, an integral form, slightly different from the Nakamura model, which, when transformed to an equation with temperature as the independent variable, gives rise to the following equation(21):

$$\frac{X(T)}{X_\infty} = 1 - \exp\left[-\int_{T_\bullet}^{T} K(T)n\left(\frac{T_o - T}{R}\right)\frac{dT}{R}\right] \qquad [2.6.10]$$

Both the Kamal model and the Nakamura model reduce to the Avrami equation for n=1. The differential form is frequently more useful than the integral form in process simulation. The model of Nakamura et al., in its differential form, can be represented as follows(21):

$$\frac{d\theta}{dt} = nK(T)(1-\theta)\left[\ln\left(\frac{1}{1-\theta}\right)\right]^{\left(\frac{n-1}{n}\right)} \qquad [2.6.11]$$

where $\theta = X(T) / X_\infty$. Dietz(91) noted that neither Kamal model nor Nakamura model accounted for the slow secondary crystallization. He proposed a modified rate equation which he mentioned to be a modification of the Nakamura formulation.

$$\frac{d\theta}{dt} = nK(T)(1-\theta)t^{n-1}\exp\left(\frac{-a\theta}{1-\theta}\right) \qquad [2.6.12]$$

Actually, the above relationship is a modification of the Kamal model as it reduces to the differential form of Kamal model for a=0(21). The model proposed by Deitz is useful for polymers showing extensive secondary crystallization but it has the disadvantage of evaluating an additional parameter "a".

Several investigators have attempted to use non-linear regression methods to fit non isothermal data directly(21,92,97). Patel and Spruiell fitted the non isothermal data using a differential form of Nakamura model {equation(2.6.11)}. They simplified the differential equation (2.6.11) into the following:

$$\frac{dY}{dt} = nK(T)(Y)^{\frac{n-1}{n}} \qquad [2.6.13]$$

where,

$$Y = \ln\{1/(1-\theta)\}$$

and $$K(T) = k^{1/n} = k_0\exp\left(\frac{-U^*}{T(T-T_\infty)}\right)\exp\left(\frac{-C_3}{T\Delta Tf}\right).$$

The values of k_0 and C_3 were evaluated by non-linear regression method for the range of experimental cooling rates and were assumed to be valid for higher cooling rates often observed in processing.

Crystallization Kinetics in Melt Spinning:

Crystallization in melt spinning is not only governed by non isothermal conditions but also the orientation of the polymer chains developed due to the stress in the spinline. From the equation of force balance along the spinline, it is evident that the rheological force and diameter of the fiber vary along the spinline. Hence the stress that causes the development of orientation also varies along the spinline.

Molecular orientation has a strong effect on crystallization. A thermodynamic description of the effect of orientation on crystallization was first presented by Flory(98). He presented a theoretical formulation in which the reciprocal of absolute temperature for incipient crystallization was predicted to decrease linearly with a simple function of elongation and average number of chain segments between the cross linkages of network polymer. The crystallization kinetics of molten polyethylene subject to a constant shear stress has been investigated theoretically and experimentally by Kobayishi and Nagasawa(99). They reported an increase in the temperature of crystallization due to a decrease in the change in entropy, ΔS, at constant shear stress. They also suggested that the superstructures of a specimen crystallized from a sheared melt might be quite different from that of a specimen crystallized without shear. The morphology of the specimen is strongly affected by molecular orientation. The crystal orientation changes with applied stress(100,101) and the spherulitic morphology changes to a non-spherulitic type morphology.

Few descriptions of crystallization kinetics of a polymer melt under stress are available. The effect of orientation on crystallization kinetics has been discussed by Ziabicki(102), Dunning(103) and Kobayishi and Nagasawa(99). Kobayishi and Nagasawa attempted to formulate the growth rate of nuclei in terms of the free energies

of the deformed and undeformed(quiescent) states. Ziabicki attempted a phenomenological analysis of nucleation and growth rate in terms of the invariants of molecular displacement gradient tensors(102) and showed that, for simple deformations such as uniaxial extension, the crystallization rate functions could be expressed as functions of orientation factors. Kobayishi and Nagasawa(99) presented the following relationship between the growth rates of quiescent and oriented conditions:

$$\frac{G(oriented)}{G(quiescent)} = \exp\left[-\left(\frac{4b_o\sigma_s\sigma_e}{kT}\right)\left(\frac{1}{\Delta f_{def}} - \frac{1}{\Delta f}\right)\right] \qquad [2.6.14]$$

where,

b_o = width of nucleus on growth surface

σ_s = free energy per unit area on the growth surface

σ_e = free energy per unit area on a surface normal to the chain direction

k = Boltzmann constant

T = absolute temperature

Δf_{def} = change in free energy for crystallization in presence of orientation

and Δf = change in free energy for quiescent crystallization.

Assuming the difference in change in free energy of crystallization in presence of orientation and the free energy of quiescent crystallization to be due to the entropy difference between the oriented and the isotropic amorphous region, Katayama et al. derived the following form for the overall rate of crystallization:

$$K(T,f_a) = K(T)\exp\left[\frac{4b_o\sigma_s\sigma_e T_m}{k\Delta H_f T\Delta T}\left(1 - \frac{1}{1 + C\left(\frac{T}{\Delta T}\right)f_a{}^2}\right)\right] \qquad [2.6.15]$$

where f_a is the amorphous orientation factor and C is an arbitrary constant.

An extension of the half time analysis to include the orientation effect in crystallization kinetics during melt spinning has been proposed by Patel and Spruiell(105):

$$K = K_o \exp\left[-\frac{U^*}{R(T-T_\infty)}\right]\exp\left[-\frac{C_3}{T\Delta Tf + Cf_a^2T^2}\right] \qquad [2.6.16]$$

where K is related to the crystallization half time, $t_{1/2}$, by "$K=\{(\ln 2)^{1/n}\}/t_{1/2}$" and n is the Avrami index. In the equation (2.6.16), K_o and C_3 are evaluated by the method of non-linear regression from quiescent isothermal crystallization data. The constant C is determined by trial and error method such that the various profiles such as the diameter and temperature profiles obtained, when crystallization kinetics along with other inputs is put into a mathematical model for melt spinning, match the corresponding experimental profiles obtained from melt spinning experiment. The model proposed by Patel and Spruiell is used in the mathematical model for Spunbonding.

The Continuous Cooling Transformation (CCT) curves used in metallurgy and solid state physics to illustrate phase transition can also be used as a conceptual tool for polymer crystallization. This idea was coined by Spruiell and White(106) and can be used to show the locus of points at which crystallization begins during continuous cooling of a polymer on a temperature versus log(time) plot for both quiescent and stressed state. It can also serve as a tool for comparing crystallization of melts under stress to quiescent melts and the crystallization of different polymers.

2.7 Orientation and Birefringence:

Quantitative analysis of orientation in fibers was started by Hermans(107). He defined orientation factor as a ratio of the resultant polarization anisotropy of a given fibrous system to the maximum theoretical polarization anisotropy in the principal directions of polarization. Thus:

$$f_H = \frac{\overline{\alpha_{II} - \alpha_{\perp}}}{\alpha_1 - \alpha_2} \qquad [2.7.1]$$

where α_{II} and $\alpha_{\perp}$ are the polarizabilities in the directions parallel and perpendicular to the fiber axis respectively. In terms of the angle between the polymer chains and the reference axis, z, the Hermans orientation function can be represented as follows:

$$f_H = \frac{3\langle \cos^2 \Phi_{c,z} \rangle - 1}{2} \qquad [2.7.2]$$

where $\Phi_{c,z}$ is the angle between the chains and the reference axis, z.

Birefringence is defined as the difference of principal refractive indices between the direction of extension and the direction perpendicular to it. The birefringence, Δn, at low and moderate stresses, is linearly related to the difference between the principal stresses through the stress-optical coefficient:

$$\Delta n = C_{op} \Delta \sigma \qquad [2.7.3]$$

where,

$$\Delta \sigma = \sigma_{11} - \sigma_{22}.$$

According to the theory of rubber elasticity of small deformations, the stress-optical coefficient is related to the absolute temperature by(108):

$$C_{op} = \frac{2\pi}{45kT}\frac{\left(n^2+2\right)^2}{n}(\alpha_1 - \alpha_2) \qquad [2.7.4]$$

where n is the average refractive index, k is Boltzmann constant and α_1 and α_2 are the principal polarizabilities of the polymer chain segment under investigation.

The relationship between optical retardation, Γ, and the intensity of the monochromatic light is given by (109):

$$I = c\sin^2(\pi\Gamma/\lambda) \qquad [2.7.5]$$

where I is the intensity of the incident beam, λ is the wavelength of light, and c is a constant depending on the intensity of the entering beam and the angle between the principal axis of the sample and the optic axis of the polarizer. Actually, this constant also depends on the absorption and the scattering by the sample and on the optical system(110).

Matsumoto and Bogue(110) investigated the effect of stress on birefringence under non isothermal conditions for amorphous polymers. They observed that stress is proportional to birefringence even under nonisothermal conditions till about the level of 10^7dyne/cm^2 beyond which the stress increased more rapidly than birefringence with deformation.

2.8 Structure Development in Fiber Formation:

The end properties of melt spun fibers largely depend on the structure formation during spinning. Molecular orientation, crystallinity (in the case of semicrystalline

polymers) and morphology together constitute the structure of the fiber. All these parameters not only depend on the type of polymer being spun but also the processing conditions such as spinning speed, extrusion temperature and secondary drawing and other post-spinning processing. For example, in the melt spinning of linear polyethylene, spherulitic morphology is observed at very low take up speeds whereas row nucleated untwisted lamellae are formed at high speed spinning(78,106). At very low take up speeds spherulitic morphology similar to that observed in polyethylene crystallized from quiescent melts is observed because of absence of stress in the spinline. Investigations by Dees and Spruiell(78) on structure development during melt spinning of polyethylene suggested a model that accounted for change in the crystalline morphology as well as the change in the crystallization temperature with change in spinning speed. As spinning speed increases from very low to moderate values, there's a rapid transition from spherulitic structure to a row nucleated structure. Under these conditions, the row structure has lamellae growing out from "fibril nuclei" perpendicular to the fiber axis and these lamellae twist in a fashion similar to the twisting that occurs in the lamellar crystals growing out from the center of spherulites. Strain induced fibril nucleus causes crystallization to occur at temperatures far above those at which crystallization occurs for a quiescent melt cooled at similar rates. Further increase in spinning speed suppresses the twisting of the lamellae and decreases the interlamellar spacing(long periods). The variation of the orientation functions along the crystal axes of polyethylene with spinning speed has been explained by Dees and Spruiell with the above model(78). These ideas have also been applied to polypropylene by Spruiell and White(106). Mechanical properties of as-spun fibers of both polyethylene and polypropylene can be correlated with the structure developed during spinning. Investigations by various researchers have shown that the

elastic modulus and tensile strength increase and the elongation to break decreases with c-axis crystalline orientation function(106, 111,112,113).

The development of structure in melt spinning of isotactic polypropylene has been subject to considerable investigation(106,113-121). Melt spun isotactic polypropylene contains three phases, namely, amorphous, smectic and crystalline(monoclinic). The proportion of these three phases can be altered by varying processing conditions only upto a certain limit. The work of Nadella et al. (113) gives birefringence and crystalline orientation functions, f_a, f_b and f_c as functions of spinline stress. Birefringence of the as-spun fiber increases with increase in spinline stress. The crystalline orientation functions show the same general trend as those of linear polyethylene for different extrusion temperature but reduce to the same curves when plotted against spinline stress independent of extrusion temperature(106).

The mechanical properties of spun fibers from isotactic polypropylene can be correlated with spinline stress. This comes from the fact that the structural features that control the mechanical properties of the fiber are themselves determined by, among other variables, the stress in the spinline. Structural features such as c-axis crystalline orientation factor and birefringence(a measure of average orientation) increase with spinline stress. Tensile strength, yield strength and Young's modulus of the fiber increase and percent elongation to break decreases with increase in spinline stress(106).

The effect of molecular weight on structure and mechanical properties of spun filaments of isotactic polypropylene has been studied by Ross(122) and Lu and Spruiell(119). Polypropylenes of three different melt indices were taken for experimentation by Lu and Spruiell(119). The final birefringence of the spun filaments showed considerable difference in magnitude, the lowest viscosity sample having the

minimum value, at low take-up velocities. Higher final birefringence for higher molecular weight sample was explained with the argument that higher viscosity(or molecular weight) sample needed more force and hence stress in the spinline for the fiber to draw down to the same diameter(or take-up speed). The same logic has been extended to explain why there is an increase in final birefringence with decrease in extrusion temperature for the same sample and take-up speed. They also suggested that the paracrystalline smectic phase in the fiber is favored by high cooling rate and low stresses in the spinline. Thus, controlling the cooling rate and/or stress, one could alter the proportion of these three phases present in fibers spun from isotactic polypropylene.

Crystallization kinetics also plays an important role in the structure development. The crystallizability of the virgin resin affects the end properties of the spun filaments. This effect has been recently investigated by Lu and Spruiell(121). Isotactic polypropylenes of similar molecular weight, polydispersity and rheological behavior but different crystallization kinetics were investigated. The quiescent crystallization kinetics was altered by addition of nucleating agents or through copolymerization. Increasing the quiescent crystallization kinetics caused crystallization to occur closer to the spinneret at higher temperatures. This resulted in lower molecular orientation of the as-spun filament and hence higher elongation-to-break because of the ability of the less oriented chains to elongate more before breaking. These effects were more prominent in low stress(or low take-up velocity) spinning. Higher takeup velocities and spinline stress reduced the effect of differences in quiescent crystallization due to the influence of on-line stress-induced (molecular orientation-enhanced) crystallization.

2.9 Development of Mathematical Model for The "Reicofil" Spunbonding Process:

A mathematical model has been developed for the "Reicofil" Spunbonding process at the University of Tennessee, Knoxville(9). The Reicofil spunbonding process, originally developed by Reifenhauser GmbH, Troisdorf, Germany' bears many similarities to the conventional melt spinning process. The differences of the process from the melt spinning process include the draw down conditions of the fiber, the conditions of ambient temperature and the boundary conditions. A schematic figure of the Reicofil Spunbonding process is given in Figure 2.2. In the Reicofil system, the melt is forced by spin pumps through special spinnerets having a large number of holes. In melt spinning, the draw down force is provided from the bottom of the spinline through a godet or an airjet. In the Reicofil system, the drawing of the fibers occurs through high velocity air surrounding the spinlines. As the molten polymer comes out of the spinneret, air through the primary blow duct (see Fig. 2.2) continuously cools the fibers. Temperature of this air is controlled. Immediately below the primary blow ducts, secondary blow ducts supply auxiliary air at room temperature. A blower at the bottom of the enclosed spinline chamber creates a suction that sucks the fibers and mixed air down from the cooling chambers. The continuous filaments pass through a venturi(low pressure zone) onto the distributing chamber and then onto the moving belt for thermal bonding (see Fig. 2.2).

Comparison of the results predicted by the model with experimental values for a range of processing conditions have been accurate for final diameter and final crystallinity within the range of experimental errors. Though the birefringence results

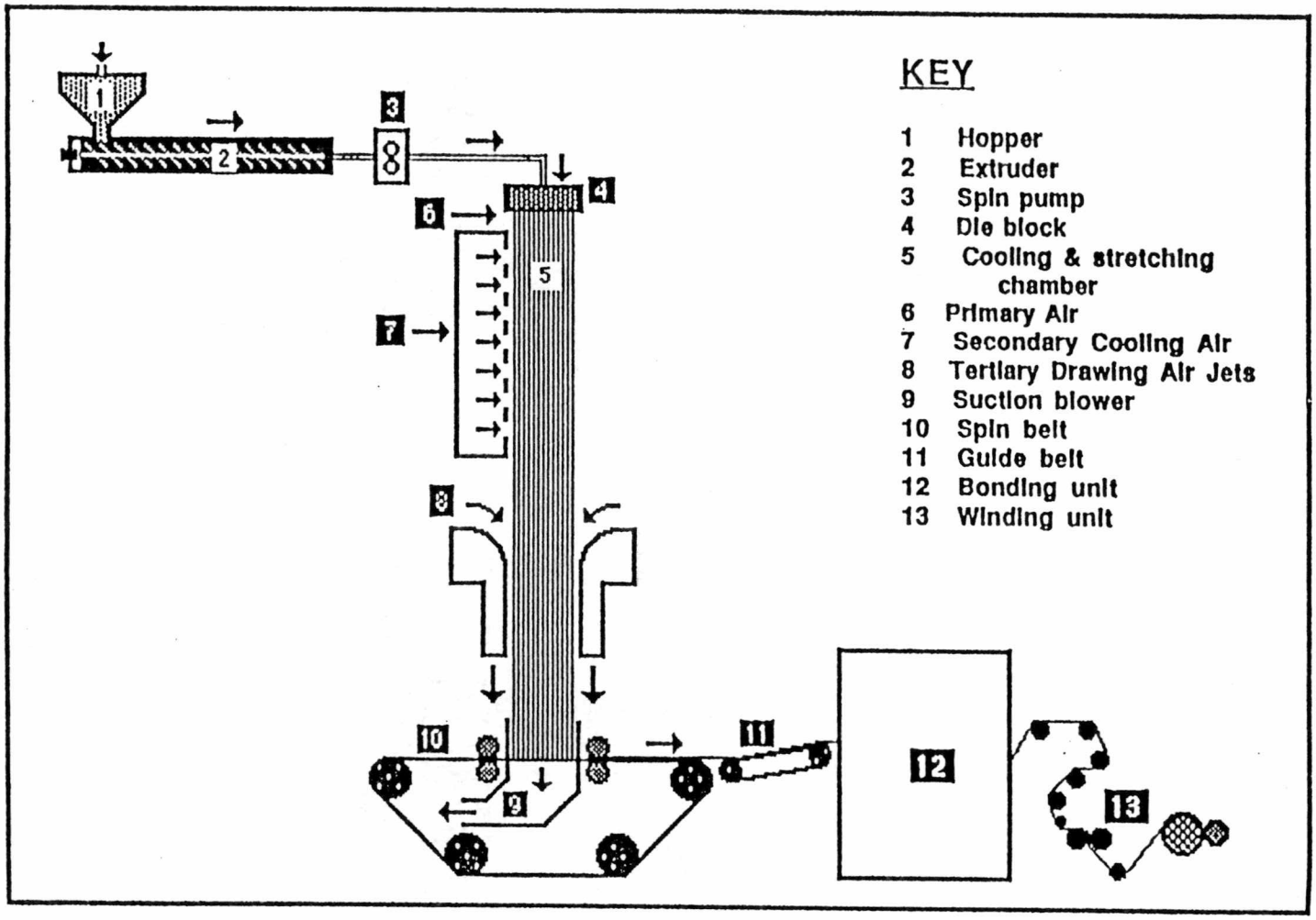


Figure 2.2 Schematic diagram of the "Reicofil" Spunbonding process.

predicted by the model showed a trend that matched the trend of the experimental data, the accuracy was not as good as that for final diameter final crystallinity. A more detailed description of the model and its predicted results can be found in reference-9.

CHAPTER 3

EXPERIMENTAL MATERIALS, EQUIPMENT AND METHODS:

A part of the present research was to carry out melt spinning studies on polypropylene. The aim was to investigate the effect of molecular weight as well as molecular weight distribution of polypropylene in melt spinning.

3.1 Materials:

Nine samples of isotactic polypropylene used in the present research were provided by Exxon Chemical company. Based on the qualitative information provided by Exxon Chemical Company, the entire set can be divided into three groups in terms of the melt flow rate of the 'as-received' resins. At each particular range of melt flow rate, three samples of varying molecular weight distribution, indicated qualitatively as narrow, medium and broad were provided as shown in Table 3.1. From the data on Table 3.1 it is clear that the 'as-received' samples are in three distinct ranges of melt flow rate(MFR), viz., 16 to 18, 35 to 42 and 74 to 78. The GPC data on five of these samples and the dynamic viscosities of the nine samples obtained by using a cone and plate viscometer at 180 ^{o}C in the 'as-received' state were measured by Exxon Chemical Company and are presented in Table 3.2 and Figures 3.1 through 3.3 respectively.

Table 3.1 Classification of experimental polypropylene samples.

Sample ID	Melt Flow Rate(MFR) of as-received samples	Melt Flow Rate(MFR) of post-extrusion samples	Molecular Weight Distribution(MWD)
1	16	24	Narrow
2	16	22	Medium
3	18	32	Broad
9	35	40	Narrow
4	37	45	Medium
5	42	44	Broad
6	75	95	Broad
7	74	86	Medium
8	78	85	Narrow

Table 3.2 GPC data of the experimental polypropylene samples.

Sample ID.	MFR	M_n	M_w	M_z	M_w/M_n	M_z/Mw	M_{z+1}/M_w
1	16	47864	174,880	325,633	3.65	1.86	3.0
3	18	38501	226,175	843,377	5.87	3.73	8.2
9	35	42097	147,050	270,373	3.49	1.83	3.0
8	78	31080	117,918	196,470	3.79	1.67	2.5
6	75	36669	138,818	448,647	3.79	3.23	8.0

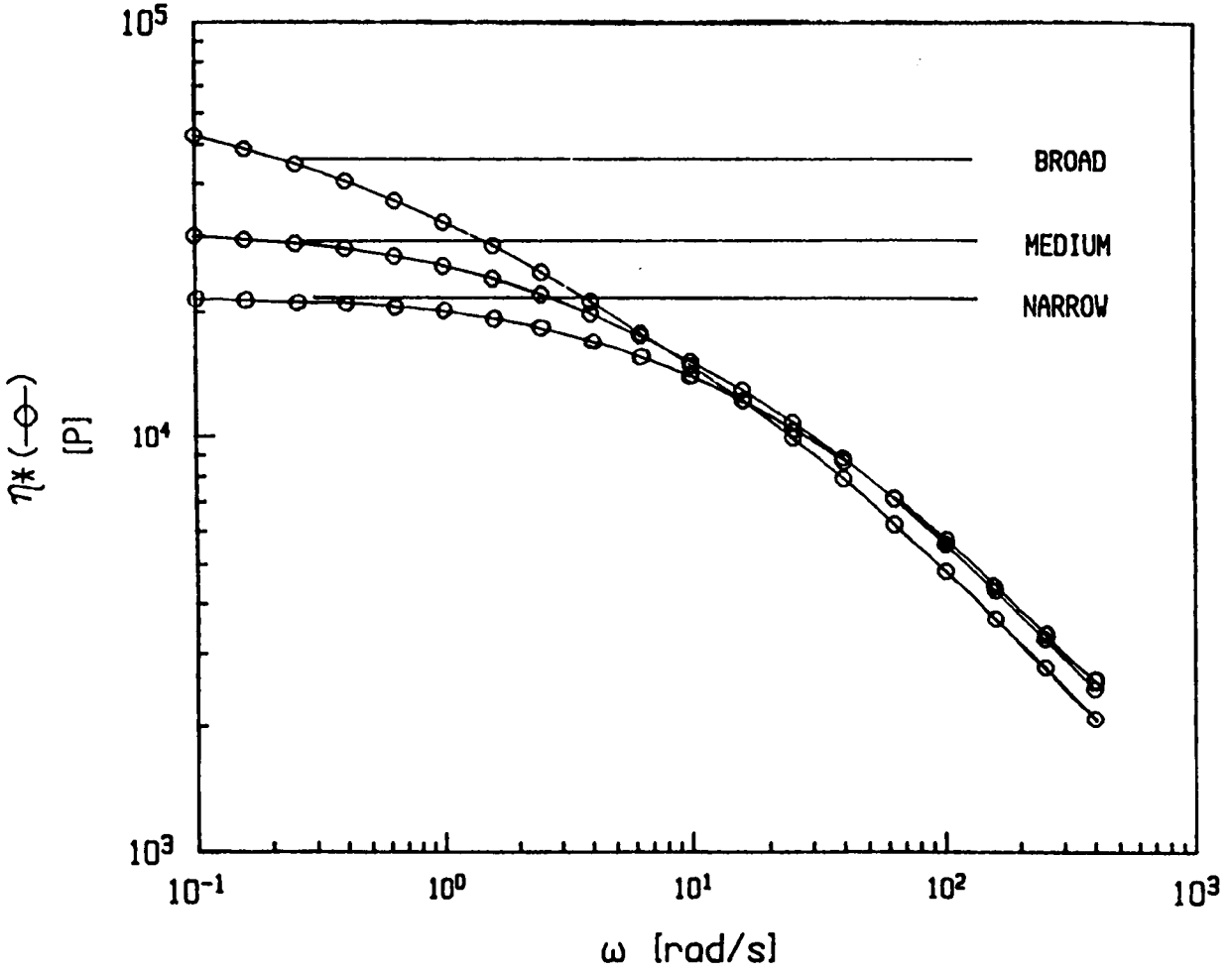


Figure 3.1 Dynamic viscosity for the 16-18 MFR resins as a function of angular frequency. (Temperature = 180 °C)

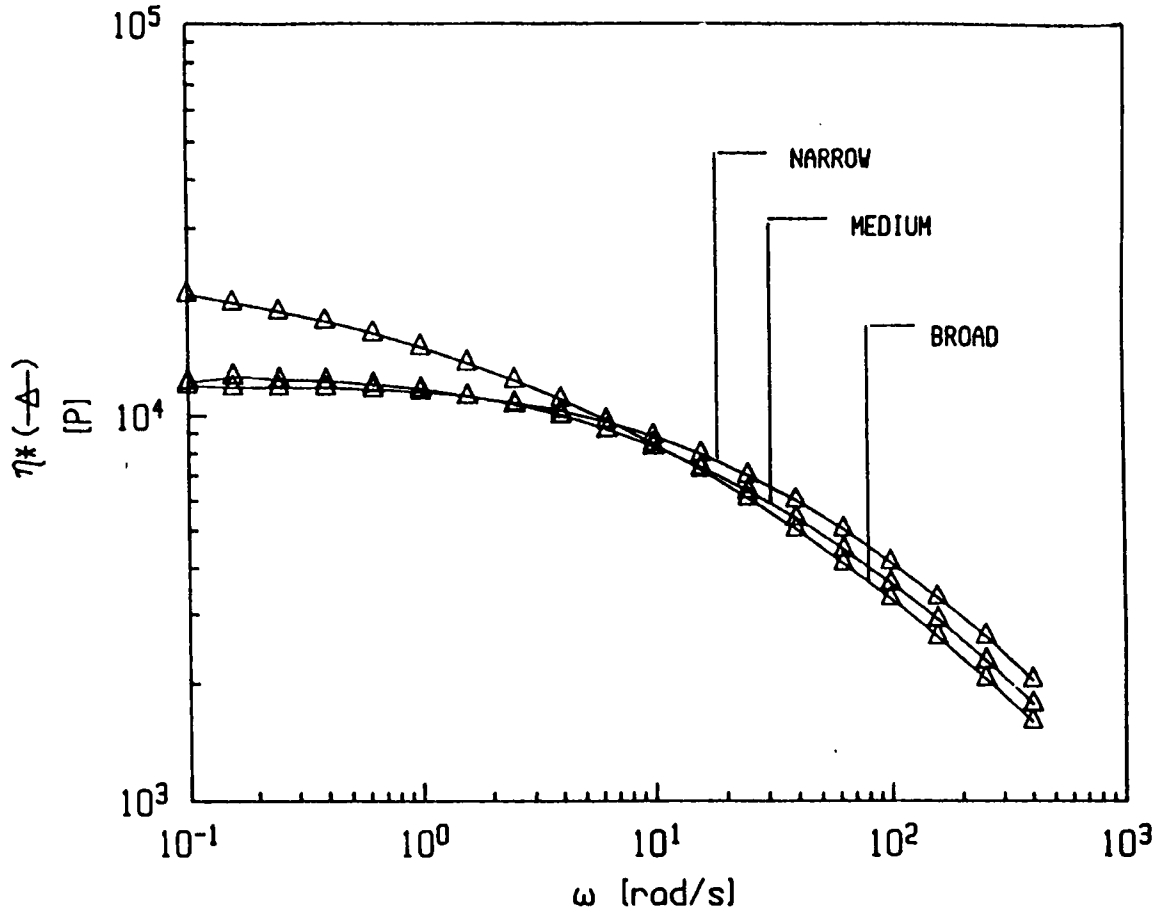


Figure 3.2 Dynamic viscosity for the 35-42 MFR resins as a function of angular frequency. (Temperature = 180 °C)

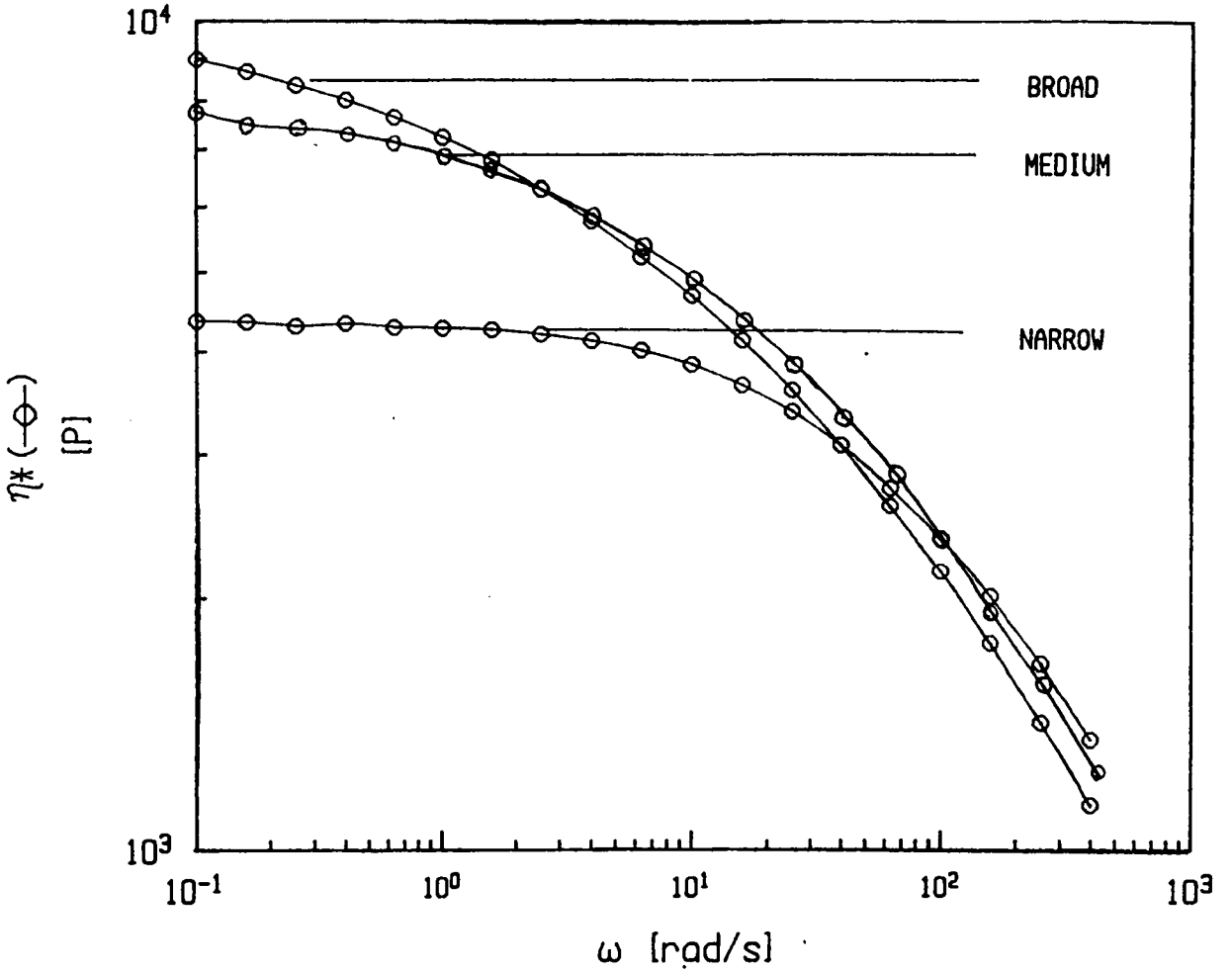


Figure 3.3 Dynamic viscosity for the 74-78 MFR resins as a function of angular frequency. (Temperature = 180 °C)

The melt flow rates of the various samples after they were extruded in the melt spinning equipment were also measured by Exxon Chemical Company. These data are summarized in the third column of Table 3.1. A comparison of the MFRs of the 'as-received' resins with those of the corresponding 'post-extrusion' samples indicate that the polymers undergo degradation in the extruder, particularly the 16-18 MFR samples. They were extruded at 240 °C whereas the other samples were extruded at 210 °C, as discussed in the next chapter. This degradation is not unusual because the residence time of the molten polymer in the reservoir before being spun is around 20 minutes. In the present research the polymer samples are referred to by their MFRs in the 'as-received' state.

3.2 Melt Spinning:

Melt Spinning Equipment:

The melt spinning machine used in the present study was designed by Fourne Associates of Germany(shown schematically in Figure 3.4). The Fourne extruder had a single screw of length 300 mm and diameter 13 mm. The polymer was fed in the form of pellets from a seven liter nitrogen purged hopper. Heat was supplied to the barrel by two band type heaters. To facilitate feeding of the polymer from the hopper and prevent immediate melting of the polymer at the throat by contact with the hot barrel, cooling water was circulated just underneath the hopper at the throat of the barrel. The molten polymer was delivered at a pressure of 1.0×10^3 to 3×10^3 psi to a Zenith constant volume displacement gear pump. The spinning head temperature was maintained by two band type heaters similar to those along the barrel. Molten polymer from the gear pump was forced through a filter mesh and then a capillary die of diameter 0.762 μm and an L/D ratio of 5.0. The mass flow rate of the molten polymer was controlled by adjusting the speed of the gear

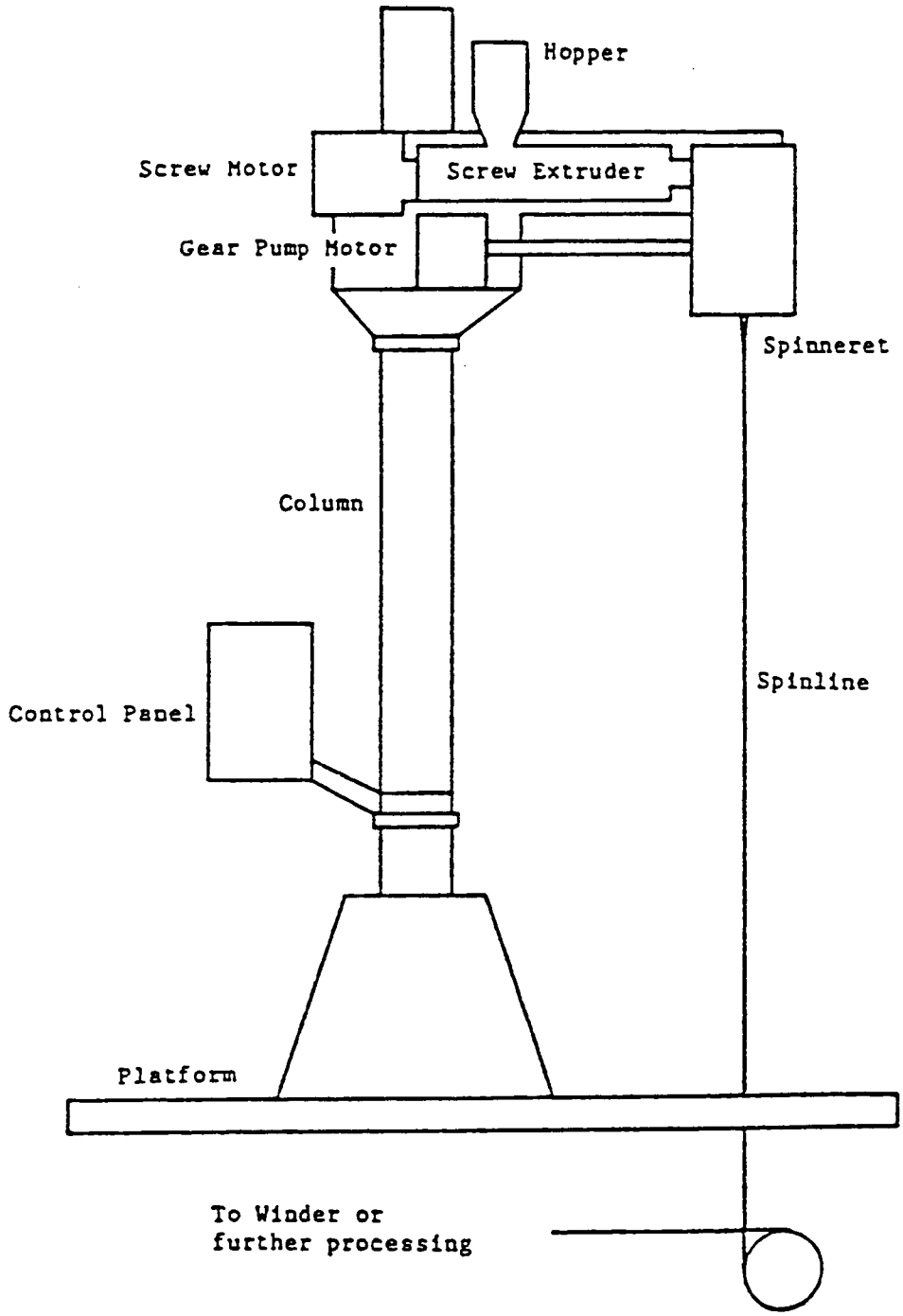


Figure 3.4 Schematic diagram of the melt spinning set up.

pump and the back pressure was maintained by controlling the rpm of the extruder screw. The extruder and the spinning head block was mounted on a vertical steel column which allowed vertical movement of the extruder and the spinning head assembly and, hence, variation of spinline length. The filament exiting the die was drawn down by an airjet drawdown device with air pressure upto about 100 psi, enabling spinning speeds up to 6000 meters/min.

3.3 On-line Measurements:

Diameter Measurement:

The on-line diameter measurements were done by a Zimmer diameter monitor(model 460A/2) and Digital Display Controller(model 466/2) supplied by Zimmer OHG, Germany. This instrument operated on a non-contact electro-optic principle, permitting measurements on both opaque and semitransparent materials. The range of diameter measurement by the Zimmer system was 0 to 2 mm with a resolution of 0.5 μm. The displayed diameter was averaged over 11 cm of filament length. It was necessary to calibrate the instrument before use with a set of metal wires with diameters in the range of 25 μm to 1.6 mm. The Zimmer was interfaced with an IBM PC AT for data acquisition in which the interval between successive data points and the number of data points could be chosen as desired. The Zimmer was mounted on a movable carrier to take measurements at different positions from the spinneret. The data collected at each position was fed to a computer program developed during previous research at the University of Tennessee, Knoxville(31) which computed the average diameter and its distribution after correcting for the transparency in case of semi-transparent fibers.

Birefringence Measurement:

On-line birefringence of the running filaments for the nine samples of polypropylene were measured as a function of distance by an Olympus polarizing microscope(model 206080). An Olympus four order Berek compensator(model CTPI-200205) was used to measure the optical retardation. The arrangement is shown schematically in Figure 3.5. The same movable stand used for the Zimmer system to measure the diameter at different positions along the spinline was also used as the stand for the Olympus microscope. A small V-groove, arc shaped aluminum guide was used to help stabilize the spinline within the microscope viewing field. The birefringence was computed by dividing the retardation by the filament diameter. There might be a small effect on the birefringence profile due to friction between the guide and the running filament(119). However, it was minimized by carefully adjusting the position of the guide in relation to the running filament.

Temperature Measurement:

The on-line temperature profiles were measured using a Hughes PROBEYE 3300 infrared thermal imaging system. This system does not measure the temperature of the fiber directly. The radiant power received by the infrared camera is measured and the detector displays the temperature at which a black body would emit the same radiant power. However, This temperature is referred to as the 'apparent' black body temperature because the radiant power received by the camera not only includes the radiation from the fiber surface but also the radiation coming from the surroundings which was partially reflected by and transmitted through the fiber surface before it reaches the instrument. The Hughes imaging system divides the entire fiber in view into one hundred horizontal sections which are scanned separately. The analog thermal imaging data is digitized after each horizontal

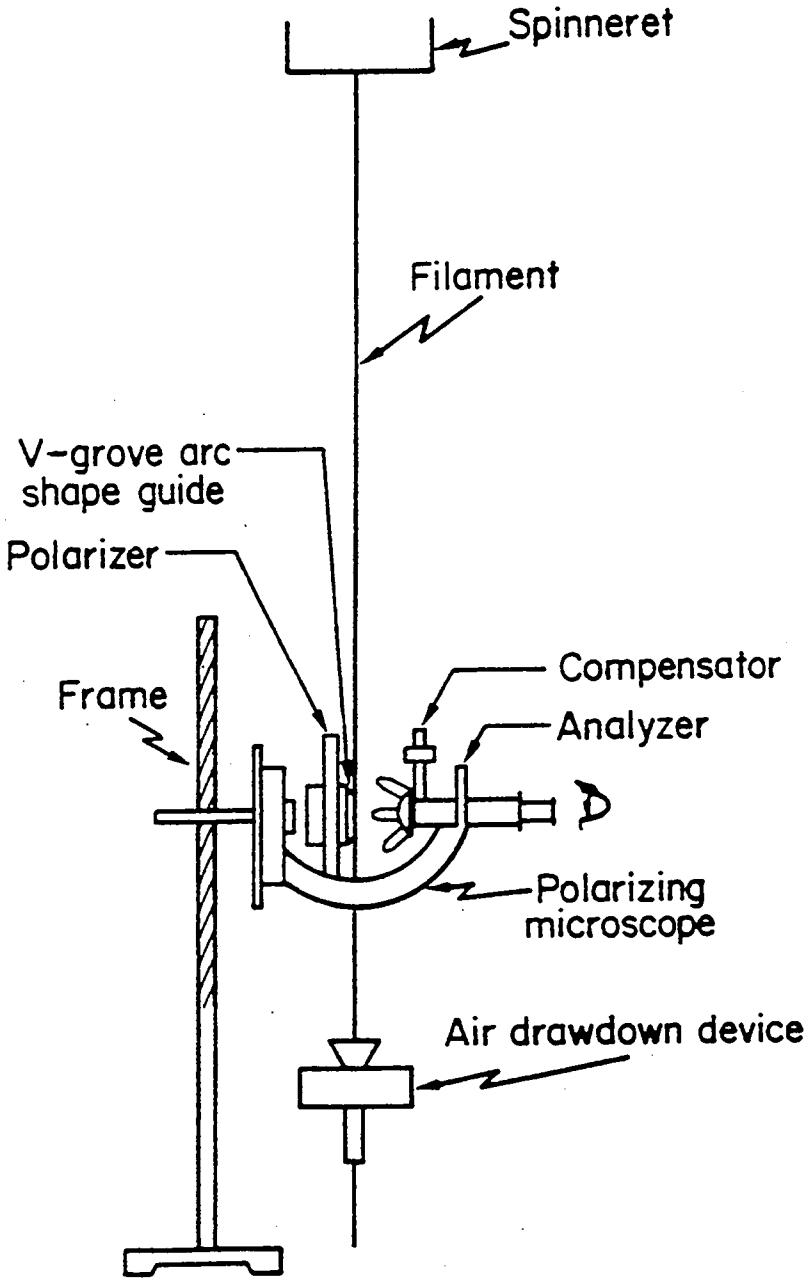


Figure 3.5 Schematic arrangement for birefringence measurement.

scan and the apparent black body temperature is displayed after the entire scene is covered. In order to obtain the actual filament temperature, it is necessary to know the emissivity of the fiber surface at that temperature. Emissivity of polypropylene fiber surface has been measured by Hajji(11) and the black body temperature profile was converted to the actual filament temperature profile by using a computer program that included the emissivity of polypropylene as a function of temperature and diameter(11).

Tension Measurement:

It is difficult to measure the tension at the bottom in a running spinline because the running fiber often sticks to the measuring head and breaks. This is particularly true in the melt spinning of polyethylenes. Hence the tension was measured using a Rothchild Tensiometer(model INTEG R-1198) as a function of fiber diameter and air pressure in the suction venturi, for stationary fibers. Fibers of different diameters were inserted in sufficient lengths in the drawdown device so that the effective length of these fibers experiencing the drag is the same as the length of the portion of a continuous filament which would experience the air drag while running through the drawdown device. These fibers were held stationary and the tension was measured. Tension at the bottom of the spinline for fibers of diameter and air pressure other than the measured points was obtained by interpolation between the two nearest points. However, the force measured this way would be greater than the force experienced by a running fiber of same diameter and at same pressure because the velocity of drag air relative to the moving fiber is less than the relative velocity when the fiber is stationary, or, in other words, the velocity of drag air relative to a fiber moving in the same direction is less than the absolute velocity of air (which is same as the velocity of drag air relative to a stationary fiber)(123). This correction is treated in Chapter 4.

CHAPTER 4

MELT SPINNING STUDY OF POLYPROPYLENE

Polypropylene is one of the most common polymeric materials used for both household and industrial purposes. Fundamental study of melt spinning of isotactic polypropylene dates back to the 1960s, when the polymer had just become available for commercial use. Extensive research on various aspects of polypropylene such as molecular weight, crystallizability and molecular weight distribution etc. that affect its melt spinning has been conducted in the laboratories of the University of Tennessee in the recent past(119,121,124). The aim of the present research was to analyze and compare polypropylene samples of varying molecular weight and molecular weight distribution in melt spinning. This study was intended to be more systematic and complete in examining these effects than was the case in the previous studies.

4.1 Preliminary Studies of Spinnability:

For the purpose of the present research, nine different polypropylene samples were supplied by Exxon Chemical Company. These samples were discussed in Chapter-3. As described in that chapter, the entire set of nine samples can be divided into three

groups, each group containing three samples of varying molecular weight distribution (Table 3.1).

Some difficulties were observed in preliminary spinning runs, especially for broad and medium MWD samples. At higher air pressures in the suction venturi the broad MWD samples and some medium MWD samples showed unsteadiness and frequent breaking of the filament in the spinline. Hence the spinnability of those samples were tested in terms of maximum air pressure in the suction venturi for continuous spinning at different temperatures in the range of 210 °C to 250 °C. It should be noted that the maximum air pressure for continuous spinning did not necessarily give a steady spinline without transverse vibrations. The results, including the condition of the spinline at maximum air pressure for continuous spinning, are summarized in Table 4.1. As seen from the table, the spinnability of any sample increases with spinning temperature only till a particular value above which increase in temperature has negligible effect on spinnability. The 18 MFR broad MWD sample seems to level off at a temperature of 240 °C whereas the 75 MFR broad MWD sample attains its maximum spinnability in terms of air pressure in the suction venturi at an extrusion temperature of 220 °C. Note that all the broad MWD samples are observed to have substantial vibration before breaking whereas the 37 MFR medium MWD sample gives a steady spinline even at its maximum speeds at different temperatures. The 16 MFR narrow MWD sample could be spun at maximum air pressure that could be provided by the compressed-air line in the laboratory, viz. 75 psi(g), at extrusion temperatures of 230 °C and 240 °C. Similarly, the 35 MFR and the 78 MFR narrow MWD samples could be spun at 75 psi(g) air pressure in the suction venturi at 210 °C. Based on these results, extrusion temperatures were selected for subsequent on-line measurements and detailed experimentation. The selected extrusion temperature for the 16-18 MFR group was 240

Table 4.1 Spinnability test for 'difficult-to-spin' polypropylene samples.

Sample ID	MFR	MWD	Extrusion Temp.(°C)	Maximum Air Pressure for Continuous spinning(psig)	Spinline condition (Vibrations, Steady etc)
3	18	Broad	210	-	-
			220	10	Vibrations
			230	15	Vibrations
			240	20	Vibrations
			250	20	Vibrations
4	37	Medium	200	3	Vibrations
			210	20	Vibrations
			220	24	Steady
			230	30	steady
			240	30	-
5	42	Broad	200	2	Vibrations
			210	12	Vibrations
			220	20	Vibrations
			230	27	Vibrations
			240	30	Vibrations
6	75	Broad	200	15	Vibrations
			210	20	Vibrations
			220	25	Vibrations
			230	25	Vibrations
			240	22	Vibrations

°C whereas the extrusion temperature chosen for all other samples was 210 °C. In spite of poor spinnability of the broad MWD samples, they were spun at the same temperature as the narrow MWD samples of the same MFR range for the purpose of comparison of diameter and birefringence profiles that indicate the structure development in the fiber.

Diameter uniformity of the as-spun filaments is an important property of the melt spinning process. The diameter uniformity for samples of different molecular weight distribution(MWD) can be analyzed by comparing the filament diameter distribution at a certain distance from the spinneret. The distribution of diameter of the fiber in the form of fraction of a total of 2000 observations of diameter at a distance of 220 cm from the spinneret was obtained. These distributions are shown in Figures 4.1 to 4.3. All the observations are for an air pressure of 5 psi(g) in the suction venturi. For the samples in the range of 16 MFR, the diameter distribution of the narrow MWD sample lies between 31 microns and 37 microns whereas the 18 MFR broad MWD sample has data points distributed from 32 to 48 microns, Figure 4.1. The narrow and broad MWD samples in the range of 35 MFR have a diameter distribution span of 5 microns and 15 microns respectively, Figure 4.2. Similar observations are made for the different MWD samples in the range of 75 MFR, Figure 4.3. In all the cases the diameter distribution for the medium MWD samples are observed to be in between the diameter distribution span of the narrow MWD and the broad MWD samples. This observation of increasing diameter distribution span with broadening molecular weight distribution can be correlated with decreasing highest air pressure for spinning with broadening molecular weight distribution, Table 4.1. Thus, the uniformity of filament diameter is associated, at least qualitatively, with the ultimate spinnability of the polymer. The above experimental observation generalizes that, for melt spinning of the present set of polypropylenes, the

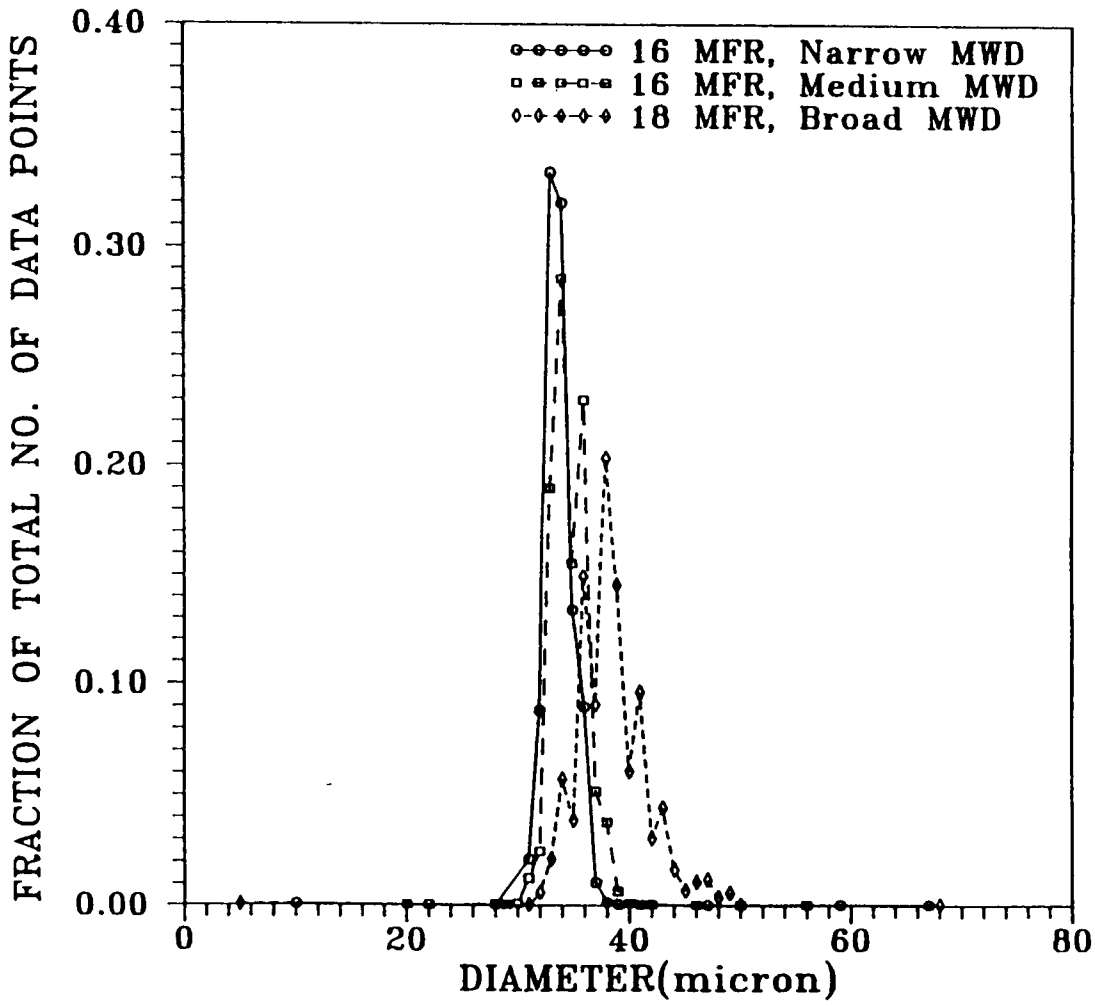


Figure 4.1 Diameter distribution of running filaments of 16-18 MFR at 220 cm below the spinneret spun under low air pressure of 5 psi(g).

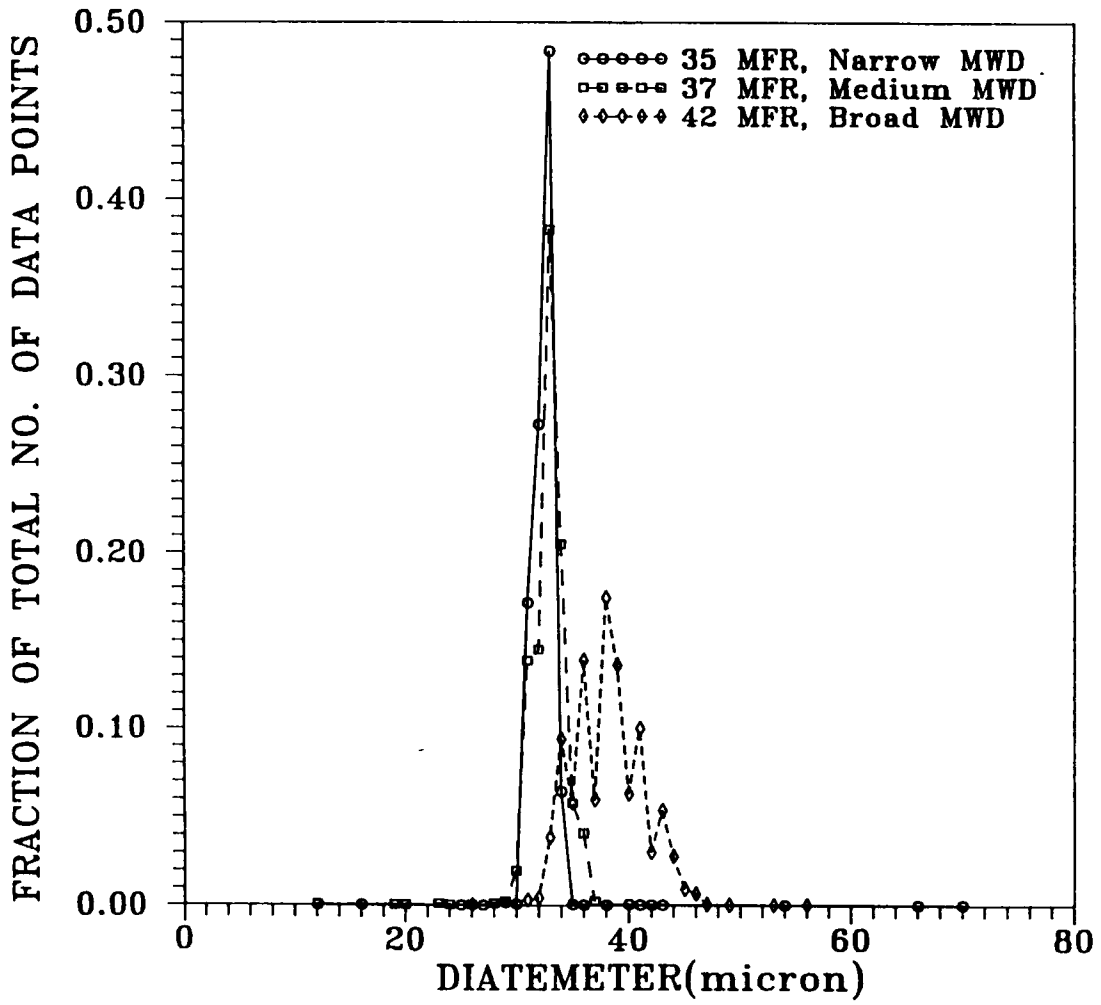


Figure 4.2 Diameter distribution of running filaments of 35-42 MFR at 220 cm below the spinneret spun under low air pressure of 5 psi(g).

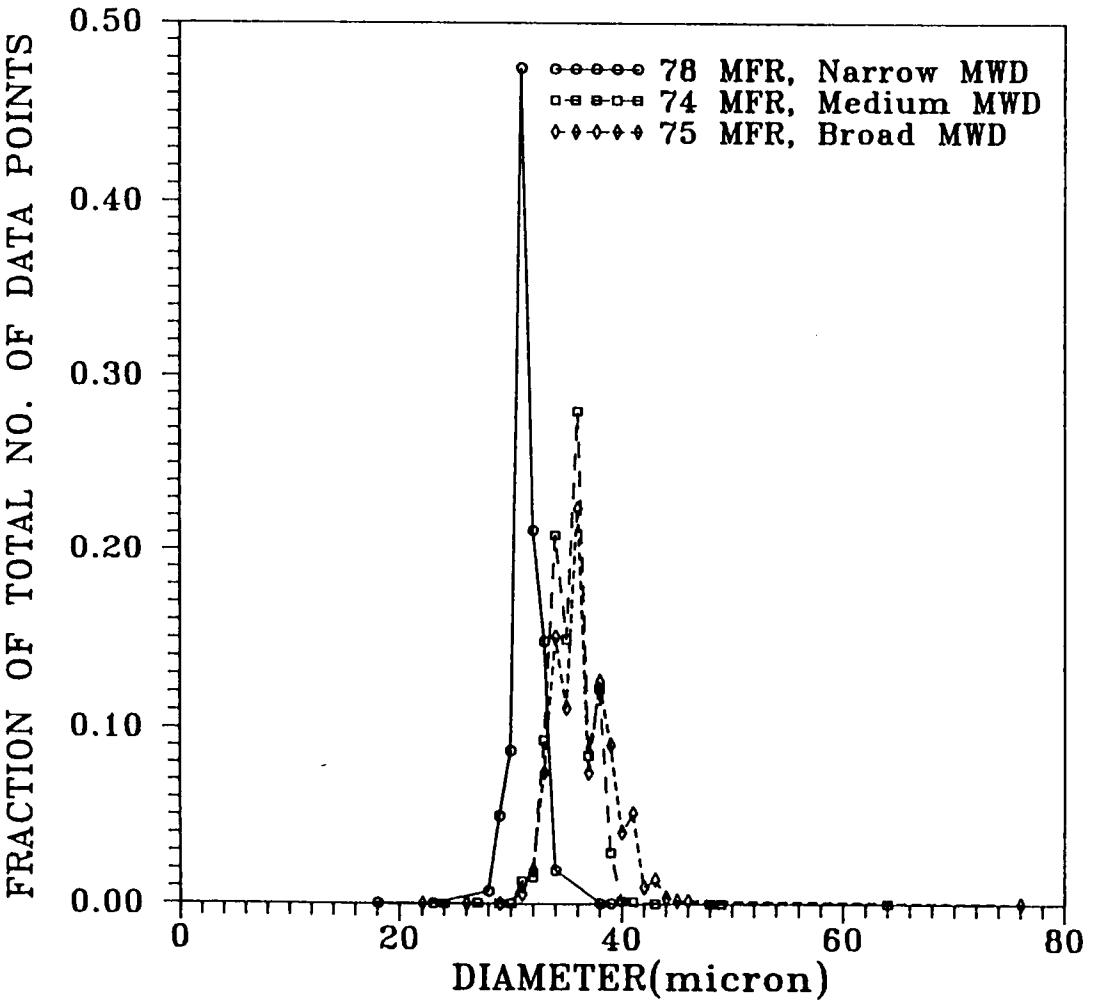


Figure 4.3 Diameter distribution of running filaments of 74-78 MFR at 220 cm below the spinneret spun under low air pressure of 5 psi(g).

spinnability at any extrusion temperature decreases and the variation in the diameter of the filament increases with broadening of molecular weight distribution.

4.2 Structure and Properties of As-spun filaments:

Each sample was spun at two different speeds at the spinning temperatures selected above. The processing conditions are summarized in the Table 4.2 for the low spinning speeds or lower air pressure in the suction venturi and Table 4.3 for the higher spinning speeds or higher air pressures in the suction venturi. The indicated spinning speeds are determined from application of the continuity equation to the on-line diameter measured at 220 cm from the spinneret. The lower spinning speeds were obtained by using a constant air pressure of 5 psi(g) in the suction venturi for drawdown of the fiber whereas the higher speeds were obtained, whenever possible, with an air pressure of 25 psi(g) in the suction venturi, Table 4.3. The higher air pressures in the suction venturi for the medium and broad MWD samples, as shown in Table 4.3 are not necessarily the same as the maximum possible air pressure as shown in Table 4.1. Lower pressures were used because of the difficulty in doing on-line measurements for those samples due to substantial vibrations in the spinline at the highest possible air pressure for spinning which is shown in Table 4.1. Tables 4.2 and 4.3 show that different samples were spun at different speeds even though the air pressure in the suction venturi was kept the same, viz. 5 psi(g), for the lower spinning speeds. Generally, the spinning speed increased with increase in MFR or with narrowing of the MWD for a given suction venturi air pressure.

The average diameter and birefringence of the as-spun filaments are presented and are compared with the corresponding on-line values measured at 220 cm from the

Table 4.2 Processing conditions of polypropylene samples at low air pressure.

Sample ID	MFR	MWD	Extrusion Temp.(°C)	Mass Flow Rate(g/min)	Supply Air Pressure to Suction Venturi(psig)	Spinning speed (m/min)
1	16	Narrrow	240	1.64	5	1917
2	16	Medium	240	1.53	5	1736
3	18	Broad	240	1.55	5	1438
9	35	Narrrow	210	1.62	5	1963
4	37	Medium	210	1.59	5	2075
5	42	Broad	210	1.61	5	1435
6	75	Broad	210	1.69	5	1741
7	74	Medium	210	1.70	5	1843
8	78	Narrrow	210	1.69	5	2245

Table 4.3 Processing conditions of polypropylene samples at high air pressure.

Sample ID	MFR	MWD	Extrusion Temp.(°C)	Mass Flow Rate(g/min)	Supply Air Pressure to Suction Venturi(psig)	Spinning speed (m/min)
1	16	Narrrow	240	1.64	25	3347
2	16	Medium	240	1.53	25	3226
3	18	Broad	240	1.55	15	2011
9	35	Narrrow	210	1.62	25	3267
4	37	Medium	210	1.59	15	2966
5	42	Broad	210	1.61	10	1648
6	75	Broad	210	1.69	15	2227
7	74	Medium	210	1.70	25	3376
8	78	Narrrow	210	1.69	25	3902

spinneret in the Tables 4.4 and 4.5 for the lower and higher air pressures in the suction venturi, respectively. It is noteworthy that the off-line diameters tend to be slightly higher than the on-line values, while the off-line birefringences tend to be slightly lower than the on-line values. This apparently is due to the elastic contraction occurring in the filaments when the drawdown stress is removed. There may also be some relaxation of the chains after spinning. The density and crystallinity as measured by the density gradient column and then other mechanical properties of the as-spun filaments are given in the Tables 4.6 and 4.7 for the low and high air pressures in the suction venturi, respectively.

Since the spinning speeds of the various samples varied, a graphical representation of the density and birefringence of the as-spun filaments can give a better picture for comparing different samples at the same spinning speed. The densities and birefringences of different samples versus the corresponding spinning speeds are shown in Figures 4.4 and 4.5, respectively. As seen from Figure 4.4 or Tables 4.6 and 4.7, for the same range of MFR, the filaments spun from the broad MWD samples tend to develop highest crystallinity whereas the fibers obtained from the narrow MWD samples have the lowest crystallinity. The fibers spun from the medium MWD samples have a crystallinity in between that of the narrow and the broad MWD samples. Also, the crystallinity increases with spinning speed. The fiber elongation before breaking is lowest for the narrow MWD samples and it increases with broadening of MWD and decreases as the spinning speed increases . But another interesting observation is that the samples show a reverse trend when the tensile strength is considered, i.e., the narrow MWD samples have the highest tensile strength and the tensile strength of the as-spun filaments decreases with broadening of MWD, Tables 4.6 and 4.7. Also, as shown in Figure 4.5 or Tables 4.4 and 4.5, the samples tend to follow the same order as the tensile

Table 4.4 Comparison of on-line and off-line data for fibers spun using 5 psi(g) air pressure*.

Sample MFR	Sample MWD	On-line Diameter (μm)	Off-line Diameter (μm)	On-line Birefringenc (x1000)	Off-line Birefringence (x1000)
16	Narrow	34.79	39.6	18.62	16.2
16	Medium	35.22	41.9	16.98	17.5
18	Broad	38.38	42.3	15.8	15.5
35	Narrow	34.11	38.22	17.96	18.4
37	Medium	32.87	38.5	16.92	16.9
42	Broad	39.77	42.3	15.1	14.1
75	Broad	36.99	41.5	13.98	13.1
74	Medium	36.06	42.9	15.94	14.54
78	Narrow	32.58	37.67	17.62	16.1

* On-line measurements are done on running filaments at 220 cm below the spinneret.

Table 4.5 Comparison of on-line and off-line data for fibers spun using higher air pressure*.

Sample MFR	Sample MWD	On-line Diameter (μm)	Off-line Diameter (μm)	On-line Birefringenc (x1000)	Off-line Birefringence (x1000)
16	Narrow	26.33	29.2	22.54	20.7
16	Medium	25.86	31.4	19.21	17.7
18	Broad	32.96	36.9	16.25	15.7
35	Narrow	26.43	29.0	21.21	19.1
37	Medium	27.49	33.6	20.26	18.72
42	Broad	37.11	40.4	15.98	14.73
75	Broad	32.71	34.8	16.85	14.83
74	Medium	26.64	29.92	19.83	17.05
78	Narrow	24.71	30.85	22.82	21.52

*On-line measurements are done on running filaments at 220 cm below the spinneret.

Table 4.6 Characteristics of as-spun fibers spun using 5 psi(g) air pressure.

Sample MFR	Sample MWD	Density (g/cm^3)	Crystallinity (%)	E ($Pa \times 10^6$)	Tensile strength ($Pa \times 10^6$)	Elongation to break (%)
16	Narrow	0.8967	42.1	1.0	0.18	315
16	Medium	0.8993	44.5	0.97	0.123	405
18	Broad	0.9029	47.85	1.0	0.097	614
35	Narrow	0.8975	42.8	1.15	0.158	310
37	Medium	0.9004	45.53	1.43	0.117	380
42	Broad	0.9013	46.37	1.48	0.095	540
78	Narrow	0.8922	37.83	0.9	0.146	270
74	Medium	0.8995	44.7	1.08	0.087	450
75	Broad	0.9010	46.1	1.26	0.073	700

Table 4.7 Characteristics of as-spun fibers spun using higher air pressures*.

Sample MFR	Sample MWD	Density (g/cm^3)	Crystallinity (%)	E ($Pa \times 10^6$)	Tensile strength ($Pa \times 10^6$)	Elongation to break (%)
16	Narrow	0.9026	47.6	1.78	0.183	300
16	Medium	0.9029	47.85	1.1	0.125	370
18	Broad	0.9032	48.13	1.02	0.099	610
35	Narrow	0.9023	47.3	1.48	0.162	250
37	Medium	0.9037	48.6	1.47	0.14	360
42	Broad	0.9014	46.46	1.47	0.091	550
78	Narrow	0.8967	42.1	1.49	0.17	200
74	Medium	0.9018	46.83	1.37	0.108	370
75	Broad	0.9013	46.4	1.29	0.086	560

* The various higher air pressures in the suction venturi for different samples are given in Table 4.3.

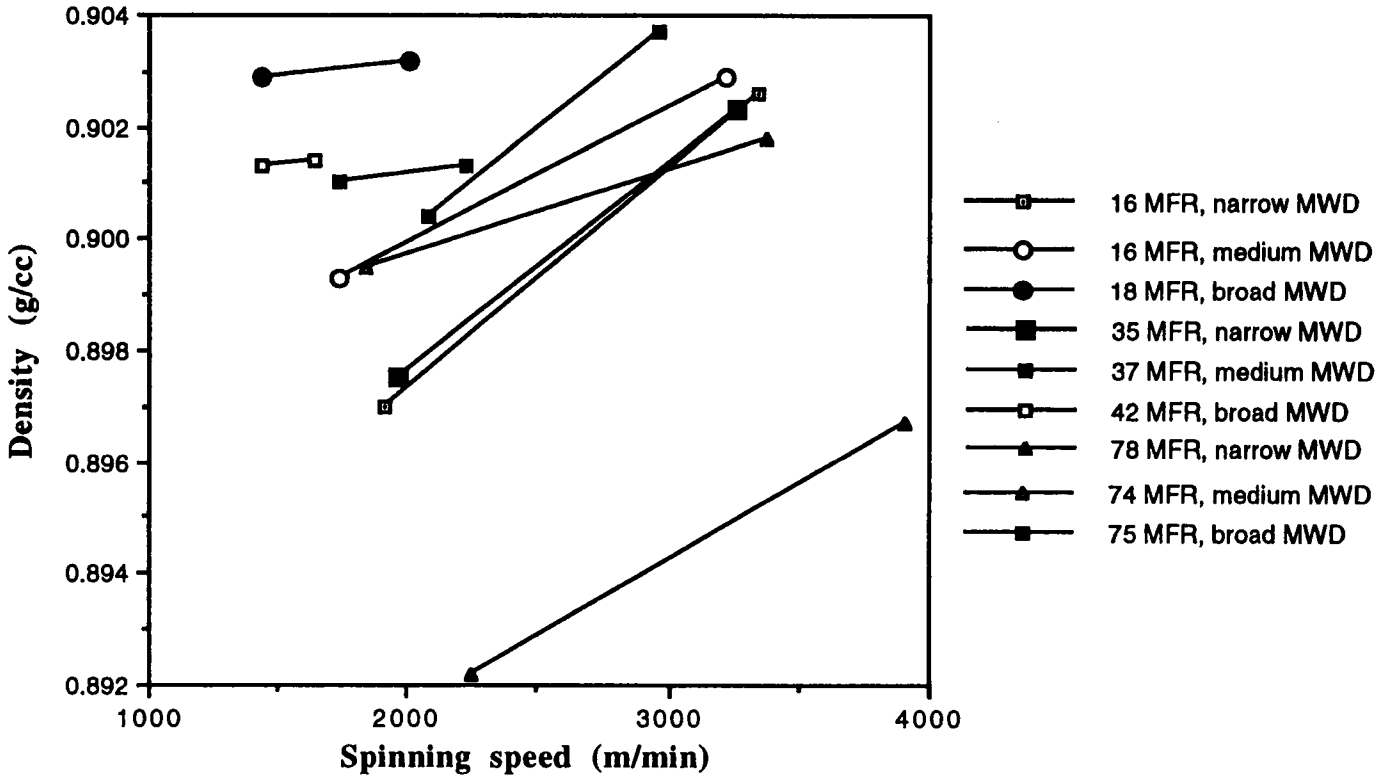
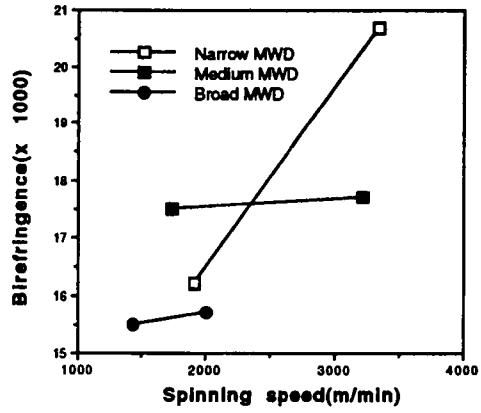
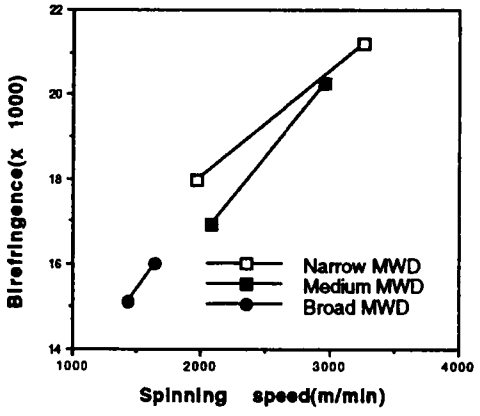


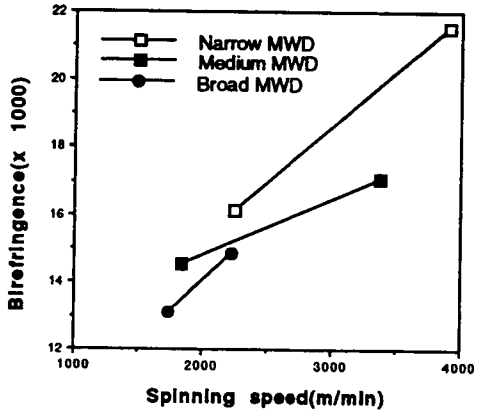
Figure 4.4 Graphical representation of density versus spinning speed of as-spun fibers.



(a) 16-18 MFR samples.



(b) 35-42 MFR samples.



(c) 74-78 MFR samples.

Figure 4.5 Graphical representation of birefringence versus spinning speed of as-spun fibers.

strength where the birefringence of the as-spun filaments is concerned, i.e., the narrow MWD samples have the highest birefringence whereas the broad MWD samples in the same range of MFR have the lowest birefringence. As seen from Fig. 4.5, the birefringence of the as-spun filaments increases with spinning speed. X-ray patterns of the as-spun filaments indicated that the structure of the filaments was largely monoclinic, but for the narrow MWD samples it became somewhat more smectic in nature as the MFR increased. Broadening of the MWD tended to shift the structure back towards the monoclinic α form even at the highest MFR.

4.3 On-line Profiles During Melt Spinning:

The on-line diameter profiles for the samples in the same range of melt flow rate for melt spinning with 5 psi(g) air pressure in the suction venturi are given in Figures 4.6 to 4.8. A comparison of the diameter profiles of the 35 MFR narrow MWD sample spun under 5 psi(g) and 25 psi(g) air pressure in the suction venturi is presented in Figure 4.9. The nature of the on-line temperature profiles of different polypropylene samples in the same range of melt flow rate are illustrated in Figure 4.10 where the temperature profiles of the three different samples in the MFR range of 74-78 for 5 psi(g) air pressure in the suction venturi are given. The on-line birefringence profiles are shown in Figures 4.11-4.13. Figure 4.14 gives a direct comparison of the development of birefringence along the spinline for the six samples in the MFR ranges of 35-42 and 74-78. The birefringence profiles of the samples for the higher spinning speeds are given in Figures 4.15-4.17.

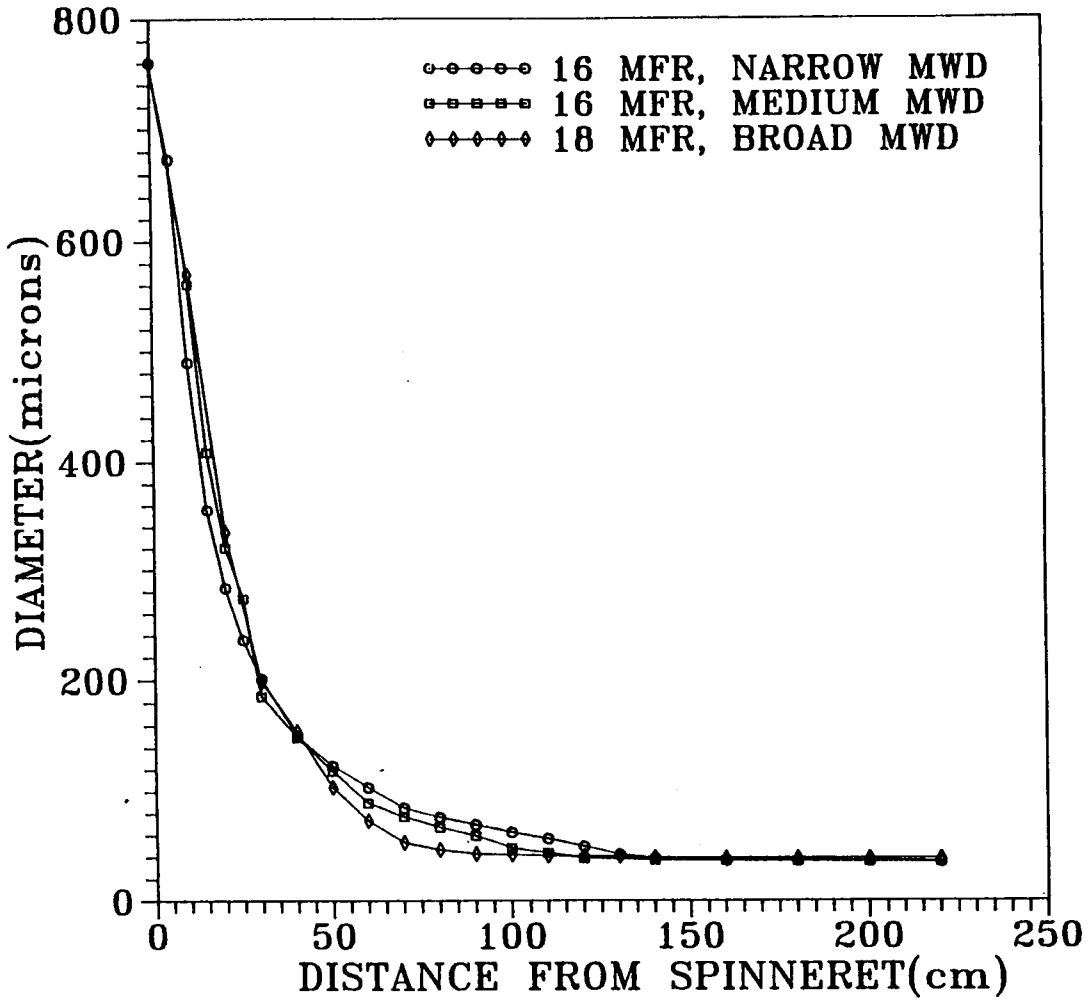


Figure 4.6 On-line diameter profiles for the 16-18 MFR resins spun under low air pressure of 5 psi(g).

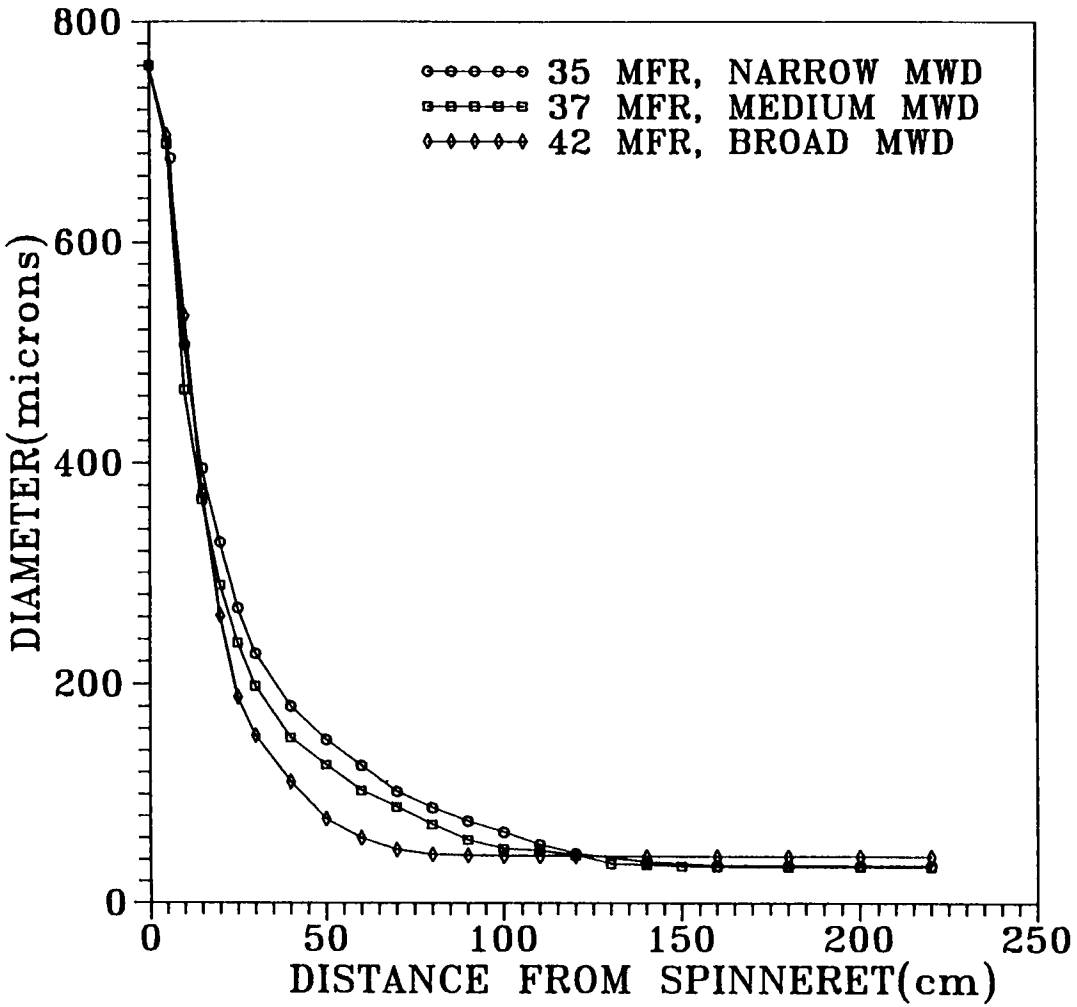


Figure 4.7 On-line diameter profiles for the 35-42 MFR resins spun under low air pressure of 5 psi(g).

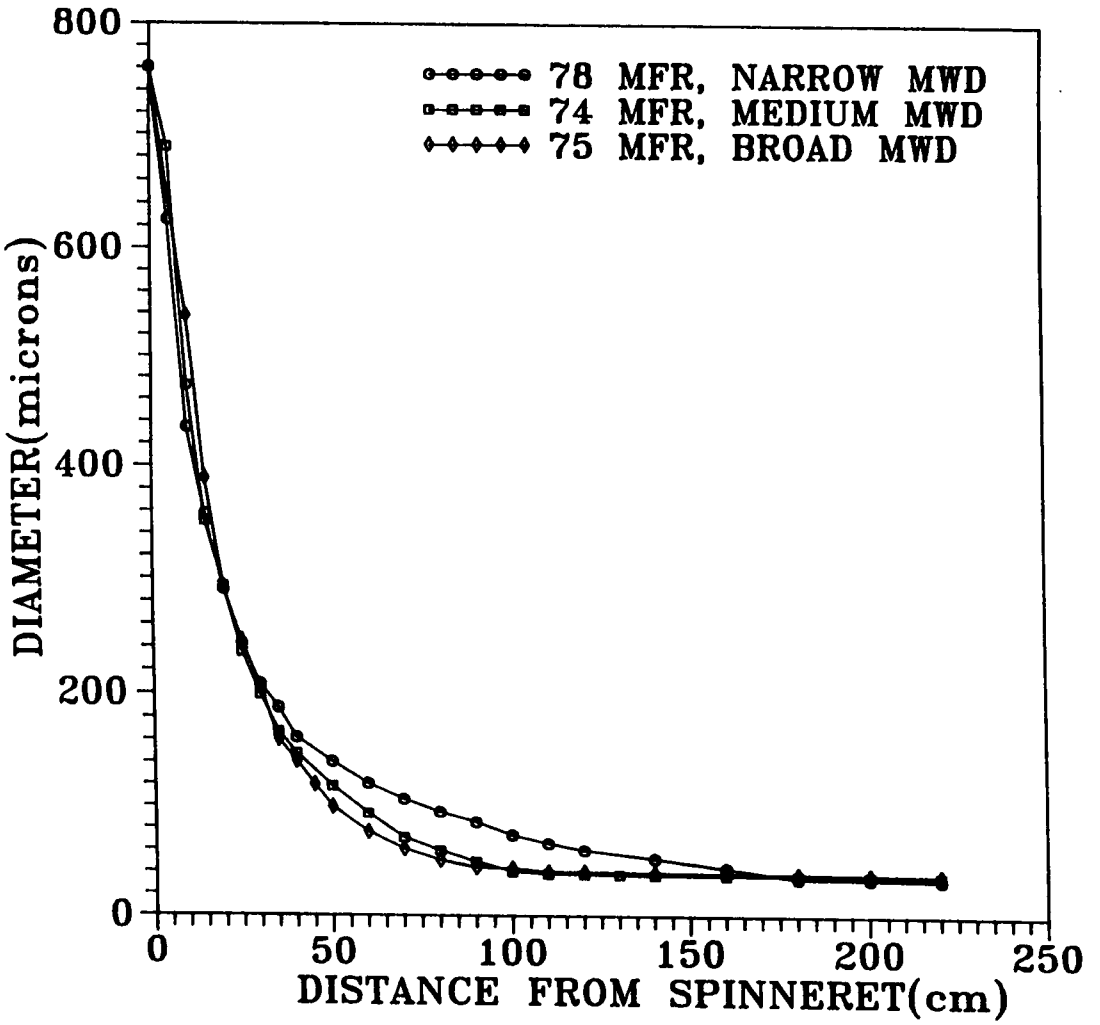


Figure 4.8 On-line diameter profiles for the 74-78 MFR resins spun under low air pressure of 5 psi(g).

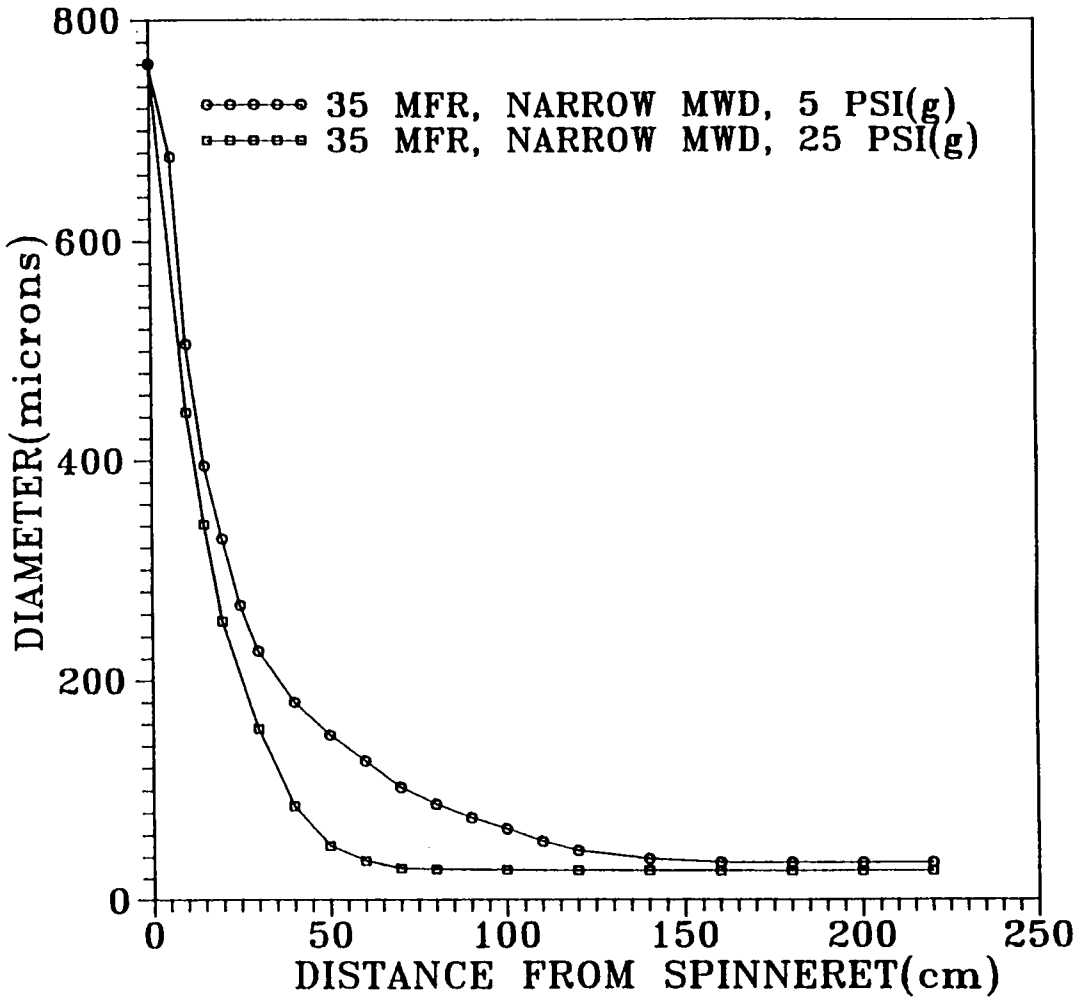


Figure 4.9 Comparison of on-line diameter profiles spun under different air pressures.

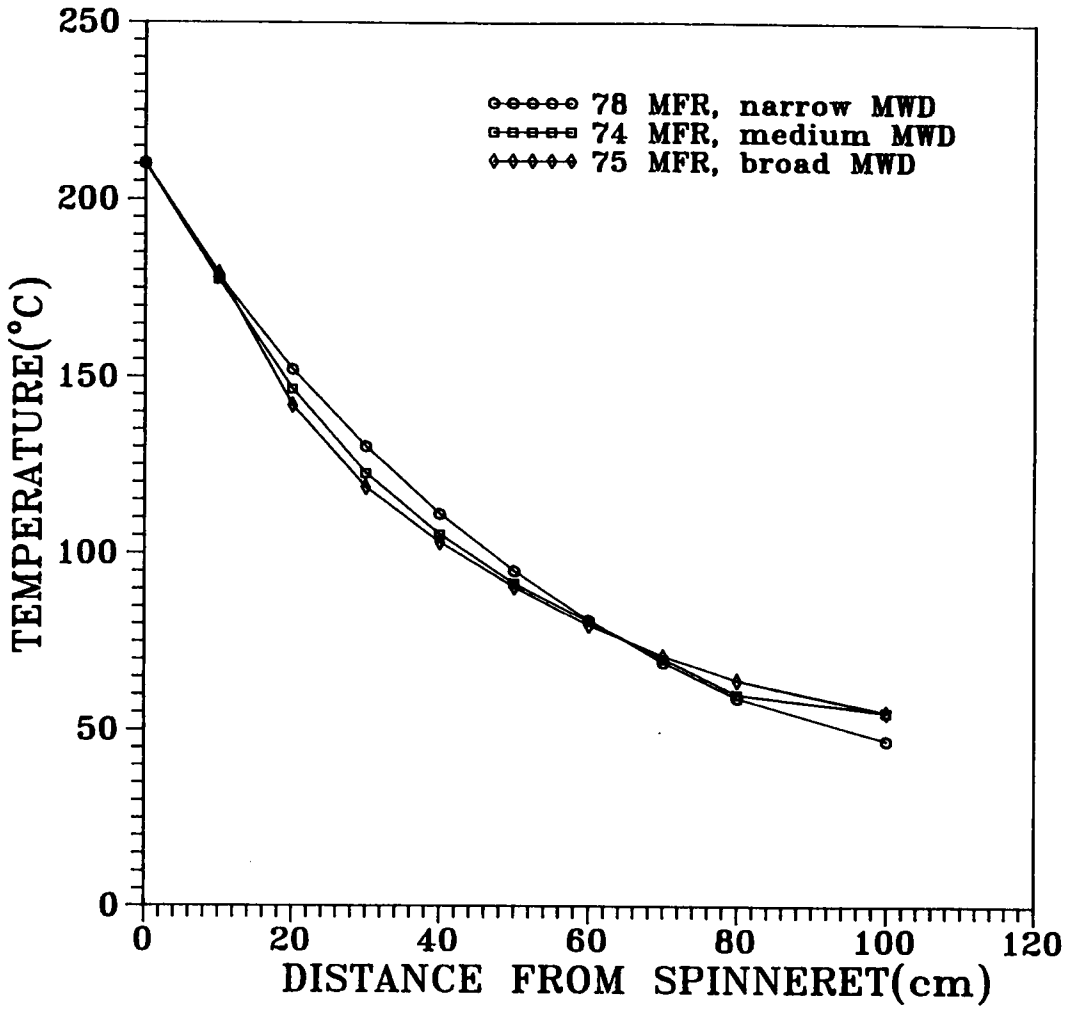


Figure 4.10 Comparison of the temperature profiles of the resins of the 74-78MFR range at 5 psi(g) air pressure.

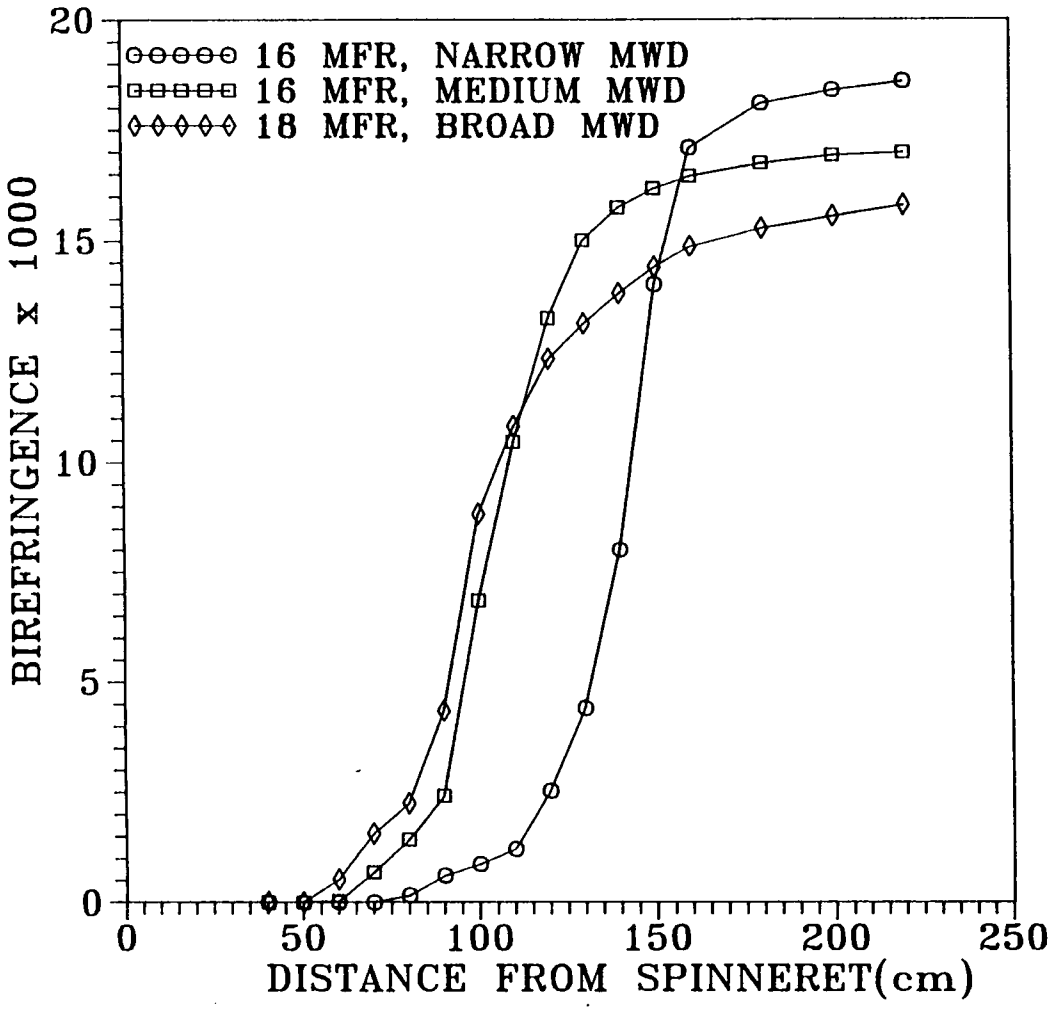


Figure 4.11 On-line birefringence profiles for the 16-18 MFR resins spun under low air pressure of 5 psi(g).

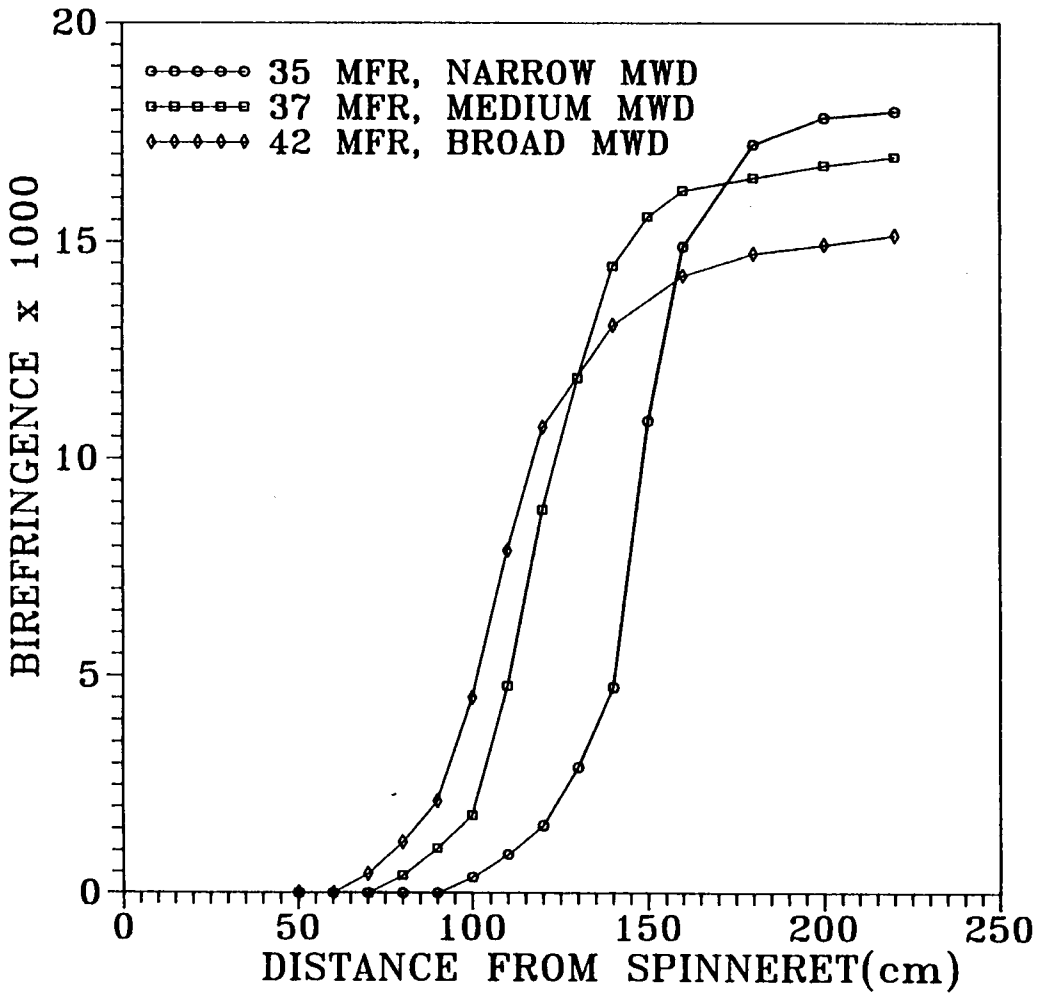


Figure 4.12 On-line birefringence profiles for the 35-42 MFR resins spun under low air pressure of 5 psi(g).

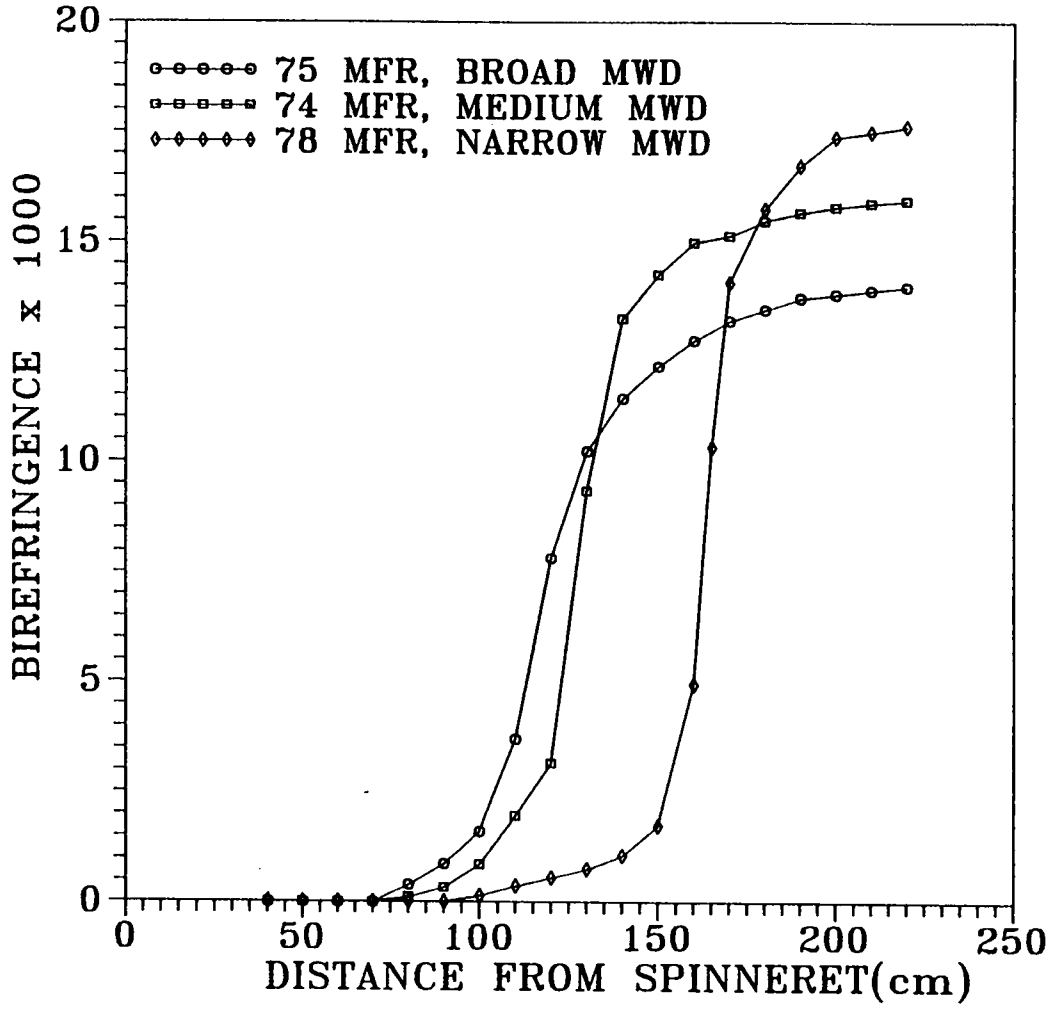


Figure 4.13 On-line birefringence profiles for the 74-78 MFR resins spun under low air pressure of 5 psi(g).

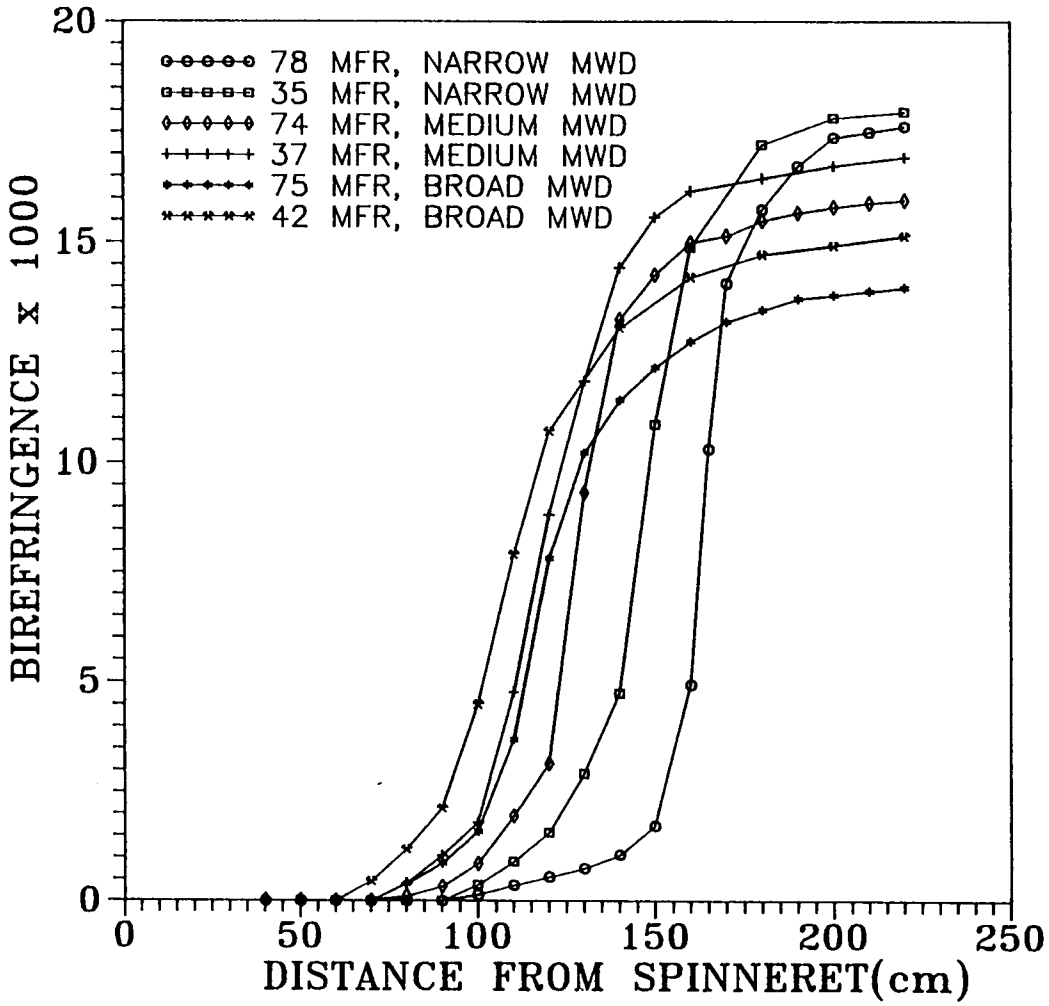


Figure 4.14 Comparison of on-line birefringence profiles of the resins of 35-42 MFR and 74-78 MFR.

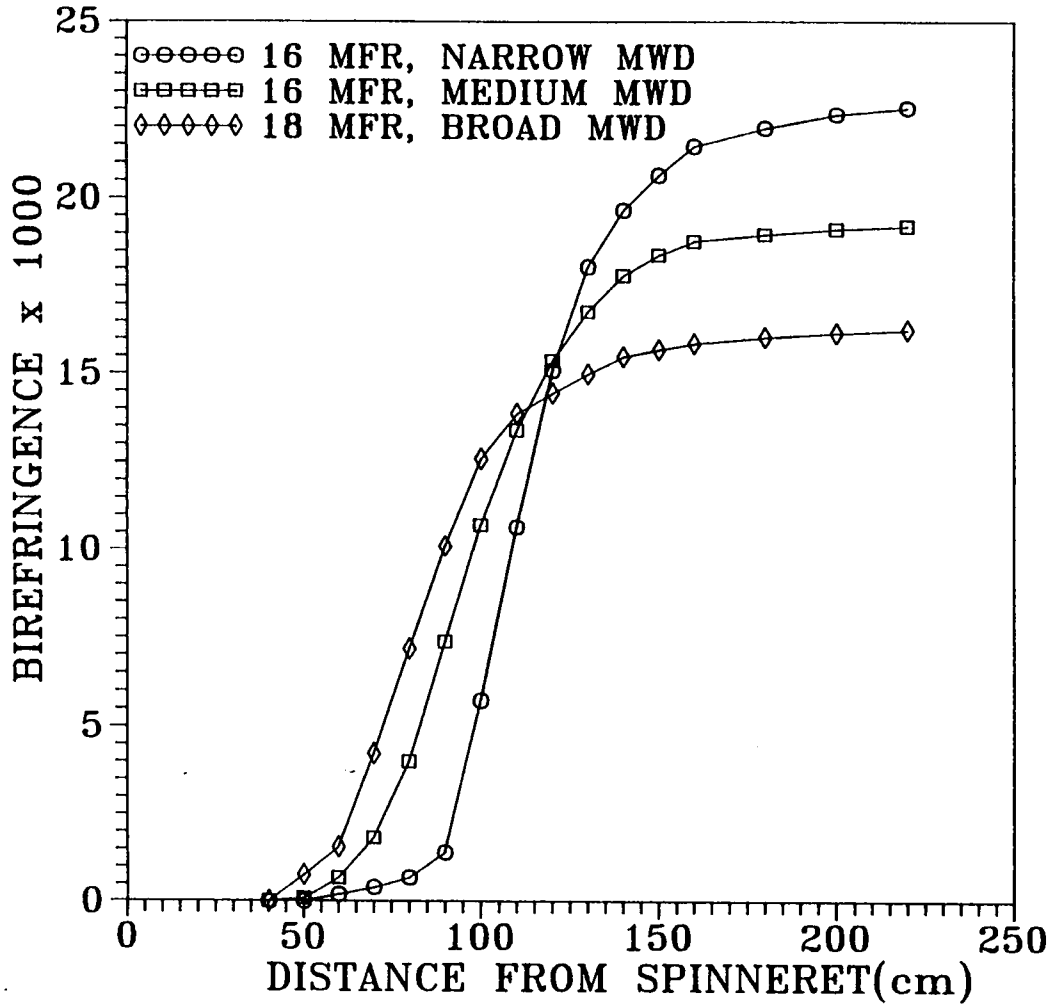


Figure 4.15 On-line birefringence profiles for the 16-18 MFR resins spun under high air pressure(the values of different air pressure are given in Table 4.3).

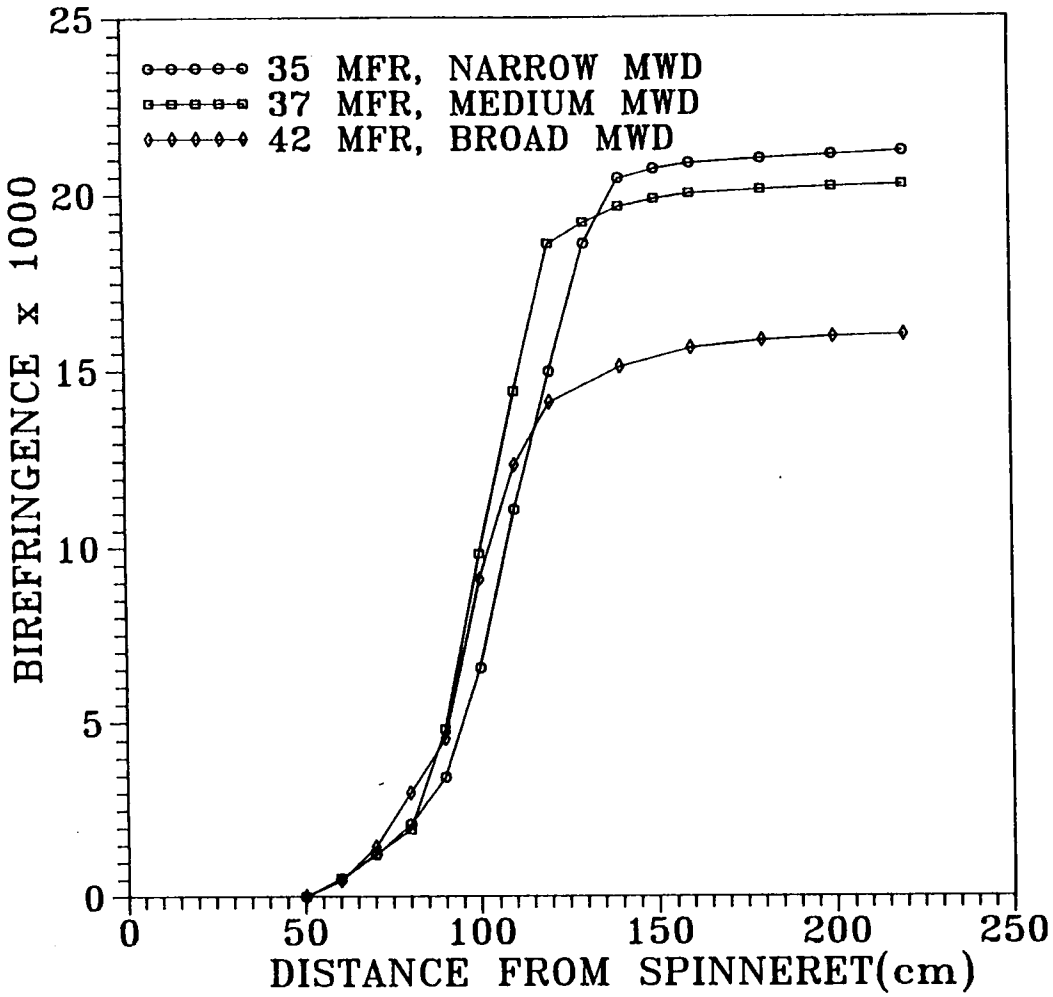


Figure 4.16 On-line birefringence profiles for the 35-42 MFR resins spun under high air pressure(the values of different air pressure are given in Table 4.3).

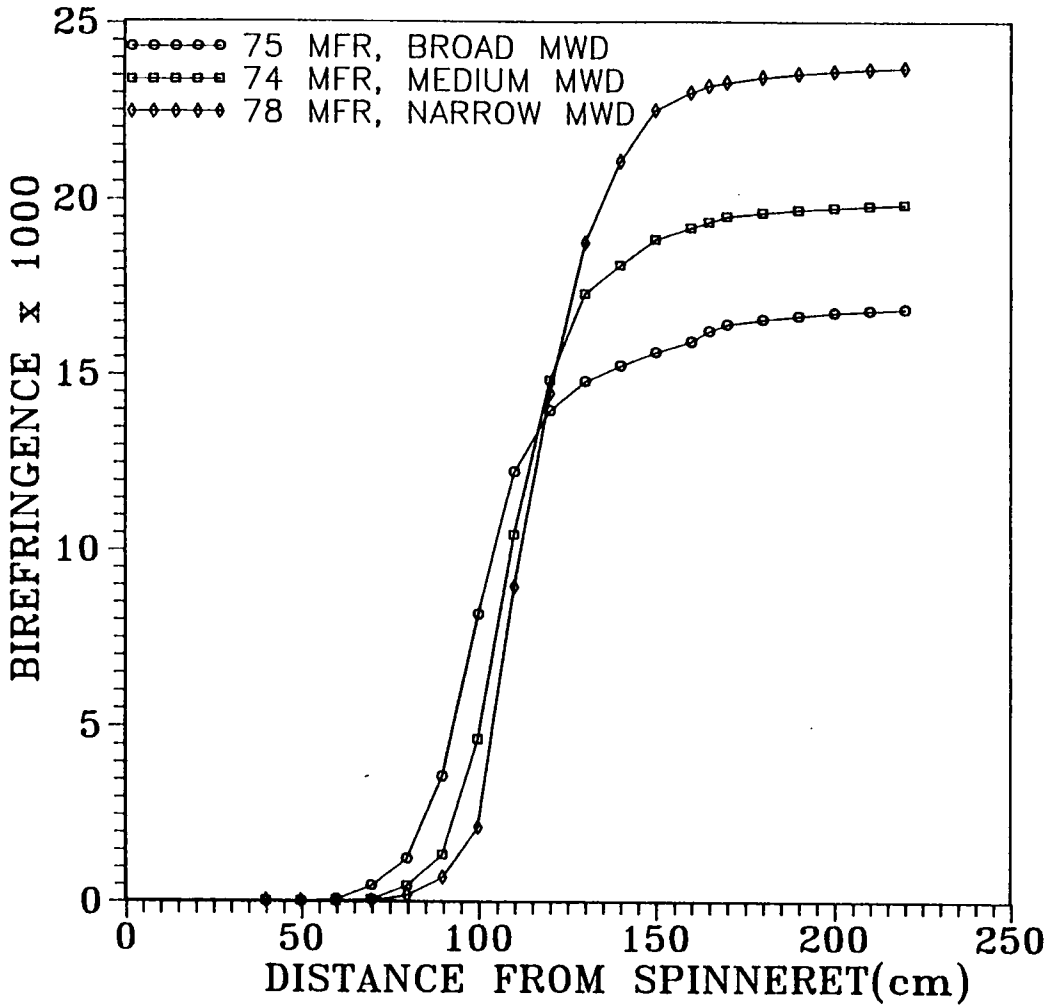


Figure 4.17 On-line birefringence profiles for the 74-78 MFR resins spun under high air pressure(the values of different air pressure are given in Table 4.3).

As seen from Figures 4.6 to 4.8, the diameter profile changes with variation in molecular weight distribution in each MFR range. The filament draws down faster with broadening of molecular weight distribution in each MFR range. In general, the filament draws down rapidly in the region of few centimeters below the spinneret which is true for all the three samples of varying MWD in the same MFR range. However, the molecular weight distribution seems to have a distinct effect on fiber drawdown as the filament moves farther from the spinneret. The broad MWD sample approaches its final diameter closer to the spinneret than the narrow MWD sample. The medium MWD sample draws down in between the broad and narrow MWD samples, Figures 4.6 to 4.8. As the spinning speed increases, the filament draws closer to the spinneret because of higher stress on the fiber which causes higher drawdown in the section of the spinline where the filament is hot and the local viscosity is lower. An example is presented in Figure 4.9 where the diameter profiles of the 35 MFR narrow MWD sample at 5 psi(g) and 25 psi(g) air pressure are compared. At 25 psi(g) the fiber approaches its final diameter at a distance of 70 centimeters from the spinneret whereas at 5 psi(g) it reaches its final diameter at 140 cm from the spinneret. A comparison of the diameter profiles of the narrow MWD samples from Figures 4.6 to 4.8 shows that the filament approaches its final diameter closer to the spinneret as the resin viscosity increases or the melt flow rate decreases. For example, the 16 MFR and 78 MFR narrow MWD samples approach their final diameters at distances 130 and 170 cm from the spinneret respectively, Figures 4.6 and 4.8. Note that the 16 MFR narrow MWD sample was spun at 240 °C. The difference in the distances at which the 16 MFR and 78 MFR narrow MWD samples would approach their respective final diameters would be greater if the 16 MFR narrow MWD sample was spun at 210 °C. The 35 MFR narrow MWD sample approaches its final diameter at a distance in between the above two values., viz. at 140 cm from the

spinneret. This observation is consistent with earlier results of Lu and Spruiell(124). The temperature profiles of the three different samples in the MFR range of 74-78, Figure 4.10, show that the more rapid drawdown of the broad MWD sample in the upper part of the spinline results in a slightly faster cooling of the broad MWD sample, compared to the narrow MWD sample. In the lower part of the spinline (below about 70 cm from the spinneret) there is a crossover of the cooling curves. The on-line birefringence profiles in Figures 4.11 to 4.13 show that the broad MWD samples tend to have lower final birefringence than the narrow MWD samples of the same range of MFR in agreement with the trends observed in as-spun samples. The medium MWD samples tend to have a final birefringence in between that of the narrow and the broad MWD samples of the same range of MFR.

As seen in the figures 4.11-4.13, the birefringence picks up closest to the spinneret for the broad MWD sample and farthest form the spinneret for the narrow MWD sample. For the medium MWD sample, the birefringence develops at a distance from the spinneret which is in between that for the narrow and the broad MWD samples. However, once the birefringence starts to increase rapidly, it develops faster for the narrow MWD samples and reaches a higher value than for the broad MWD samples. A common feature in all the three Figures 4.11-4.13 is the comparative shape of the curves. As shown in Fig. 4.11, birefringence development of the 18 MFR broad MWD sample starts at a distance of 50 cm below the spinneret and rises gradually over the next 130 centimeters along the spinline, that of the 16 MFR medium MWD sample starts at 60 cm from the spinneret and develops more rapidly and goes to a final higher value than the broad MWD sample. The birefringence curve of the 16 MFR narrow MWD sample starts to develop at 70 cm below the spinneret and rises rapidly in the range of 110 to 150 cm from the spinneret with a final value higher than both the medium and the broad

MWD samples. Similar trends are observed for samples in the range of 35-42 MFR and 74-78 MFR, Figures 4.12 and 4.13. A direct comparison of the birefringence profiles of all the nine samples is not possible because they were spun at different extrusion temperatures for reasons already mentioned earlier in this chapter. However, a comparison of the profiles of the six samples in the 35-42 MFR and 74-78 MFR ranges is presented in Figure 4.14, since all these samples were spun at 210 °C. Compare the following samples. 35 MFR narrow MWD to 78 MFR narrow MWD, 37 MFR medium MWD to 75 MFR medium MWD and 42 MFR broad MWD to 75 MFR broad MWD. It can be seen that birefringence develops closer to the spinneret with decreased melt flow rate (or increased viscosity) for samples of similar MWD. Also note that the birefringence curves of the medium and broad MWD samples in the 74-78 MFR range rise closer to the spinneret than the 35 MFR narrow MWD sample in spite of the lower MFR of the latter resin. The detailed discussion and implications of all the profiles as well as the off-line data is given in the following section.

4.4 Analysis and Discussion of Role of Molecular Weight and its Distribution in the Melt Spinning of Polypropylene:

From the characteristics of the as-spun filaments as shown in Tables 4.4-4.7 and Figures 4.4 and 4.5 the following can be inferred: A lower birefringence in spite of the higher crystallinity in the filaments spun from the broad MWD samples in each MFR range suggests that the broad MWD samples have lower average amorphous orientation in the fiber than the medium and narrow MWD samples. This can be further qualified by the data on tensile strength and elongation to break. The higher tensile strength of the narrow MWD suggest that the narrow MWD samples have higher amorphous

orientation. Previous research has shown that the tensile strength of polypropylene fibers is related to the amorphous orientation in the fibers and that an increase in the amorphous orientation increases the tensile strength(125). A higher amorphous orientation in the narrow MWD samples than the medium and broad MWD samples in the same range of MFR can also be seen from the data on the fiber elongation before breaking. The highest elongations in case of the broad MWD samples suggest that the polymer chains in the as-spun filaments from the broad MWD samples are not as much oriented as the chains in the narrow MWD samples and hence they can be extended more before breaking. The medium MWD sample shows a percentage elongation to break that is intermediate between the narrow and broad MWD samples in the same MFR range. Similarly the tensile strength of the medium MWD samples lie in between that of the narrow and broad MWD samples of the same MFR range, Table 4.6. This indicates that, with broadening of molecular weight distribution, the amorphous orientation in the fiber decreases for the same range of spinning speed.

Two factors primarily affect the fiber drawdown during melt spinning of semicrystalline polymers. They are: i) rheological effects and ii) crystallization effects. One aspect of the rheological effect on fiber drawdown during melt spinning of polymers is well understood. For a given overall drawdown ratio, a higher viscosity polymer draws down closer to the spinneret where the molten polymer is hotter and hence the local viscosity is lower. A comparison of the shear viscosities for the polypropylene samples in each MFR range (Figures 3.1-3.3, Chapter-3) indicates that the broad MWD samples have the highest zero shear viscosity but are more shear thinning in nature than the medium and narrow MWD samples in the same MFR range. The narrow MWD samples show the lowest zero shear viscosity but also have the least shear thinning nature. The medium MWD samples lie in between the broad and the narrow MWD

samples . The difference in the dynamic viscosity in the low frequency range with broadening of molecular weight distribution may partially explain the variation in the diameter profiles of the various samples in the same MFR range but with different MWD. The rheological property of the polymer changes as the volume element moves away from the spinneret because of the change in temperature of the polymer. Also the elongation rate first increases and then decreases. Polypropylenes are elongation-thinning polymers. Therefore, the elongation-thinning behavior can be expected to be different for the samples with different MWD even if they are in the same range of MFR as shown by their shear-thinning behavior in Figures 3.1-3.3 of Chapter-3. However, it is difficult to ascertain the magnitude and importance of these effects. The rheological effect is superimposed by the crystallization effect in the spinline. Onset of crystallization increases the local viscosity of the polymer and causes the fiber to draw down closer to the spinneret. Hence the effect of lower viscosity may be off-set by crystallization of the polymer earlier in the spinline. An interesting comparison is the relative behavior of the diameter profiles of the 35 MFR narrow MWD sample and the broad and medium MWD samples in the MFR range of 74-78. When spun under 5 psi(g) air pressure in the suction venturi and in the same range of spinning speed (see Table 4.2), both the 75 MFR broad MWD sample and the 74 MFR medium MWD sample draw down faster and approach their final diameter at a distance of 100 cm from the spinneret whereas the 35 MFR narrow MWD sample approaches its final diameter at a distance of 140 cm from the spinneret, compare the respective diameter profiles from the Figures 4.7 and 4.8. A comparison of the dynamic viscosities of these samples from Figures 3.2 and 3.3 of Chapter-3 shows that the 35 MFR narrow MWD sample has a higher dynamic viscosity than both the 75 MFR broad MWD and the 74 MFR narrow MWD samples in the experimental range of angular frequency. Therefore, a faster

drawdown of the latter samples can be attributed to the crystallization effect which overrides the rheological effect during fiber spinning.

The above experimental observations indicate a complicated effect of molecular weight distribution on the filament drawdown and structure development of polypropylene resins. The results for samples of different MFRs but similar MWDs are consistent with the fact that as the viscosity increases the diameter draws down closer to the spinneret where the local viscosity is lower and that more force is required for a higher viscosity resin at the bottom of the spinline to attain the same spinning speed as that of a lower viscosity resin. Hence the stress on the fiber rises faster along the spinline for the higher viscosity resin. This causes development of molecular orientation on the fiber closer to the spinneret inducing "molecular orientation-enhanced" crystallization (also known as "stress-induced" crystallization). Thus, the birefringence rises earlier along the spinline with increased viscosity. This effect was experimentally verified by Lu and Spruiell(121). They compared the birefringence profiles of polypropylene samples, with melt flow rates of 35 and 300 but similar polydispersity, spun in the same range of spinning speed. They found out that the fiber spun from the 35 MFR resin developed birefringence earlier along the spinline than the fiber spun from the 300 MFR sample, Figure 7, Reference 121. The present data show that the same effect is also observed with broadening of molecular weight distribution of samples in the same MFR range. A possible explanation is that, at any point along the spinline, the molecular orientation of broad MWD sample is less uniform than that of a narrow MWD sample for the same level of stress and temperature, i.e.; there is a variation in molecular orientation with the size of the polymer chain. A resin with a broad MWD has a larger fraction of molecules with chain lengths different from the average value compared to that of a narrow MWD sample with similar MFR. Complete information on molecular

weights and their distribution based on Gel Permeation Chromatography(GPC) for all the experimental samples is not available at present. However, the available data on five of the nine samples was presented in Chapter-3. The 18 MFR broad MWD and 75 MFR broad MWD samples have z-average molecular weights(M_z) in the range of 2.5 times the M_z of the 16 MFR narrow MWD and 78 MFR narrow MWD samples, respectively, even if the samples in the same MFR range have similar number average molecular weight(M_n), see Table 3.1 of Chapter-3. This indicates that these two broad MWD samples have a larger fraction of molecules with chain length different from the average chain length compared to the respective narrow MWD samples. The ideal assumption in fiber spinning regarding molecular orientation is that all the polymer chains undergo elongational deformation to the same extent and hence have the same molecular orientation at same temperature and level of stress. However, from a realistic point of view, it can be expected that different chains undergo different elongational deformation which depends on the entanglement of the molecules in the melt. It is known that two resins of similar polydispersity but different melt flow rate (i.e.; different number average molecular weights and hence chain lengths) show different orientation and crystallinity for the same spinning speed. If a resin contains an appreciable fraction of long chains in addition to the short chains thereby showing a higher value of M_z and M_{z+1} then the long molecules will tend to orient more than the shorter molecules due to larger entanglement for the same spinning speed. The entanglement and orientation of the long chain molecules leads to the formation of "row nuclei" as first discussed by Hill and Keller(126,127). This nucleates crystallization causing it to occur closer to the spinneret for the broad MWD sample than for a narrow MWD sample with similar MFR.

It is observed that the medium and broad MWD samples in the 74-78 MFR range develop birefringence earlier along the spinline than the 35 MFR narrow MWD sample

even if all three are spun in the same range of spinning speed(see Table 4.2), Fig. 4.14. This can be explained by assuming that both the medium and broad MWD samples in 74-78 MFR range contain a fraction of polymer molecules that have a higher chain length than the average molecule in the 35 MFR narrow MWD sample. Consequently that fraction of polymer molecules of the medium and broad MWD samples in 74-78 MFR range are more susceptible to forming "row nuclei" than the average molecule in the 35 MFR narrow MWD sample at any point along the spinline for the same spinning speed due to higher entanglement of the large molecules which leads to greater elongation of those molecules and "row nucleation", thus causing the onset of crystallization. This causes the fibers spun from the medium and broad MWD samples in 74-78 MFR range to develop birefringence earlier along the spinline than the fiber spun from the 35 MFR narrow MWD sample. This argument can be further supported by comparing the GPC data of the 75 MFR broad MWD resin with the 35 MFR narrow MWD resin given in Table 3.1 of Chapter 3. For a direct comparison the data are presented again; the 75 MFR broad MWD resin has the following values: M_n=36,669; M_w=138,818; M_z=448,647 and M_{z+1}=1,110,544. The 35 MFR narrow MWD resin has the following corresponding values: M_n=42,097; M_w=147,050; M_z=270,373 and M_{z+1}=367,625. In spite of the larger M_z and M_{z+1} values, the 75 MFR broad MWD resin has a lower viscosity as indicated by its melt flow rate and the dynamic viscosity curve than the 35 MFR narrow MWD resin (see Figures 3.2 and 3.3 of Chapter-3). Hence it can be expected that the 75 MFR broad MWD resin contains a fraction of appreciably long polymer chains that cause it to have higher M_z and M_{z+1} values than the 35 MFR narrow MWD resin. Thus, these longer polymer chains get more oriented for the same spinning speed and cause onset of crystallization earlier along the spinline, Fig. 4.14. A comparison of the temperature profiles of the three different samples in the MFR range of

74-78 indicated that the broader MWD sample cools slightly faster in the upper part of the spinline due to the faster filament drawdown. However, there is a cross-over at about 70 cm from the spinneret. This cross-over and the slow-down in the cooling rate of the broad MWD sample compared to the narrow MWD sample supports the idea that crystallization occurs nearer the spinneret for the broad MWD sample, the slow-down in cooling rate resulting from the release of the heat of crystallization at an earlier point in the spinline for the broad MWD sample. This further implies that the onset of crystallization in the case of the broad MWD sample means crystallization at a higher temperature (or lower supercooling). Greater entanglements of the long chain molecules in the broad MWD samples may depress the crystallinity level that is developed, but higher crystallization temperature leads to higher crystallinity , probably as a result of more α-form in the broad MWD samples and more smectic form in the narrow MWD samples. This interpretation is in agreement with the higher as-spun densities of the broad MWD samples compared to the narrow MWD samples. Also the rate of crystal growth in case of the broad MWD sample may be lower than that in the narrow MWD sample because of higher temperature of crystallization for the broad MWD sample. This can explain why the birefringence curve of the broad MWD sample starts to rise earlier along the spinline but rises at a lower rate than the birefringence curve of the narrow MWD sample of the same range of MFR.

The entire argument presented above revolves around the assumption that chains of different size experience different ability to nucleate crystallization within the same melt. This is a logical extension of the fact that, while spinning two resins of different viscosity at the same speed, higher force or stress is needed to spin the resin of higher viscosity (and hence, longer average polymer chain if both the resins have similar MWD), thus giving rise to different orientation of the polymer chains and hence different

"stress-induced crystallization" effects. This uneven orientation of the polymer chains in the broad MWD samples may be the cause of lower spinnability of the broad MWD samples of the present research. During fiber spinning, elongation of the chains and chain slipping to some extent occur simultaneously. During chain slipping, the longer polymer chains can be expected to experience more shear force due to chain slipping than the shorter chains. This argument is analogous to the load transfer to the fibers in a "fiber reinforced composite" subjected to deformation. In a fiber reinforced composite (where the fibers are aligned in the direction of applied force) subjected to extentional deformation, the force is transferred from the matrix to the fibers through shear stress in the fiber-matrix interface. But the transfer of load depends on the length of the fibers in the matrix, and, below a critical length which depends on the modulus of elasticity of the fibers, the load cannot be supported to extent of maximum value. If the same logic is qualitatively applied to the polymer chains for chain slipping, the longer chains can be expected to support more shear force than the short chains during chain slipping. In effect, a higher shear force may cause the longer chains to orient more than the shorter chains giving rise to onset of crystallization earlier in the spinline. The higher shear force on the long polymer chains may also rupture those chains and eventually lead to a break of the filament.

The effect of molecular weight distribution on structure development becomes less pronounced as the spinning speed increases. The birefringence profiles for melt spinning using higher air pressure in the suction venturi are shown in Figures 4.15-4.17. As the spinning speed increases the birefringence curve for all the samples start to rise closer to the spinneret. At 25 psi(g) air pressure, the 16 MFR narrow and medium MWD samples start birefringence development at 50 cm from the spinneret and the birefringence curves rise in the range of 90 to 120 cm and 60 to 140 cm from the

spinneret for the narrow MWD and medium MWD samples, respectively. The birefringence of the 18 MFR broad MWD sample starts to develop at 40 cm from the spinneret and rises over a range of 40 to 150 cm from the spinneret, Fig. 4.15. Similar trends are observed for the other samples. However, the effect of spinning speed is more pronounced on the narrow MWD samples than the broad and the medium MWD samples of the same MFR range. For example as the spinning speed of the 16 MFR narrow MWD sample increases from 1917 m/min. to 3347 m/min., the development of birefringence shifts by a distance of 30 cm along the spinline whereas for the 16 MFR medium MWD sample, as the spinning speed increases from 1736 m/min. to 3226 m/min., the birefringence curves shifts by a distance of only 10 cm along the spinline, compare the Figures 4.11 and 4.15. Similarly, as the spinning speed of the 78 MFR narrow MWD sample increases from 2245 m/min. to 3902 m/min., its birefringence curve shifts by 50 cm along the spinline whereas the birefringence curve of the 74 MFR medium MWD sample shifts by only 20 cm along the spinline for an increase in spinning speed from 1843 m/min. to 3376 m/min., compare Figures 4.13 and 4.17. The broad MWD samples are not taken for direct comparison because of their considerably different spinning speeds. Similar to the lower spinning speeds, the final birefringence values appear to decrease with broadening of molecular weight distribution.

4.5 Application of 'Inversion Procedure' for Measurement of Apparent Elongational Viscosity:

As mentioned in Chapter 2, the "Inversion Procedure" can be employed to compute the apparent elongational viscosity of any polymer at any range of spinning speed. The inputs to the inversion procedure are the experimental diameter and

temperature profiles and the tension at the bottom of the spinline. A force balance along the spinline is used with the tension at the bottom of the spinline as a boundary condition to obtain the stress at any point on the spinline. The stress, when divided by the rate of elongation, gives the apparent elongational viscosity. Since the boundary condition influences the rheological force in the fiber for all the points, an accurate measurement of the tension at the bottom of the spinline is necessary for correct results.

Tension measurement at the bottom of the spinline:

It was pointed out in Chapter 2 that measurement of tension at the bottom of a running spinline is difficult because the fiber often sticks to the measuring head and breaks. For this reason an off-line tension measurement technique has been established(123). In this method, filaments of different diameters are inserted in sufficient length into the suction venturi to which air is supplied at various pressures. Sufficient length of the filaments inside the suction venturi is necessary so that the fibers inserted experience a drag force over the length which is the same as that of a running fiber. The force on the fiber is then measured on the tensiometer. A plot showing the force on stationary fibers of different diameters for various air pressures in the suction venturi is given in Figure 4.18.

However, it must be noted that the force measured using the above technique is the force when the filament is stationary and the drag force is due to the absolute velocity of air in the suction venturi. During actual experimentation, the drag force on the fiber is due to the velocity of air relative to the velocity of the fiber. The velocity of the running filament can be calculated from the mass flow rate of the polymer using the continuity equation. The spinning speeds are mentioned in Tables 4.2 and 4.3 for the low and high air pressures respectively. A theoretical prediction of the air velocity is possible provided

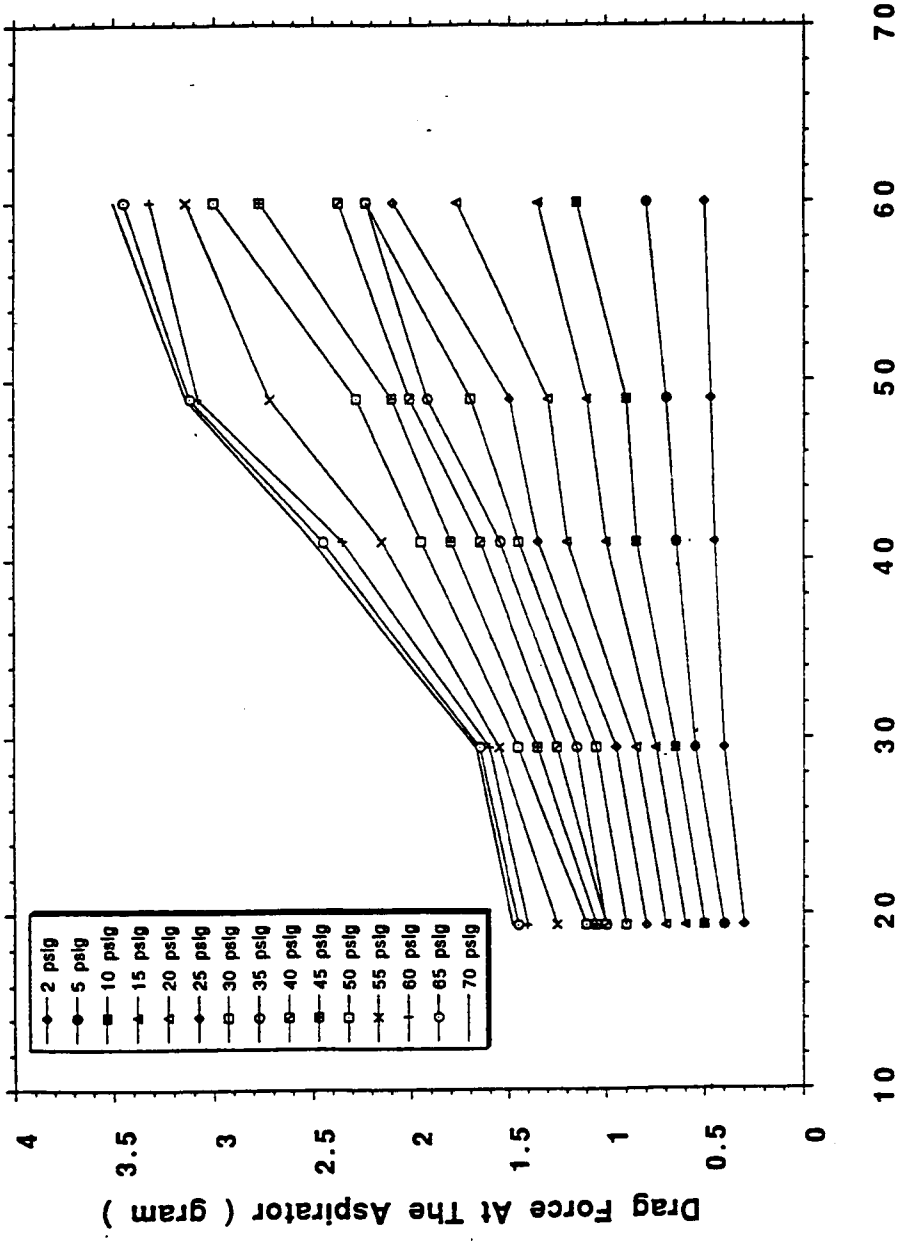


Figure 4.18 Drag force versus fiber diameter for different air pressures in the suction venturi.

accurate geometrical configuration of the suction venturi and the surroundings to which the air is released from the venturi is known. Theoretical prediction also requires the temperature data of the inlet and outgoing air streams. A simpler and practical method would be to find out the velocity of air using the Bernoulli's equation:

$$P_1 + \rho_1 \frac{V_1^2}{2} + \rho_1 g z_1 = P_2 + \rho_2 \frac{V_2^2}{2} + \rho_2 g z_2 \qquad [4.3.1]$$

where P_1 and P_2 are the pressures at the points of interest, ρ_1 and ρ_2 are the densities of air, V_1 and V_2 are the air velocities, z_1 and z_2 represent the height of the fluid at the points of interest and g is constant of acceleration due to gravity. For the purpose of the present calculations, the potential head can be neglected. Thus, neglecting the compressibility effects of air, the air velocity, V, for any pressure can be given by:

$$V = \sqrt{\frac{2(P - P_{atm})}{\rho_{atm}}} \qquad [4.3.2]$$

where P is the air pressure in the suction venturi and P_{atm} and ρ_{atm} are the atmospheric pressure and density of air at 1 atm. pressure, respectively.

The correction of force for the fiber velocity is done as follows: from the plot of tension in stationary fibers of different diameters for various air pressures generated in our laboratories(128), the tension in a stationary fiber with a diameter of 35 microns at 5 psi(g) supply air pressure is 0.5 gram force or 490 dynes. A fiber of diameter of 35 microns was spun at a speed of 1917 m/min in the present research(Table 4.2). The air velocity at 5 psi(g), calculated by using a pitot tube and applying Bernoulli's equation, is 7639 m/min. Hence, the velocity of air relative to that of the fiber is 5722 m/min which corresponds to an air velocity in the suction venturi when the supply air pressure is 3.75 psi(g). The tension on a fiber of diameter 35 microns at a supply air pressure of 3.75

psi(g) is 0.4 gram force or 392 dynes. In another method of estimation of air velocity, the Bernoulli's equation is directly applied to the pressure of the air coming into the suction venturi, i.e., 5 psi(g), and that of air going out of the venturi (i.e., atmospheric pressure) and the corrected force on the bottom of the spinline also comes out to be approximately 0.4 gram force. Thus there is a difference of 98 dynes between the tension at the bottom of the spinline with and without correction. The correction of tension is very important when the spinning speed is low because the velocity of the fiber cannot be neglected compared to the air velocity. As the supply air pressure increases the effect of this correction becomes less pronounced since the air velocity rises rapidly and the fiber velocity becomes a smaller fraction of the air velocity.

The apparent elongational viscosities of the samples are given in Figures 4.19 to 4.21 where the plots are shown together for the samples of similar polydispersity but different melt flow rates. The log of apparent elongational viscosities are plotted against the reciprocal of the absolute temperature. It can be seen from Figure 4.19 that the narrow MWD samples in each MFR range are fairly linear and hence show approximate "Arrhenius" behavior in the range of conditions examined. As the spinning speed increases, all the three narrow MWD samples show a slight decrease in the respective apparent elongational viscosities. It is difficult to ascertain whether this decrease is due to some kind of elongation thinning behavior of the samples or scatter in the data. An obvious observation from the Fig. 4.19 is that the three narrow MWD samples of different MFRs have apparent elongational viscosities in three distinct regions which seems to qualitatively correlate with the melt flow rates of those samples and difference in viscosity data of Figures 3.1-3.3.

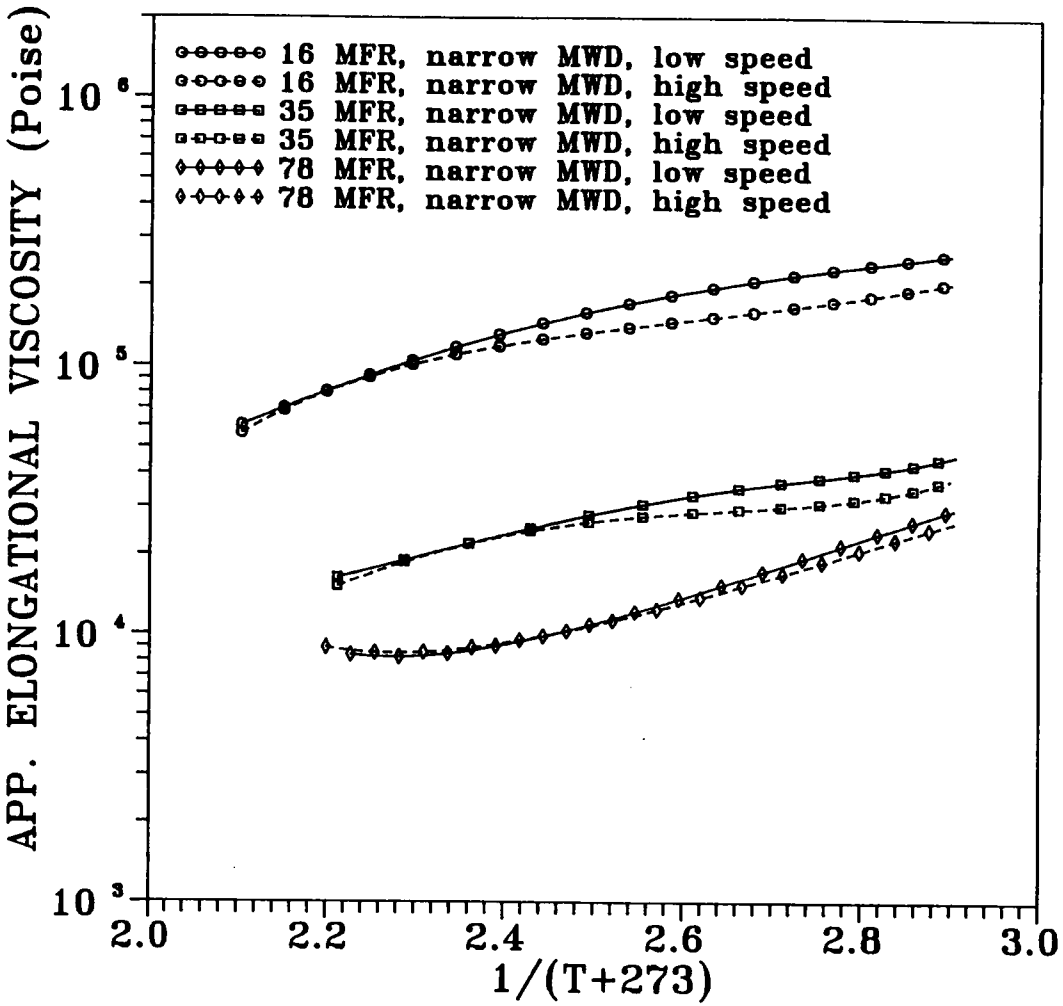


Figure 4.19 Apparent elongational viscosities for the narrow MWD samples.

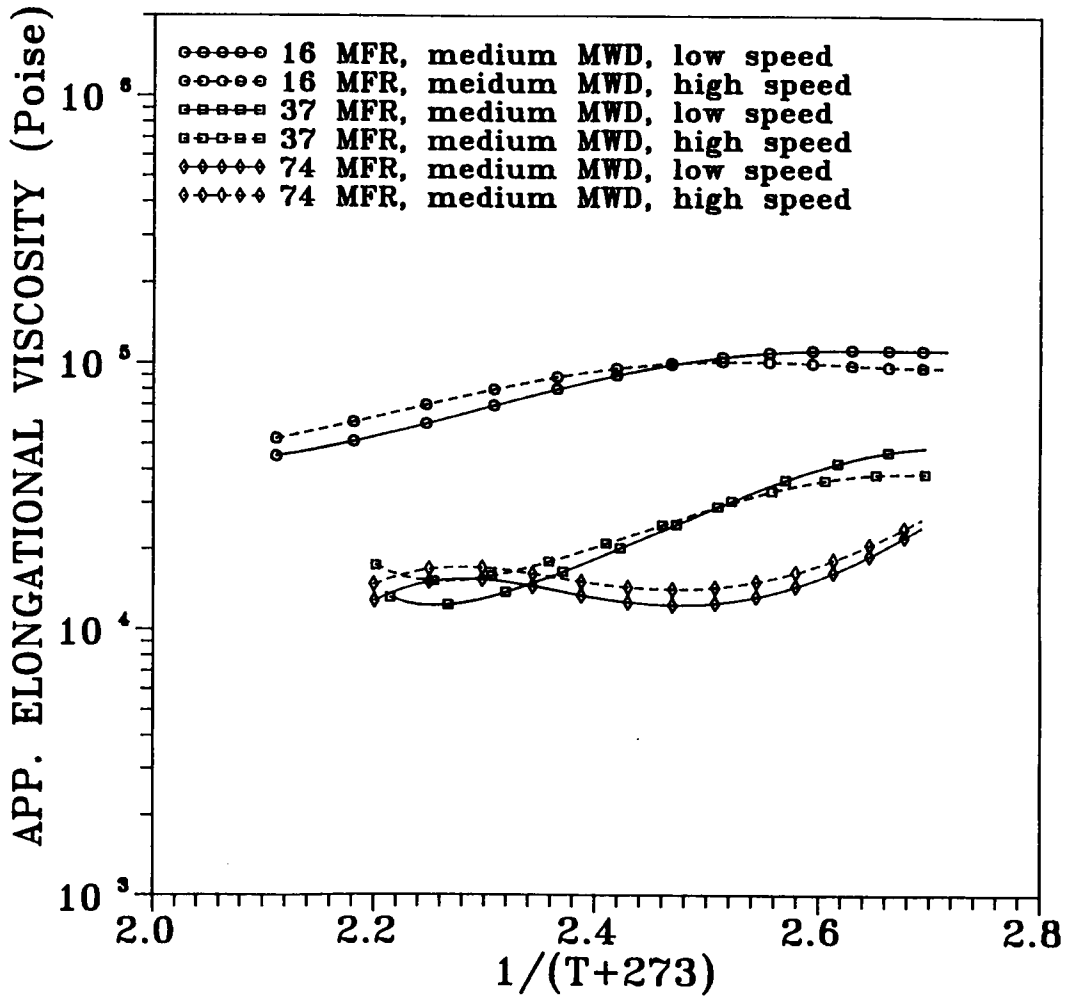


Figure 4.20 Apparent elongational viscosities for the medium MWD samples.

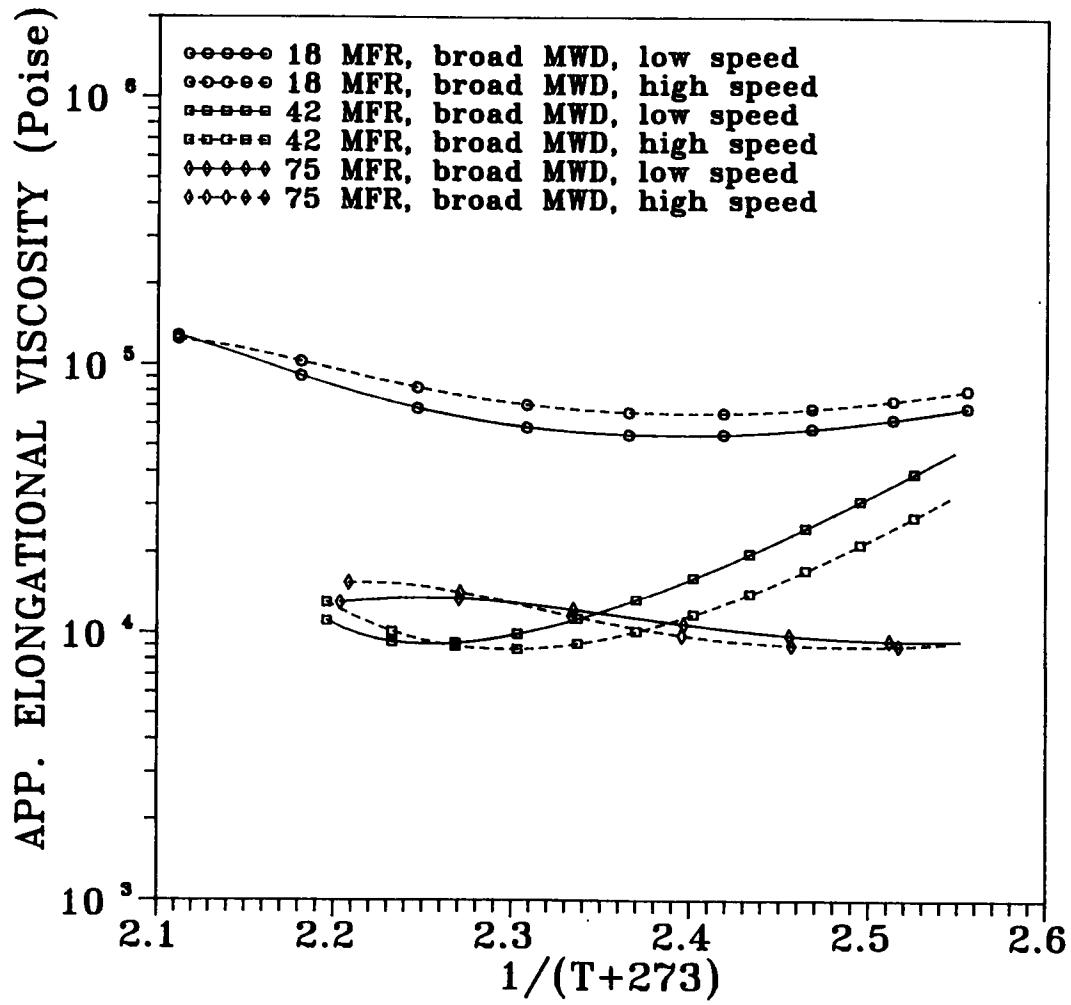


Figure 4.21 Apparent elongational viscosities for the broad MWD samples.

Deviation from the Arrhenius temperature dependence increases with broadening of molecular weight distribution. The apparent elongational viscosities of the medium and broad MWD samples of the various MFR ranges are shown only in the noncrystalline region because crystallization causes the viscosity of the sample to rise rapidly. The 42 MFR broad MWD sample can be analyzed as an example. Figure 4.22 gives the temperature profile of this sample for spinning with 5 psi(g) air pressure in terms of the reciprocal of absolute temperature versus the distance from the spinneret. A value of 1/(T+273) = 2.6 corresponds to a distance of 65 cm from the spinneret. The birefringence profile of this sample in Fig. 4.12 shows that the birefringence curve starts to rise at 60 cm below the spinneret. Thus, onset of crystallization has already taken place at 65 cm from the spinneret{or at 1/(T+273)=2.6}for this sample causing the viscosity to rise rapidly. A comparison of the Figures 4.19 to 4.21 shows that the apparent elongational viscosities of the samples of the same MFR range lie in the same order of magnitude and that the apparent elongational viscosity of each sample follows almost the same pattern within the experimental range of spinning speed indicating that the response of the samples to elongation rate does not change appreciably during the range of spinning speed of the present research. The general trend of the narrow MWD samples is a rise in the apparent elongational viscosity with decrease in temperature(or increase in the reciprocal of the absolute temperature of the filament), Figure 4.19. However, the broad MWD samples first show a slight decrease and then an increase in the apparent elongational viscosity with decrease in temperature within the range of spinning speeds. The shear viscosity data of the resins in the "as-received" state, shown in Figures 3.1 to 3.3, indicate that the broad MWD samples are more shear-thinning in nature than the medium and narrow MWD samples. Thus, it may be suggested that the apparent elongational viscosity behavior is related to the elongation thinning nature of

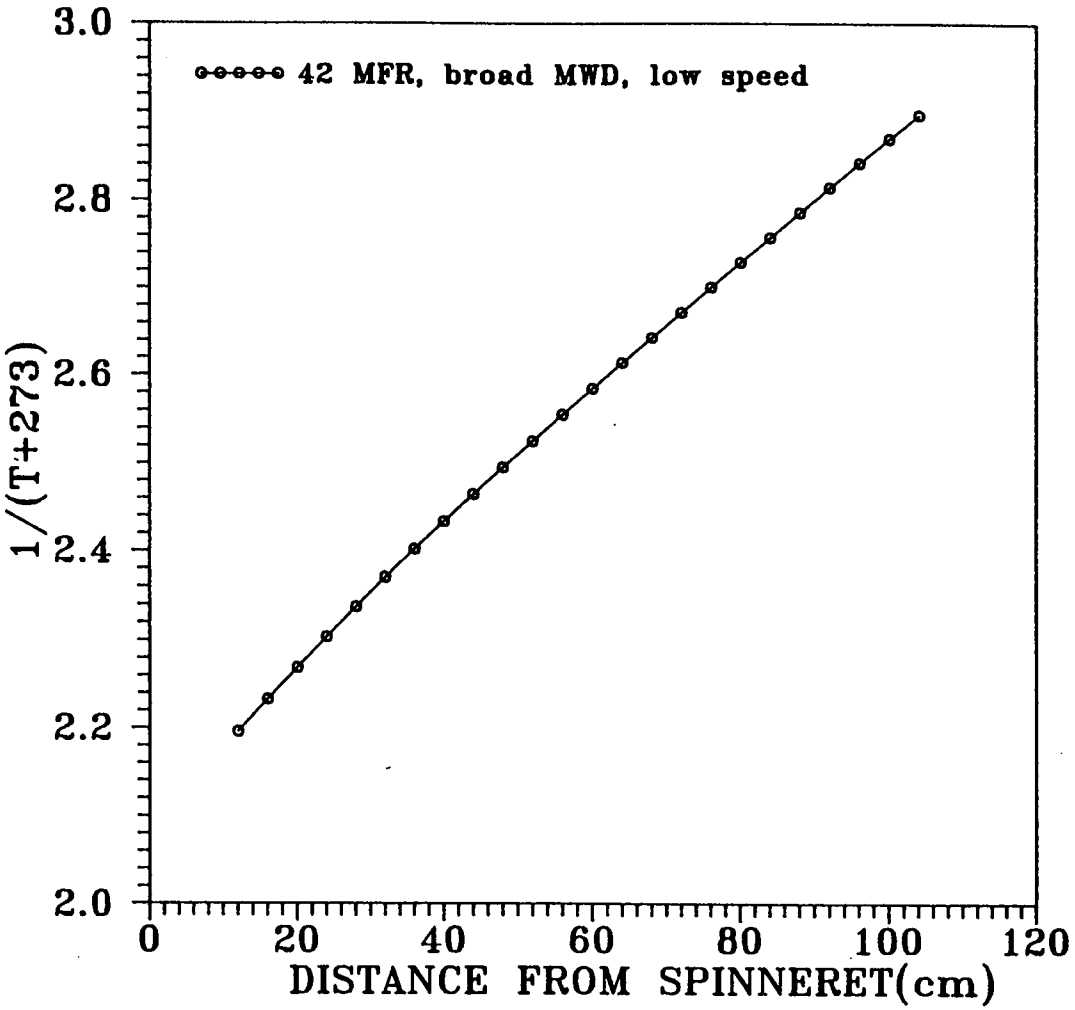


Figure 4.22 Profile of reciprocal of absolute temperature.

those samples. Hence, for the broad MWD samples, the variation of viscosity of the polymer along the spinline is thus affected by two opposing effects, viz. increase in viscosity due to the drop in the temperature of the fiber along the spinline and a decrease in the viscosity with increase in the rate of elongation the change in which is quite substantial near the spinneret. Also the deviation from the Arrhenius behavior may be caused by the long chains present in the broad MWD samples which give rise to appreciable elastic effect due to greater entanglement. The nature of the curves shown in the Figure 4.21 is similar to those reported by Matsui and Bogue(69) for polyethylenes in which the elongational viscosity first showed a decrease and then an increase with decrease in temperature(or increase in the distance from the spinneret). This was explained, using viscoelasticity theory, as the result of the die flow, i.e., the material remembers the deformation it experienced in the die for several centimeters into the spinline. Thus, from the apparent elongational viscosity curves it can be speculated that viscoelasticity plays an important role during the melt spinning of the broad MWD samples.

CHAPTER 5

INVESTIGATION OF 'REICOFIL' SPUNBONDING PROCESS VIA MATHEMATICAL MODELING

A part of this research was to investigate the "Reicofil" Spunbonding process through mathematical modeling. A mathematical model was developed for this process by the research group at the University of Tennessee(9). This model consists of a set of simultaneous differential equations developed from the application of fundamental physical principles such as conservation of mass, energy and momentum, together with some polymer specific information that must be determined from experiment for each polymer, such as the apparent elongational viscosity, crystallization kinetics, polymer density as a function of temperature, etc. The model also includes a treatment of the influence of molecular orientation on the crystallization kinetics of the spun polymer(21). The model is based on the earlier modeling efforts carried out in the laboratories of the department of Material Science and Engineering at the University of Tennessee for the conventional melt spinning process(20,105) modified to handle the specific differences between conventional melt spinning and the 'Reicofil' spunbonding process.

In Spunbonding the filament drawdown is controlled by air drag rather than a godet that imposes a fixed take-up velocity. This results in a different boundary condition for solution of the differential equations that make up the model, and as a result of this it is possible to compute the final filament diameter from the applied air flow rates and other process and polymer variables instead of treating diameter as a given quantity in the analysis(9).

In the present research the effect of a number of process and material parameters on the structure and properties of the spunbonded webs is analyzed, and potential changes in spunbonded web filament characteristics based on model predictions by varying the input process and material parameters are discussed. As a starting point, the material parameters for the same 35 MFR polypropylene discussed in reference-9 were used. The material parameters that were varied as inputs to the model were the apparent elongational viscosity and "stress induced" crystallization kinetics. These quantities are controlled by the polymer molecular weight distribution, tacticity, nature and composition of copolymerization, and additives such as nucleating agents. The process parameters studied here include extrusion temperature, and the temperature and flow rate of the cooling air. The effect of changes in mass throughput rate were described in reference-9.

Changes in the process itself may also be envisaged through the model. For example, a change of the spinline length would change the effects of gravity on the filament drawdown and, perhaps other factors. A change in the shape of the venturi can result in a change in the velocity profile within the spunbond chamber and, hence, a change in the air drag for a given air flow rate. In the present research, the effects of changes in the position of the neck of the venturi, insertion of a parallel neck section

between the sloping sections of the venturi, and changes in the length and position of this neck section are investigated.

5.1 Predicted Effects of Changes in Material Parameters:

Elongational Viscosity:

Here the model predictions for the results of spunbonding runs in which the processing conditions are kept constant, but the apparent elongational viscosity of the polymer is varied over a wide range, are presented. For this purpose the processing conditions used in the calculations are shown in Table 5.1; they are similar to one set of conditions used in the computations of reference-9 (sample 1). Tables 2 and 3 of that paper). Three different elongational viscosity functions, $\eta(T)$, were used in these calculations. One was the same as that of 35 MFR polypropylene studied in reference-9, while the other two were typical of functions that have been found experimentally for resins of about 12 MFR and 300 MFR.

The final filament diameters, crystallinities and birefringences are presented in Table 5.2. The results of the calculation of diameter, temperature and crystallinity profiles along the spinline are compared for the three resins in Figures 5.1 to 5.3. Note that, during these calculations, the crystallization constants that enter the description of the polymer's crystallization kinetics were kept constant at the same values found for the 35 MFR resin. However, the crystallization rates varied due to the influence of viscosity on the molecular orientation developed in the spinning polymer. The latter is caused by the influence of viscosity on the spinline stress as discussed below.

Table 5.1 Processing Conditions Used for Examining the Effects of Resin Variables on the Structure and Properties of Spunbonded Polypropylene Webs.

Extrusion Temperature (Celcius)	210
Mass Throughput (g/min/hole)	0.35
Quench Air Temperature (Celcius)	20
Auxilliary Air Temperature (Celcius)	30

Air Velocities in Chamber Reifenhauser Standard Conditions for 0.35 g/min/hole. See reference (9) for details.

Table 5.2 Predictions of the Model for Different Viscosity Resins.

Resin MFR	Final Filament Diameter (mm)	Final Crystal-linity (%)	Final Bire-fringence
12	41.3	64.8	0.0218
35	28.6	52.7	0.0172
300	27.1	40.3	0.0130

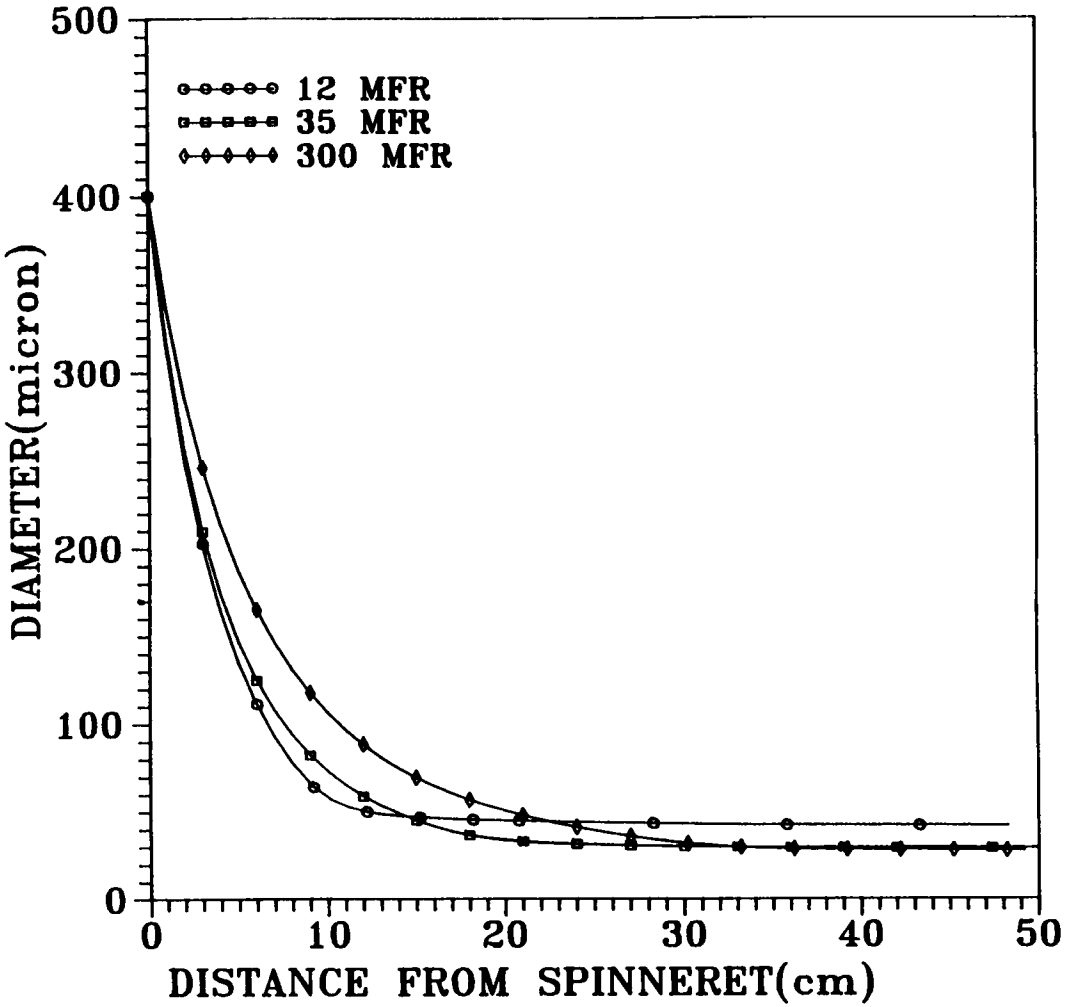


Figure 5.1. Comparison of diameter profiles for resins of three different MFRs.

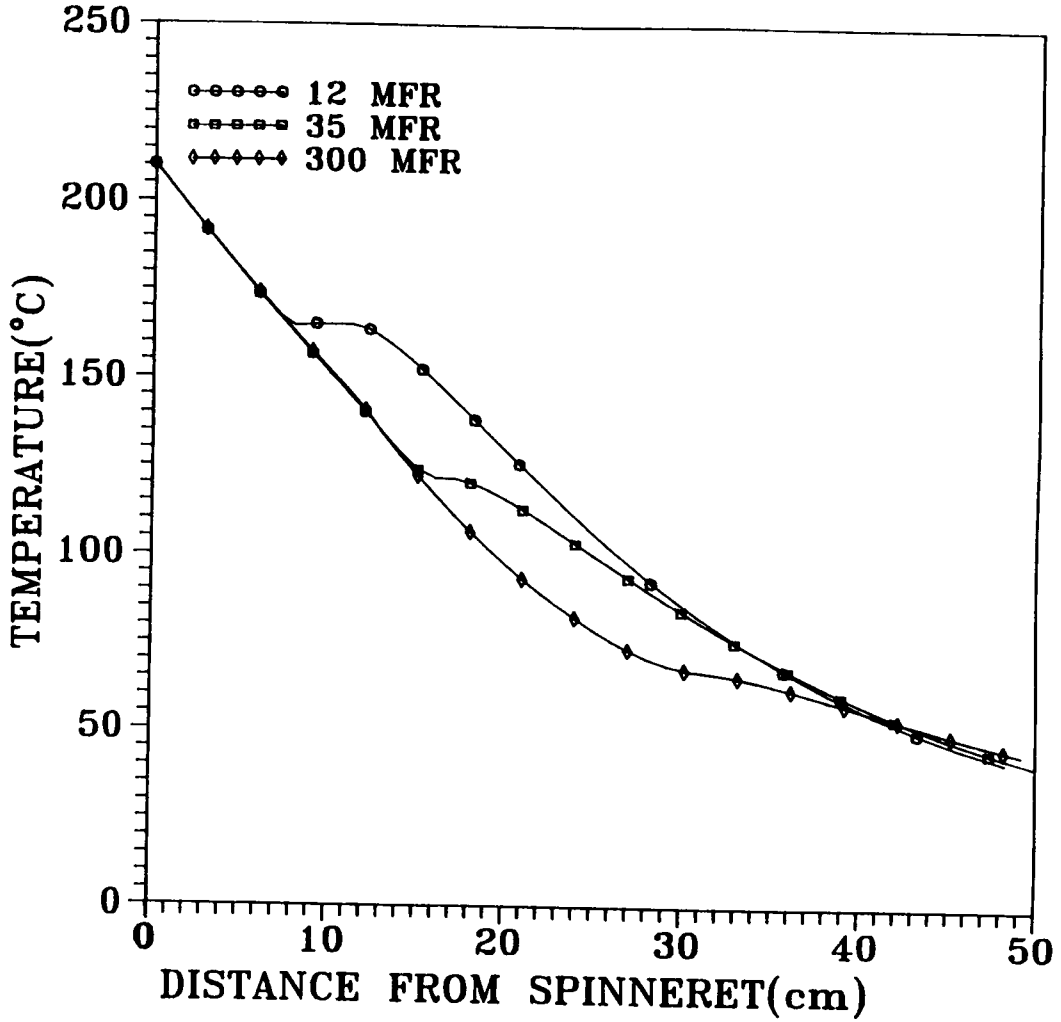


Figure 5.2 Comparison of temperature profiles for resins of three different MFRs. Note the differences in crystallization temperature.

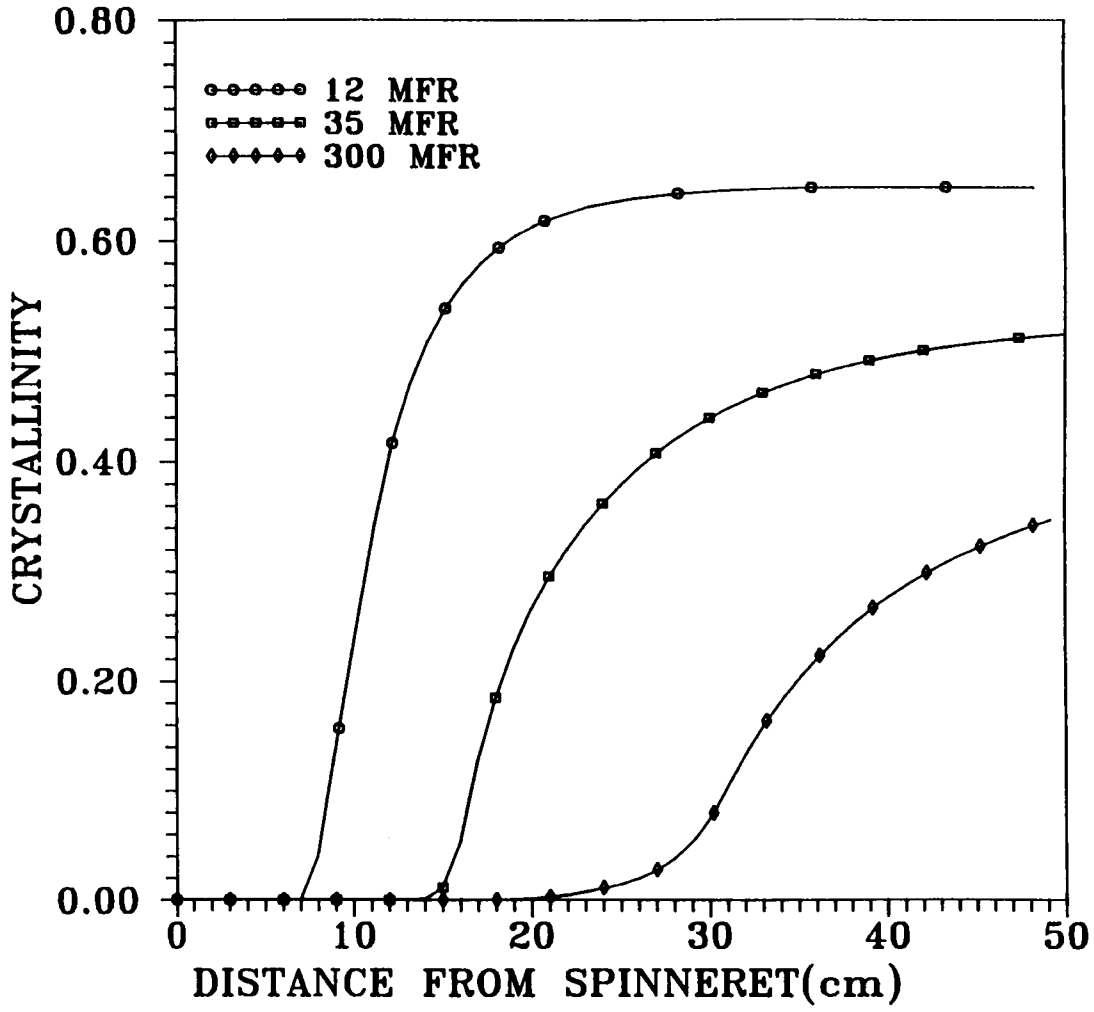


Figure 5.3 Comparison of development of crystallinity for resins of three different MFRs.

Increasing the viscosity requires higher stress levels to produce drawdown at a given temperature. Since the available air drag in the spunbonding process is essentially independent of resin viscosity, this causes the final filament diameter to increase (less drawdown) with increased resin viscosity if other process parameters remain constant, Table 5.2. Figures 5.1 and 5.2 also show that increasing the resin viscosity causes the final drawdown to occur closer to the spinneret, where the filament temperature is hotter and the local viscosity is lower. However, the stress at a given position in the spinline is higher for the higher viscosity polymer. Due to the higher stress at a given position and temperature of the spinline, stress-induced crystallization causes the crystallization to occur closer to the spinneret and at higher temperatures, Figure 5.3. The onset of crystallization causes the viscosity to increase compared to the viscosity of the polymer in the absence of crystallization and the final filament diameter is reached closer to the spinneret. The increased melt orientation and higher rates of stress-induced crystallization lead to higher final crystallinities and birefringences with increasing viscosity, Table 5.2. Note the difference in temperature of the crystallization plateau in Figure 5.2. The trends of these simulated results are consistent with experimental data measured on filaments spun on polypropylenes with different MFRs in a conventional melt spinning process(119,124).

Crystallization Kinetics:

It is well known that the crystallization kinetics of polypropylene resins vary with tacticity, copolymer contents, additives such as nucleating agents, and perhaps other molecular variables. In the present section the effects of changing the crystallization kinetics over a wide range are analyzed.

The equation used to model the crystallization kinetics is given in equation (2.6.16). This equation was proposed by Patel and Spruiell(105) and was used in the original model for the 'Reicofil' spunbonding process(9). For convenience it is written below again.

$$K = K_o \exp\left[-\frac{U^*}{R(T - T_\infty)}\right] \exp\left[-\frac{C_3}{T\Delta T f + C f_a^{\,2} T^2}\right]$$

Here, K_o, C_3 and C are experimentally determined parameters for a given resin which determine the crystallization kinetics in the process. Major effects of varying the crystallization kinetics by changing one or more of these parameters can be modeled. Variations of all three of these parameters were examined in the present investigation. The behavior can be adequately illustrated by varying C_3(only) over a range sufficient to give significant changes in crystallization kinetics. Other process and material parameters were kept constant at the values used for the 35 MFR resin case presented above.

The results of variation in the values of C_3 on the temperature and crystallinity profiles are shown in Figures 5.4 and 5.5; the final values of filament diameter, crystallinity and birefringence are given in Table 5.3. Note that as C_3 decreases, the overall crystallization rate constant K increases. Also, a value of $C_3 = 5 \times 10^5$ corresponds to the value determined experimentally for the 35 MFR homopolymer resin. As C_3 varies from 3×10^5 to 7×10^5, the position of onset of crystallization moves from 8 cm below the spinneret to 23 cm below it, Figure 5.5. The final crystallinity varies from about 63% to about 40%, and the birefringence varies from about 0.0193 down to 0.0146. As seen from Table 5.3, the final diameters of the spunbonded filaments are little affected by crystallization kinetics.

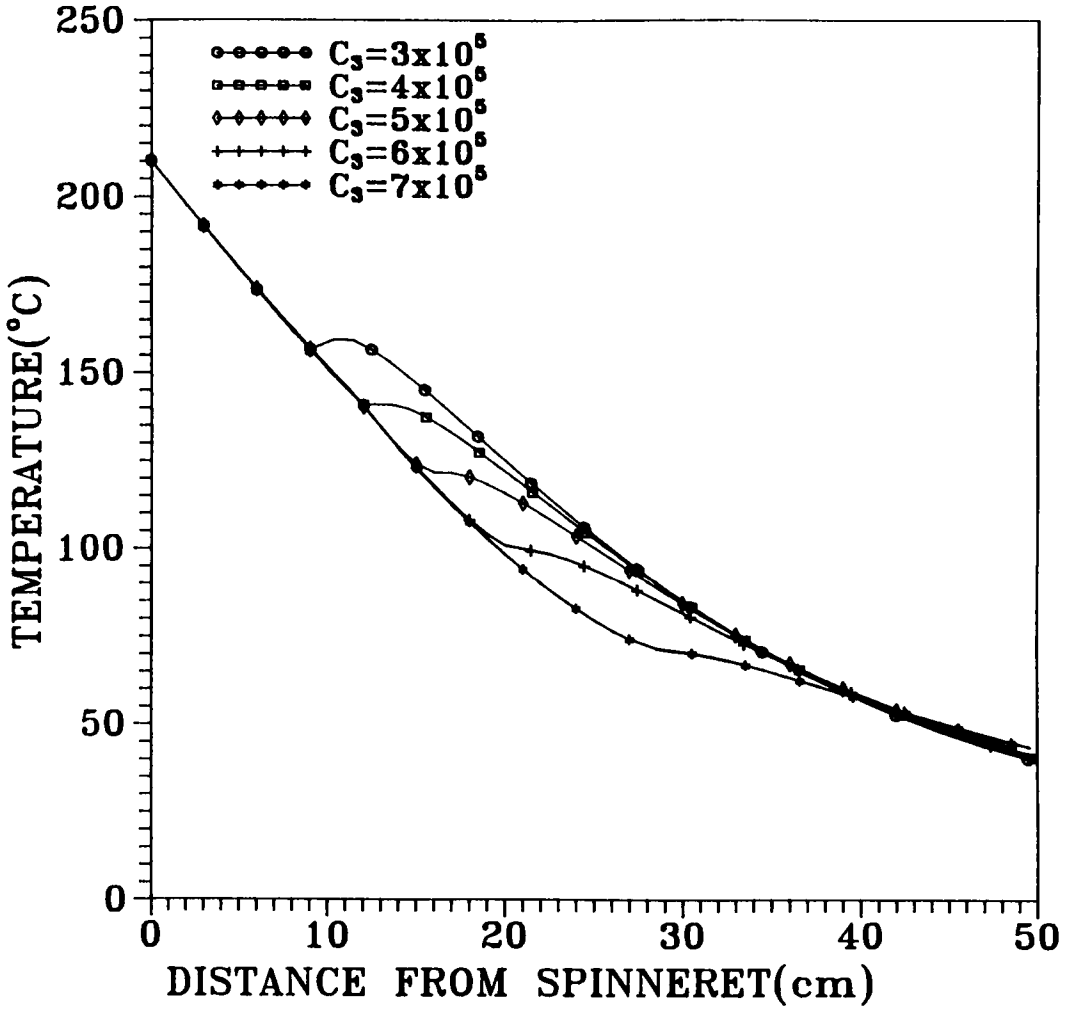


Figure 5.4 The effect of changes in crystallization kinetics on the temperature profiles. Note the differences in crystallization temperature.

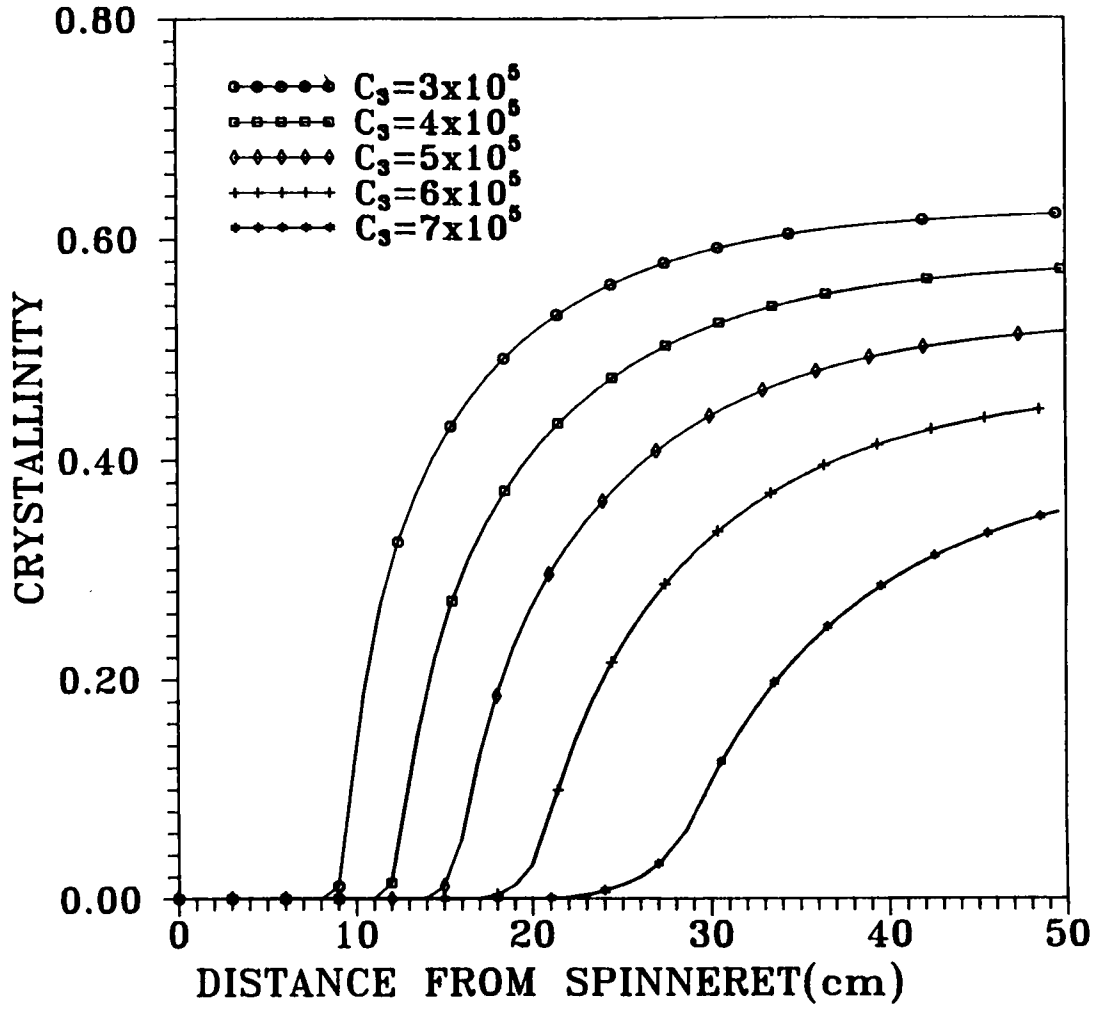


Figure 5.5 The effect of changes in crystallization kinetics on the development of crystallinity along the spinline.

Table 5.3 Predictions for Different Crystallization Kinetics.

C_3 Value	Final Filament Diameter (mm)	Final Crystal-linity (%)	Final Bire-fringence
$3x10^5$	29.3	62.6	0.0193
$4x10^5$	28.9	57.9	0.0181
$5x10^5$	28.6	52.7	0.0172
$6x10^5$	28.4	46.7	0.0161
$7x10^5$	28.2	39.4	0.0146

5.2 Predicted Effects of Changes in Process Variables:

Extrusion Temperature:

The extrusion temperature chosen for spinning a polymer is frequently a compromise. At too high a temperature the polymer may degrade or exhibit capillary break-up (drop formation) in the spinline. At temperatures near the melting point, the polymer may exhibit extrudate distortion(melt fracture), excessive die swell and requires higher stresses to extrude and produce drawdown. For polypropylenes the range of reasonably stable spinning is from about 180 °C to about 260 °C, depending on the detailed resin characteristics(119,124). A typical extrusion temperature for a 35 MFR resin used in spunbonding would be about 210 °C(9). The calculated effect of changing the extrusion temperature in the range 210-240 °C is shown in Figures 5.6 and 5.7. As the temperature of extrusion is increased the local viscosity at any point along the spinline, particularly at positions close to the spinneret, decreases. As a result of this the local stress needed for drawdown decreases too. Hence crystallization begins further from the spinneret and at higher undercoolings and drawdown occurs more slowly, i.e., over a somewhat greater range of distances from the spinneret. The final crystallinity, birefringence and diameter all decrease with increase in extrusion temperature, Table 5.4, but the effect of extrusion temperature is modest.

Cooling Air Temperature and Flow Rate:

The 'Reicofil' spunbonding process has two air blowers- a) a cool air blower where conditioned air at a controlled temperature is blown, and b) an auxiliary air blower in which the air is blown at room temperature. In principle, it is possible to control the temperature of the auxiliary air too. For the purpose of the present

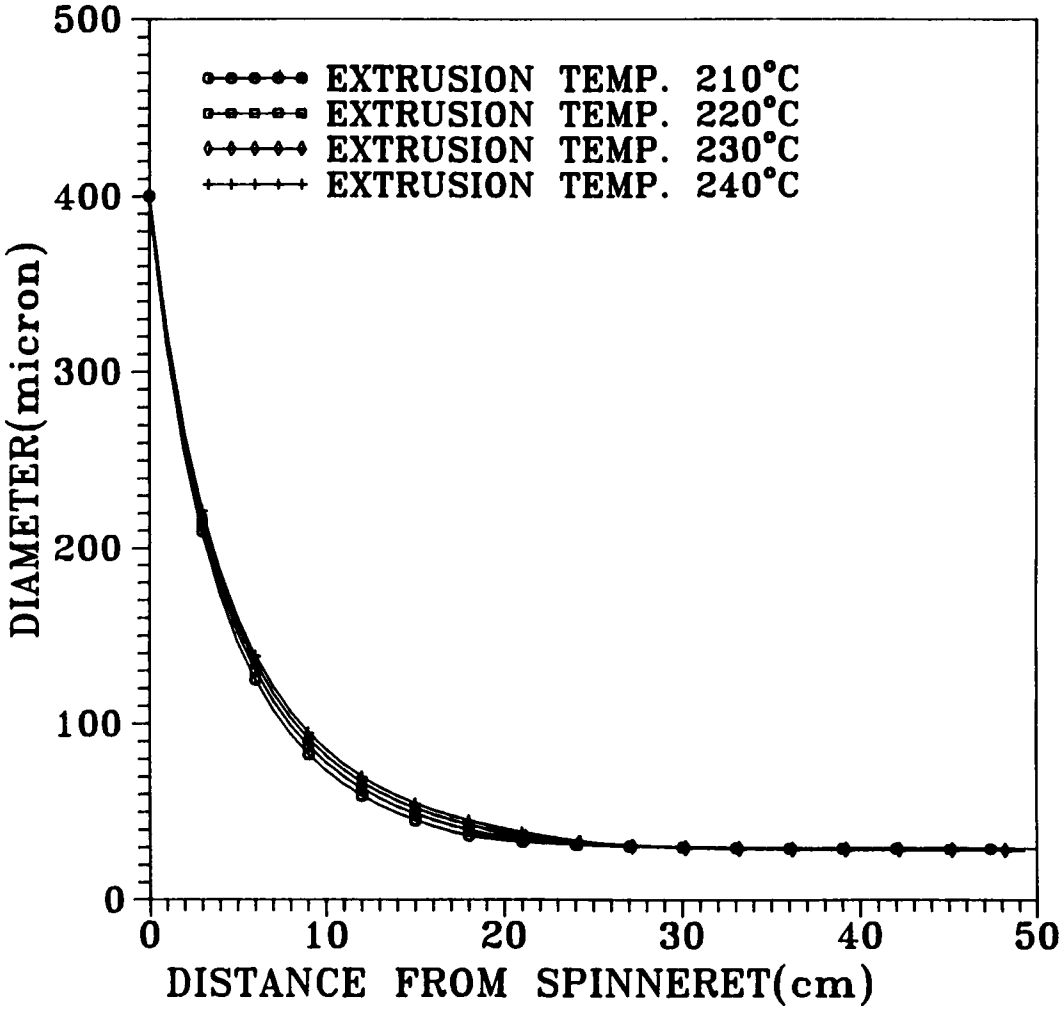


Figure 5.6 The effect of extrusion temperature on the diameter profile.

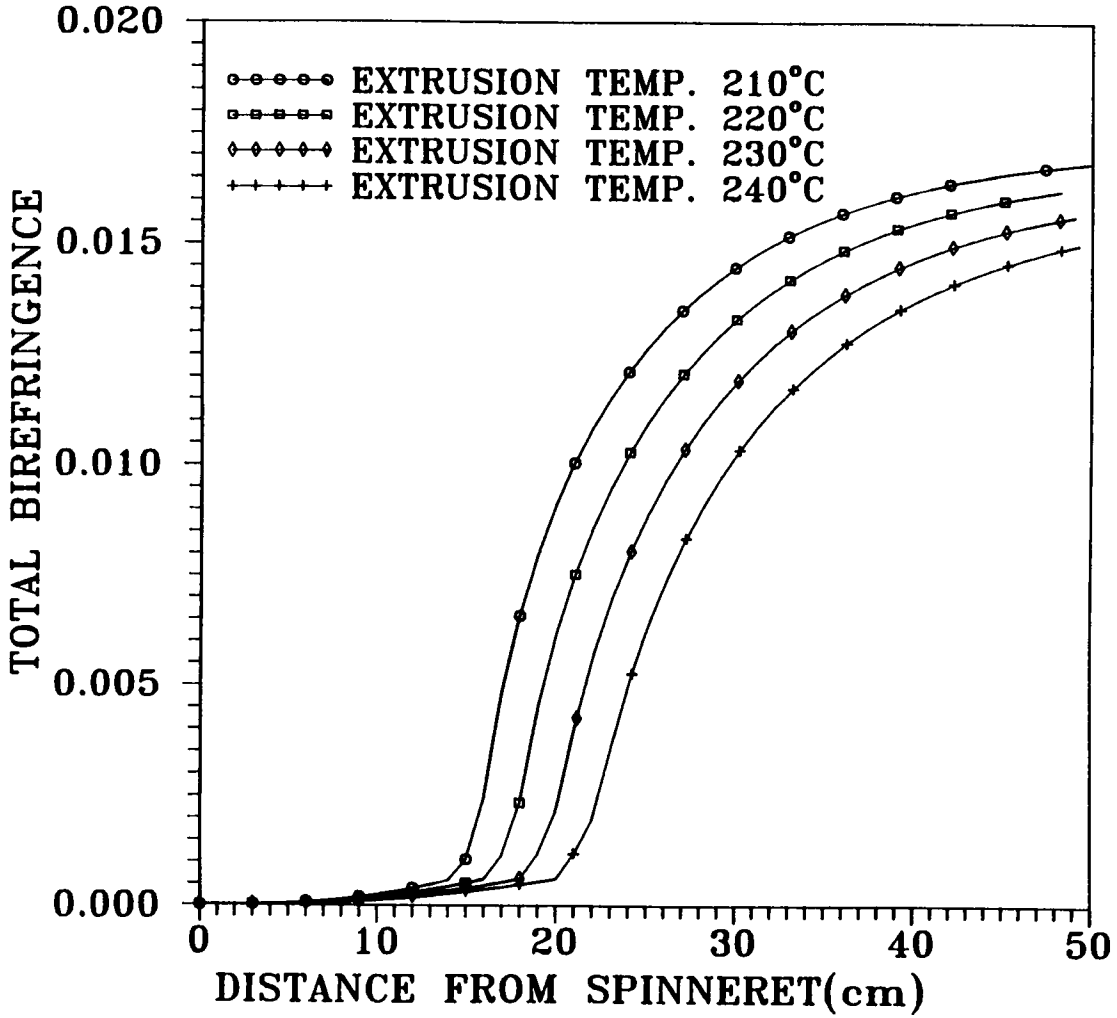


Figure 5.7 The effect of extrusion temperature on the development of total birefringence.

Table 5.4 Predictions for Different Extrusion Temperatures.

Extrusion Temperature (Celcius)	Final Filament Diameter (mm)	Final Crystal-linity (%)	Final Bire-fringence
210	28.6	52.7	0.0172
220	28.2	51.7	0.0168
230	27.8	50.7	0.0164
240	27.5	49.7	0.0155

calculations, the temperature of the auxiliary air was kept constant at 30 °C. The effect of cooling air temperature on the web filament characteristics is shown in Table 5.5, while illustrative changes in spinline profiles are given in Figures 5.8 and 5.9. As the cooling air temperature is increased from 20 °C to 150 °C the spinline cools much more slowly, and the crystallization occurs much further from the spinneret, Figure 5.9. The final diameter of the filament decreases by about 14% to about 24.7 μm but with an accompanying decrease in crystallinity from 52.7% to 40.5%. This result can again be explained in terms of stress on the spinline at different positions. The increase in the temperature of the cool air causes the viscosity of the polymer to remain at lower values for a greater distance from the spinneret and, hence, a longer elapsed time. Due to this lower viscosity along the spinline, the final diameter decreases but the stress on the spinline decreases too. Due to the decrease in stress the crystallization starts at a much lower temperature and the final crystallinity and birefringence values are lower, Table 5.5.

An increase in the air flow rate in the spunbonding chamber increases the air drag on the filaments. This increases the spinline rheological stress and results in decreased filament diameter and increased crystallinity. The final diameter, crystallinity and birefringence are presented in Table 5.6. As the air flow rate increases three fold, the diameter of the filaments, as predicted by the model, decreases form 28.6 μm to 15.3 μm, whereas the final crystallinity increases from 52.7% to 62.6%. Here it is assumed that the spinline will not break due to the increased stresses imparted by the drag forces.

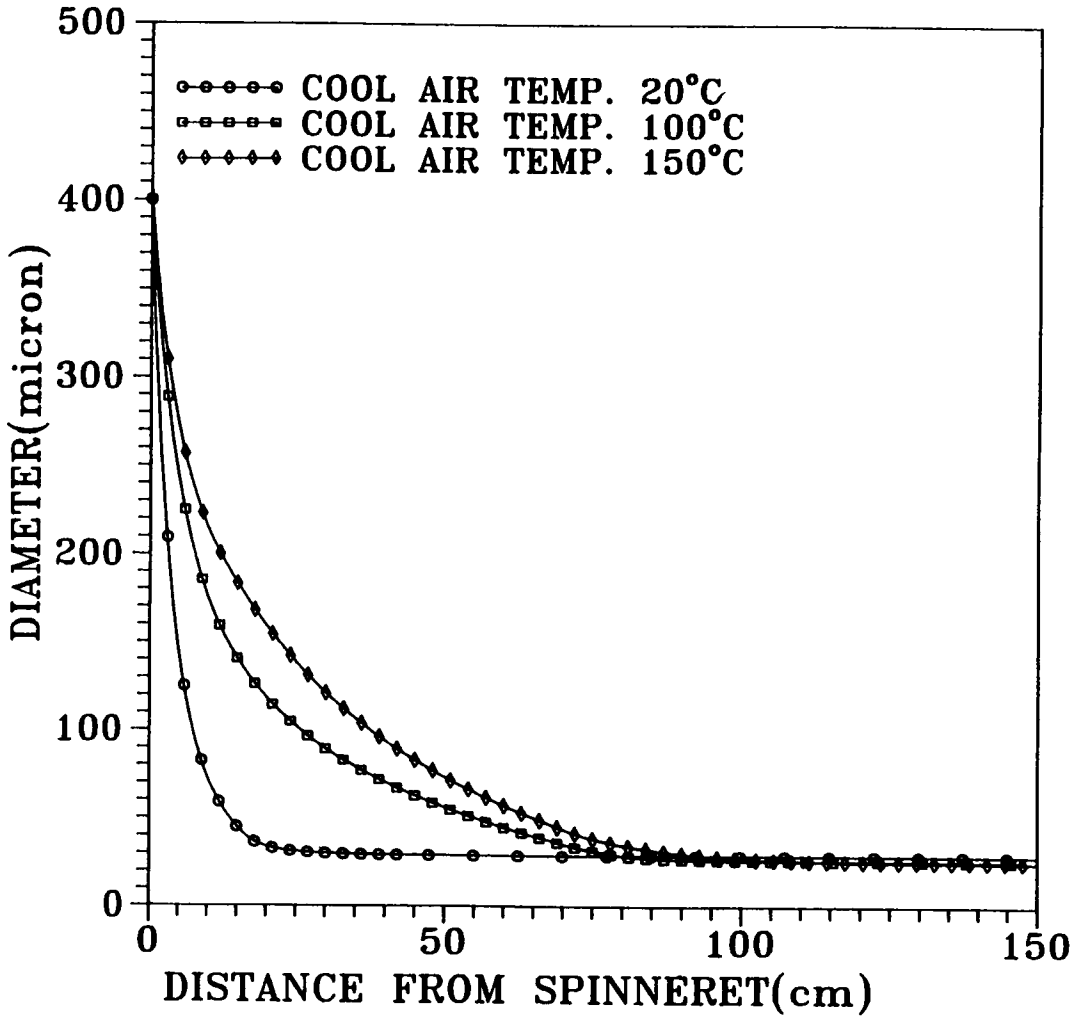


Figure 5.8 The effect of cool air temperature on the diameter profile.

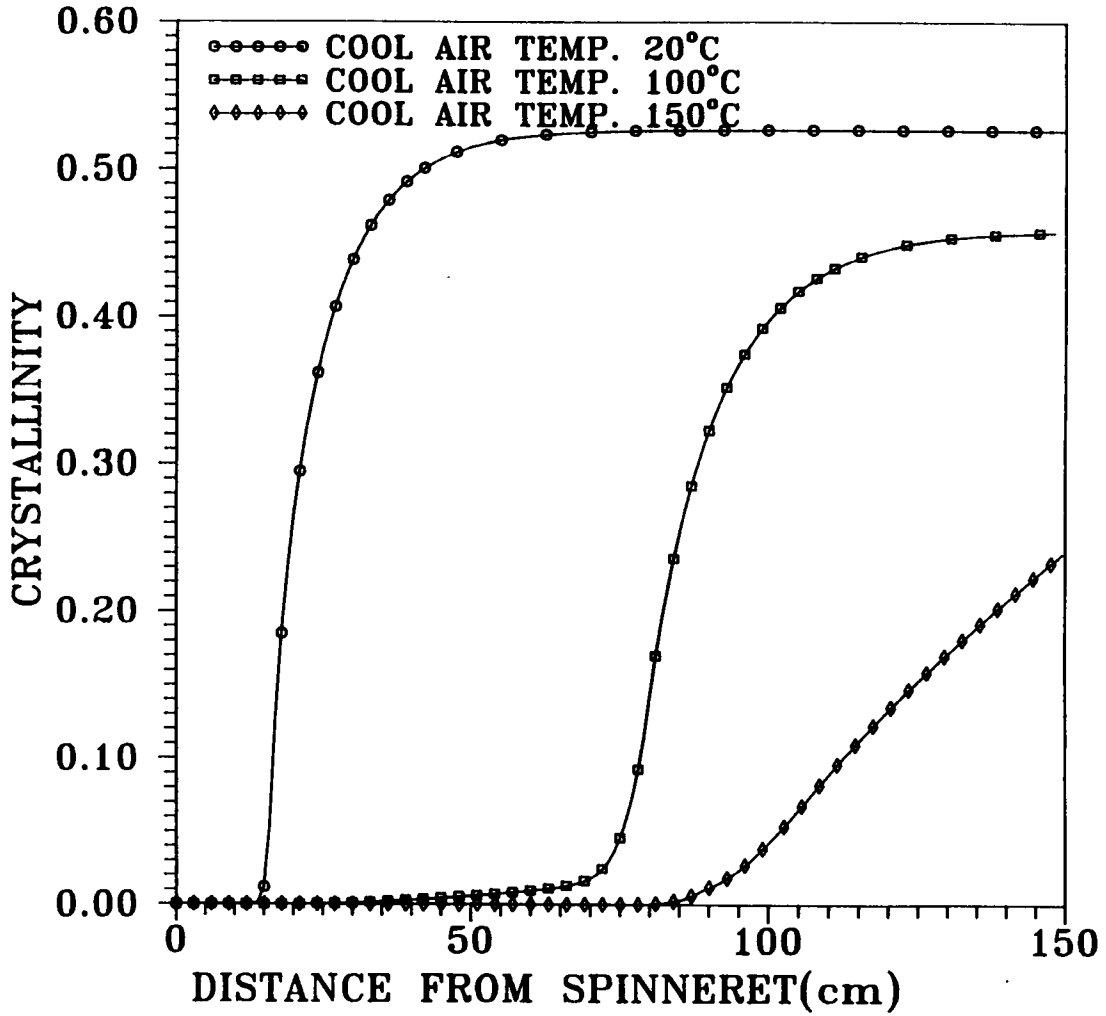


Figure 5.9 The effect of cool air temperature on the development of crystallinity.

Table 5.5 Predictions for Different Cooling Air Temperatures.

Temperature of Cooling Air (Celcius)	Final Filament Diameter (mm)	Final Crystal-linity (%)	Final Bire-fringence
20	28.6	52.7	0.0172
100	25.5	45.9	0.0152
150	24.7	40.5	0.0128

Table 5.6 Predictions for Different Air Velocity Profiles.

Air Velocity Profile	Final Filament Diameter (mm)	Final Crystal-linity (%)	Final Bire-fringence
Standard	28.6	52.7	0.0172
2x Standard	19.2	60.6	0.0231
3x Standard	15.3	62.6	0.0287

Mass Through-put Rate:

The effect of mass through-put rate was treated in reference-9. An increase of mass through-put causes the polymer to cool more slowly along the spinline, delays crystallization to greater distances from the spinneret, and results in larger final filament diameter and lower final crystallinity and birefringence.

5.3 Predicted Effects of Some Major Process Changes:

In addition to changes in material and process variables, there are changes in the basic process hardware that can be considered. In particular, changes in the length of the spinline and the position and shape of the venturi are discussed here.

Changing the overall length of the spinline by increasing the length of the venturi section has relatively little effect on the final filament diameter and structure as is illustrated by the calculated values shown in Table 5.7. There is marginal change in fiber properties as the length of the venturi section of the spinline increased from its original 489 cm to 800 cm. This is due to the opposing effects of gravity and the air drag towards the bottom of the venturi.

Venturi angle and position along the spinline have noticeable, but relatively small, effects on the final filament structure and properties. In the present discussion, the venturi angle is conveniently expressed in terms of the angle θ that the sloping section makes with the vertical, Figure 5.10. The angle θ was varied from the actual value of 2.18 degrees to 45 degrees. This has the effect of moving the position of the neck of the venturi closer to the spinneret. In carrying out these calculations, some

Table 5.7 Predictions for Different Venturi Length.

Venturi Length (cm)	Final Filament Diameter (mm)	Final Crystal-linity (%)	Final Bire-fringence
489	28.6	52.7	0.0172
600	27.5	53.9	0.0179
700	27.0	54.4	0.0181
800	26.8	54.6	0.0183

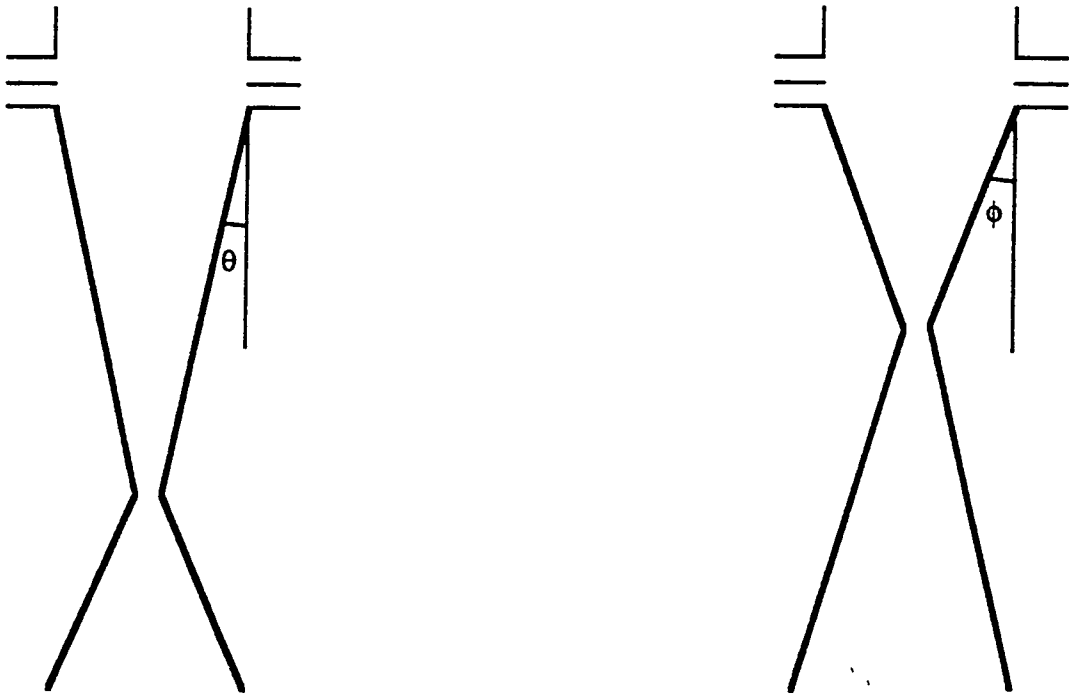


Figure 5.10. Illstration of potential changes in the venturi angle.
(a) Small venturi angle, θ
(b) Large venturi angle, ϕ

simplifying assumptions were made in order to estimate the air velocity profile in the chamber. It was assumed that a) the maximum air velocity in the venturi remains the same and b) the velocity in the upper portion of the chamber, above the venturi, and at bottom of the chamber remains the same. This provided estimated air velocity profiles for each case. With these assumptions, the diameter of the fiber decreased from 28.6 μm to 25.6 μm as θ is increased to 15 degrees. As θ is further increased the final diameter does not change appreciably as θ approaches 45 degrees. As shown in Table 5.8, the crystallinity and birefringence values increase somewhat with the increase in the angle θ , for θ values up to 15 degrees.

Inserting a more extended reduced section, i.e. a parallel section between the two sloping sections of the venturi, produces quite interesting results. Since numerous configurations are possible, the present investigation is limited to the case illustrated by Figure 5.11 with two different lengths, y, of the parallel section and two different starting positions, z, for each length. The results are given in Table 5.9. As expected the longer reduced section produces smaller filament diameters, higher crystallinity and higher birefringence. Moving the reduced section closer to the spinneret provides further reduction in diameter and increases the crystallinity and birefringence. These should be compared to the second entry in Table 5.2 or the first entry in Table 5.6 which represents the "base case" corresponding to the current actual design of the spunbond chamber. Inserting a parallel section induces an extended region where the air velocity is near its maximum value. This increases the drag and produces greater drawdown. Moving the parallel section upward along the spinline forces the drawdown to occur closer to the spinneret and increases the spinline stress. This causes further decrease in the fiber diameter and increase in the crystallinity and birefringence values.

Table 5.8 Effect of Different Venturi Angles and Positions.

Venturi Angle (degrees)	Final Filament Diameter (mm)	Final Crystal-linity (%)	Final Bire-fringence
2.18	28.6	52.7	0.0172
3.0	27.5	53.9	0.0178
7.0	26.0	55.0	0.0185
15.0	25.7	55.7	0.0189
45.0	25.7	55.7	0.0189

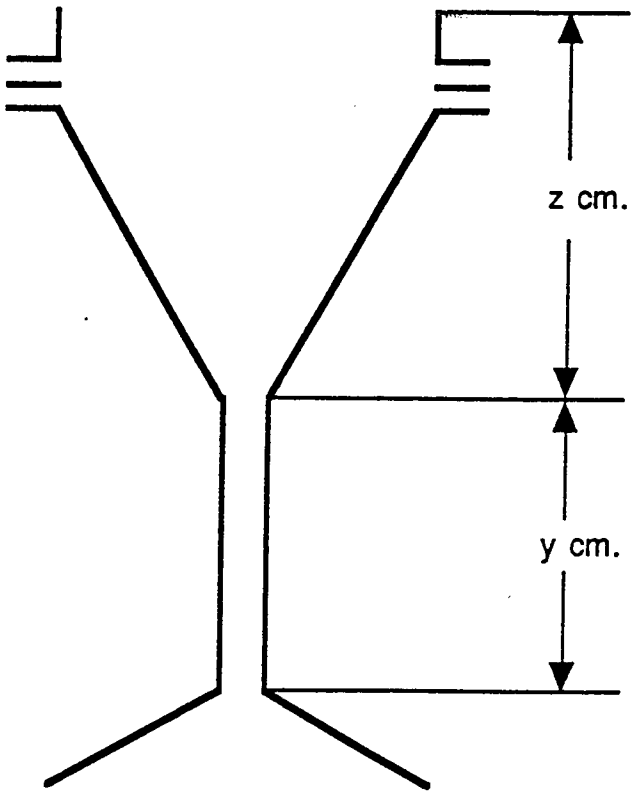


Figure 5.11. Illustration of some posible changes in the venturi design which include an extended minimum section.

Table 5.9 Effect of Increasing Length of Reduced Section in the Venturi.

Length of Reduced Section (cm)	Distance from Spinneret at Which Section Begins (cm)	Final Filament Diameter (mm)	Final Crystal-linity (%)	Final Bire-fringence
100	320	25.1	56.2	0.0192
200	270	23.2	57.8	0.0204
100	200	24.1	57.1	0.0199
200	200	22.8	58.2	0.0206

5.4 Use of the Model to Guide Experimentation:

If a specific property that is desirable for a particular application of spunbonded web can be established, the model can be used to guide the selection of process or material changes needed to achieve the desired results. An obvious case in point is the production of a web with substantially smaller filament diameters. Typical filament diameters range from about 22 to 32 μm, depending on the mass throughput, for production with commonly accepted 'Reicofil standard conditions'(9). Mass throughputs down in the range of 0.1 g/min/hole produce the smaller diameters, while the often used mass throughput of 0.35 g/min/hole gives filament diameters of about 28 μm as seen from the second entry in Table 5.2 (which are in good agreement with actual experimental results for these conditions, see reference-9, Table 3). As an illustration of the possibilities offered by the model, an attempt has been made in the present research to find conditions that might be used to prepare a spunbonded web from the standard 35 MFR resin, with filament diameters in the neighborhood of 15 μm, or less.

Based on the simulated results presented previously, the following factors have the potential to significantly reduce the final filament diameter: 1) decreasing the polymer viscosity, 2) decreasing the mass throughput per spinneret hole, 3) increasing the cooling air temperature, 4) increasing the air flow rate and, hence, the maximum air velocity in the venturi, 5) increasing the venturi angle, 6) increasing the length of the reduced section in the venturi (or otherwise changing the venturi so as to increase the maximum air velocity or the spinline distance over which the highest air velocities are applied). Some of these factors have opposing effects on spinline stress and, hence, on crystallinity and birefringence, even though they all reduce the filament diameter. For

example, increase in cooling air temperature decreases the crystallinity and birefringence while increased air flow rate increases crystallinity and birefringence, as shown in Tables 5.5 and 5.6 respectively, whereas both of them tend to decrease the final filament diameter. Certain combination of factors that reduce the filament diameters, subject to whatever constraints one desires to impose, can be picked. In doing such a "thought" experiment, it is important to avoid conditions that may lead to major problems due to factors that are not considered in the present model. For example, there is an upper limit to the stress that a spinning filament can withstand at any given temperature or position of the spinline. Above that limiting stress the spinline will break, leading to significant practical problems. The best course of action, then, is to maintain the stresses in the spinline at values consistent with prior experience for stable spinning for a particular resin. Decreasing the mass throughput to as low as 0.1 g/min/hole leads to filament diameters only in the range of about 22 μm. Thus it seems unlikely that the required reduction of diameter could be obtained with a decrease of mass throughput alone, without substantially lowering the rate of production or, perhaps, causing serious filament breakage problems.

As noted above, a reduction of filament diameter can be expected with a large increase in air flow rate and/or an increase in the length of the reduced venturi section as both effects would increase the air drag. However, increasing the air drag sufficiently to produce the desired filament diameter will lead to higher levels of spinline stress that may fracture the filaments unless some offsetting effect is used to reduce the stress levels. One possible alternative is to apply the conditions that effect a decrease in the spinline stress, while maintaining the final diameter of the filament. As seen from the modeling results, the two parameters that produce this result are 1) heated cooling and/or auxiliary air, and 2) increased extrusion temperature.

The model was used to simulate the combined effects of increasing the length of the reduced venturi section (200 cm long, starting at 270 cm from the spinneret), doubling the air flow rate and raising the cooling air temperature to 100 °C while maintaining a throughput of 0.35 g/min/hole, an extrusion temperature of 230 °C and an auxiliary air temperature of 50 °C. This simulation gives a final filament diameter of 15.0 μm, a final crystallinity of 54.4%, and a final birefringence of 0.0256. These values appear to be very near the desired diameter, while the higher birefringence might produce a stronger web for this set of conditions, if there are no other problems produced by the changes. A comparison of the spinline stress profiles for this "fine denier case" and the "base case" is shown in Figure 5.12. In the higher temperature range, the stress profiles are similar and suggest that the stresses are appropriate, at least down to the temperature where the two curves diverge. The higher stresses occurring as the resin is crystallizing in the neighborhood of 130 °C, for the fine denier case, leads to high computed birefringence. It is not known, at present, if these high stresses in this part of the spinline are sufficient to fracture the fiber. It would be intriguing to examine this possibility experimentally to see if the fine deniers and the high birefringence are really achievable.

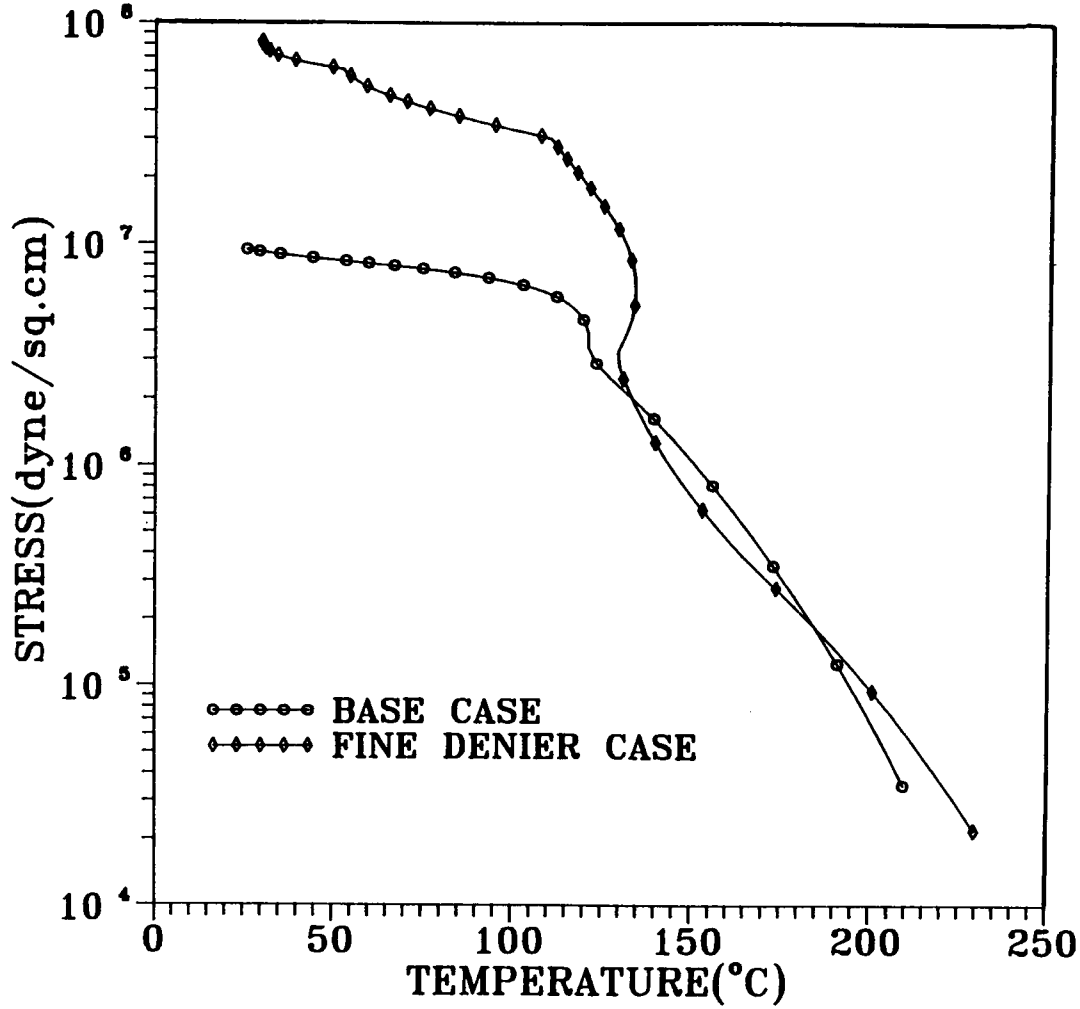


Figure 5.12 Comparison of stress versus temperature profiles for the original base case and the fine denier case.

CHAPTER 6

SUMMARY AND CONCLUSIONS

The purpose of the present research was i) experimental investigation of the effects of molecular weight and its distribution in the melt spinning of polypropylene and ii) investigation of the 'Reicofil' spunbonding process via mathematical modeling.

Three sets of polypropylene samples of different MFRs, each set comprising of three samples with similar MFRs but different MWDs , were examined. Spinnability study of the samples show that the spinnability of the resins in any set in terms of air pressure in the suction venturi decreases with broadening of MWD. The broadening of MWD is also associated with increased variation of the filament diameter during spinning.

Examination of the characteristics of the as-spun filaments reveals that the fibers spun from the broad MWD samples develop higher crystallinity and lower birefringence than the samples spun from the narrow MWD samples of similar MFR. Also, the fibers spun from the narrow MWD samples have higher tensile strength and lesser elongation before breaking than the filaments obtained from the broad MWD samples in the same range of MFR. The samples having medium MWD show properties in between that of the narrow and broad MWD samples in the same MFR

range. The crystallinity and birefringence of the filaments increase and the elongation before breaking decreases with increase in spinning speed.

On-line profiles during the melt spinning of these samples show that, for all the three ranges of MFR, the fiber draws down faster and approaches its final diameter closer to the spinneret with the broadening of MWD. Also, for any particular MFR range, the birefringence profile of the fiber starts to rise earlier along the spinline but develops more slowly and to a lower final value with the broadening of MWD. The birefringence profiles of the filaments spun from the medium and broad MWD resins of 74-78 MFR range are observed to rise earlier along the spinline than that of the fiber obtained from the 35 MFR narrow MWD sample in spite of the fact that the latter resin has a higher shear viscosity than the former samples. A comparison of the temperature profiles of the samples in the 74-78 MFR indicate that the broad MWD sample cools slightly faster than the narrow MWD sample in the upper part of the spinline. However, there is a cross-over of the temperature profiles at around 70 cm below the spinneret, presumably due to the release of heat of crystallization of the broad MWD sample which crystallizes earlier along the spinline.

From the characteristics of the as-spun filaments it can be concluded that, for similar spinning speeds, the filament develops higher crystallinity but lower average amorphous orientation with the broadening of MWD. This is evident from the data on tensile strength of the fibers and the elongation of the filaments before breaking. The higher tensile strength and lesser elongation to break for the filaments spun from the narrow MWD samples as compared to lower tensile strength and greater elongation to break for the filaments spun from the broad MWD samples of similar MFR indicate

that the fiber obtained from the narrow MWD sample has a higher average amorphous orientation.

The filament drawdown in the melt spinning of semicrystalline polymers is primarily controlled by the rheological effects and the crystallization effects. The crystallization effects, superimposed on the rheological effects, dictate the overall drawdown of the fiber. The samples show different shear thinning behavior with varying MWD. This may be correlated to the fiber drawdown to some extent. However, a comparison of the GPC data of the broad MWD samples with that of the narrow MWD samples of similar MFR indicates that the broad MWD samples contain a larger fraction of chains with higher chain length than the average value compared to the respective narrow MWD samples. It can be speculated that the longer chains in the broad MWD samples give rise to "row nuclei" due to greater entanglement and orientation than the smaller chains, thus causing onset of crystallization earlier along the spinline and hence at a higher temperature. The same argument can be employed to explain why the birefringence profiles of the fibers spun from the medium and broad MWD samples of 74-78 MFR rise earlier along the spinline than that of the fiber spun from the 35 MFR narrow MWD sample for similar spinning speed.

The measurement of tension at the bottom of the spinline is corrected for the fiber velocity relative to the velocity of the air in the suction venturi during the application of the 'inversion procedure' to obtain the apparent elongational viscosity of the samples. The correction leads to a lower value of the tension at the bottom of the spinline and hence a lower apparent elongational viscosity. The viscosities of the narrow MWD samples show approximate Arrhenius temperature dependence whereas

apparent elongational viscosities of the medium and broad MWD samples seem to deviate from it.

The effects of various material and process parameters on the structure and properties of the filaments obtained in the 'Reicofil' spunbonding process was investigated through a mathematical model developed earlier at the University of Tennessee. The model indicates that, among the material parameters, elongational viscosity is a key factor in controlling the amount of drawdown, the level of molecular orientation and the temperature of onset of crystallization, increase in viscosity leads to a higher final filament diameter, higher temperature of crystallization, higher final crystallinity and final birefringence. The kinetics of stress induced crystallization affects the extent of undercooling before the crystallization begins but has relatively small effect on the filament drawdown. The final filament crystallinity, diameter and birefringence all decrease modestly with increase in the extrusion temperature of the polymer. The cooling air temperature and the air flow rate in the drawdown chamber appear to be the most significant process variables. Increase in the cooling air temperature decreases the diameter, crystallinity and birefringence whereas an increase in air flow rate decreases the diameter while increasing the final crystallinity of the filament. Changes in the process itself can also be envisaged through the model. The effect of change in the position of the neck of the venturti along the spinline can be achieved in the model by changing the angle that the sloping sections of the drawdown chamber make with the vertical. Increasing the angle brings the neck closer to the spinline but has relatively small effects in the fiber properties. Inserting a parallel section and moving it towards the spinneret however has considerable effects, it decreases the diameter and increases the crystallinity and birefringence of the filament.

Knowing the effects of individual factors on the structure and properties of the filaments through the model can help to guide experimentation in combining different factors to achieve any specific property that is desirable for a particular application of the spunbonded webs. Some factors have opposing effects on the filament in terms different fiber properties e.g., increase in crystallinity and decrease in filament diameter. Based on the modeling results of the individual factors, for a combination of increase in extrusion temperature to 230 °C from the original 210 °C, doubling of the air flow rate, increase in the temperature of the cool air to 150 °C from 20 °C and the auxiliary air temperature to 50 °C from an original 30 °C and insertion of a parallel section instead of the neck of the venturi, the model predicts a filament of 15 microns diameter as compared to 28.6 microns diameter of the original filament. The model also shows that the spinline for this fine denier fiber has a stress similar to that of the original fiber in the higher temperature range which indicates that the stresses are appropriate.

It would be interesting to apply the results obtained from the melt spinning experiments of the present polypropylene samples in the modeling investigation of the 'Reicofil' spunbonding process. However, the melt spinning results such as the apparent elongational viscosities have to be combined with quantitative information on the crystallization kinetics of these resins, both under quiescent conditions and under stress.

REFERENCES

REFERENCES

1. M. Kaufman, "The First Century of Plastics", Plastics Institute, London(1963).

2. W. H. Carothers and J.W. Hill, J. Am. Chem. Soc., 54,1579(1932).

3. W. H. Carothers, DuPont, U.S. Patent 2,130,948(1938); DuPont, U.S. Patent 2,137,235(1938); DuPont, U.S. Patent 2,157,116(1938).

4. Encyclopedia of Polym. Sci. and Eng., John Wiley and Sons, 2nd Ed. NY, 1990, Vol.6, p. 756; Vol. 7, p. 704

5. E. A. Vaughn, *Nonwovens World Fact Book 1991*, Miller Freeman Publications Inc., San Fransisco(1990), p. 329.

6. R. G. Hill, "Book of Papers, Fiber Production Conference", Greenville, South Carolina, April 1990, p. 3A 1-4.

7. S. R.Malkan and L.C. Wordsworth, INB Nonwovens, 3, 4(1992).

8. *Guide to Nonwoven Fabrics*, 1st ed., INDA, New York(1978).

9. N. Hajji, J. E. Spruiell, F. M. Lu and S. Malkan, INDA J. Nonwovens, Vol. 4, No. 2, 16(1992).

10. B. Kunze, Paper presented in the Second Annual TANDEC Meeting, University of Tennessee, Knoxville, Oct. 13-16,1992.

11. N. Hajji, Ph.D. Dissertation, University of Tennessee, Knoxville, 1992.

12 A. Ziabicki, in *Fundamentals of Fiber Formation*, Wiley, London (1976).

13. S. Kase and T. Matsuo, J. Appl. Polym. Sci., 3, 2541(1965).

14. S. Kase and T. Matsuo, J. Appl. Polym. Sci., 5, 251(1967).

15. S. Kase and T. Matsuo, J. Text. Mach. Soc., Japan, 18, 188(1965).

16. I. Hamana, M. Matsui and S. Kato, Milliland Textile Brichte, 50, 382(1969).

17. K. Katayama and M. yoon, "Polymer Crystallization in Melt Spinning: Mathematical Simulation"; in *High Speed Fiber Spinning*, A. Ziabicki and H. Kawai ed., Wiley, New York, p. 207 (1985).

18. J. Simuzu, N. Okui and T. Kakutani, in *High Speed fFber Fpinning*, A. Ziabicki and H. Kawai ed., Wiley, New York(1985).

19. G. Vassilatos, B. H. Knox and H. R. E. Frankfort, in *High Speed Fiber Spinning*, A. Ziabicki and H. Kawai ed. Wiley, NY(1985).

20 K. F. Ziemensky and J.E. Spruiell , J. Appl. Ploym. Sci., 35, 2223(1988).

21. R. M. Patel and J. E. Spruiell, Polym, Eng. Sci., 31, 730(1991).

22. S. Kase, J. Appl. Polym. Sci., 18, 3267(1974).

23. T. Matsuo and S. Kase, Sen-i-Gakkaishi, 24, 512(1968).

24. T. Matsuo and S. Kase, J. Appl. Ploym. Sci., 20, 367(1976).

25. B. T. F. Chung and V. Iyer, Heat Transfer from Moving Fibers in Melt Spinning Process", ASME Winter Annual Meetings, Dallas Texas(1990).

26. T. Matsuo and S. Kase, J. Appl. Polym. Sci., 27, 2729(1982).

27. K. W. Hutchenson, D. D. Edie and D. M. Riggs, J. Appl. Ploym. Sci., 29, 3621(1984).

28. W. P. Bell and D. D. Edie, J. Appl. Polym. Sci., 33, 1073(1987).

29. B. C. Sakiadis, AICHE J., 7, 467(1961).

30. M. Matsui, Trans. Soc. Rheol., 20, 465(1976).

31. J. H. Bheda, Ph.D. Dissertation, University of Tennessee, Knoxville(1987).

32. A. K. Battacharya and A. Moutsoglou, ASME paper No. 82-HT 74 (1982).

33. A. K. Battacharya and A. Moutsoglou, Proceedings Seventh International Heat Transfer Conference, Vol. 3, FC34, p.111-194(1982).

34. A. Moutsoglou, Trans. ASME, J. Heat Transfer,105,830(1983).

35. S. R. S. Gupta, Acta Mechanica, 59, 123(1986).

36. D. E. Bourne, D. R. Davis and S. Wardle, Quart. J. Mech. Appl. Math,11,52(1958).

37. E. M. Sparrow, E. R. G. Eckart and W. J. Minkowycz, Trans. ASME, Series E, 83, 37(1963).

38. T. Cebeci, Trans. ASME, Series D, 92, 545(1970).

39. F. M. White, TRans ASME, Series D, 94, 200(1972).

40. J. Karnis and V. Pechok, Int. J. Heat mass Transfer, 21, 43(1978).

41. E. R. Sayles, Ph.D. Thesis, Division of Engineering, Brown University, 1982.

42. J. H. Bheda and J. E. Spruiell, J. Appl. Polym. Sci., 39, 447(1990).

43. J. R. Glicksman, Glass Technol., 9(5), 131, (1968).

44. M. B. Glauert and J. R. Lighthill, Proc. Roy. Soc. London, Ser. A, 230, 188(1955).

45. D. E. Bourne and D. G. Elliston, Int. J. Heat mass Transfer, 13, 583(1970).

46. C. Bos, Int. J. Heat mass transfer, 31, 1, 167(1988).

47. J. Simuzu, N. Okui and T. Kakutani, "Simulation of Dynamics and Structure Formation in Melt Spinning": in *High Speed Fiber Spinning*, A. Ziabicki and H. Kawai, Eds., Wiley, New York, 1985.

48. S. Kase, "Mathematical Simulation of Melt Spinning Dynamics: Steady-state conditions and transient behoior", in *High Speed Fiber Spinning*, A. Ziabicki and H. Kawai, Eds., Wiley, New York, 1985.

49. R. Lamonte and C. D. Han, J. Appl. Polym. Sci., 16, 3285(1972).

50. A. Prastaro and P. Parrini, Text. Res. J., 118(1975).

51. T. Ishibashi, A. Aoki and T. Ishi, J. Appl. Polym. Sci., 14, 1597(1970).

52. V. K. Pai and D. Hyman, Text. Res. J., 778(1984).

53. D. K Kagon and M. M. Denn, Polym. Eng. Sci., 21, 844(1981).

54. A. V. Senoy and V. M. Nadkarni, Text. Res. J., 639(1984).

55. J. C. Chang, M. M. Denn and S. Kase, Ind. Eng. Chem. Fund., 21, 13(1982).

56. L. F. G. Simons, Phil. Mag., 7, 3, 81(1927).

57. A. C. Muller, Amer. Inst. Chem. Eng., 38, 613(1942).

58. J. K. Roberts, in *Heat and Thermodynamics*, Blackie and Sons, London, 1940.

59. Nishikawa and Sano, Kagaku Logaku, 28, 275(1964).

60. R. Bird, W. Stewart and E. Lightfoot, in *Transport Phenomena*, John Wiley and Sons, New York, p. 388(1960).

61. C. J. S. Petrie, Elongational Flows, Pitman, London, 1979.

62. R. Bird, W. Stewart and E. Lightfoot, in *Transport Phenomena*, John Wiley and Sons, New York, p. 88(1960).

63. F. Trouton, Proc, Roy. Soc., A 319, 127(1906).

64. L. E. Neilsen, in *Polymer Rheology*, Marcel Dekker Inc., NY, 1977.

65. F. W. Billmayer, in *Textbook of Polymer Science*, John Wiley and Sons, p. 303(1984).

66. R. M. Patel, M. S. Thesis, University of Tennessee, Knoxville, 1988.

67. R. M. Patel and D. C. Bogue, J. Rheol., 33(4), 607(1989).

68. R. M. Patel, Ph. D. Dissertation, University of Tennessee, Knoxville, 1991.

69 M. Matsui and D. C. Bogue, Polym. Eng. Sci., 16(11), 735(1976).

70. J. D. Tsou and D. C. Bogue, J. Non-Newtonian Fluid Mech. 17, 331(1985).

71. J. G. Oldroyd, Proc. Roy. Soc., A77, 426(1950).

72. J. G. Oldroyd, Proc. Roy. Soc., A200, 523(1958).

73. W. Prager, in *Introduction to Mechanics of Continua*, Chicago, Ginn, p. 155(1958).

74. B. L. Lee and J. L. White, Trans. Soc. Rheol., 18, 467(1974).

75. D. C. Bogue, Ind. Eng. Chem. Fund., 5, 253(1966).

76. D. C. Bogue and J. L. White, "Engineering Analysis of Non-Newtonial Fluid", NATO Agrograph, #144(1960).

77. L. W. Moorland and E. H. Lee, Trans. Soc. Rheol., 4, 233(1960).

78. J. R. Dees and J. E. Spruiell, J. Appl. Ploym. Sci., 18, 1053(1974).

79. G. Marrucci, Trans. Soc. Rheol., 16, 321(1972).

80. H. H. George and M. H. E. Deeg, Paper persented at the second annual meeting of the International Polymer Processing Society, Montreal, Canada(1986).

81. Y. Fujikura, Sen-i-Gakkaishi, 27, 211(1971).

82. D. Turnbull and J. E. Fisher, J. Chem. Phys. 17, 17(1949).

83. L. Mandelkern, in *Crystallization opf Polymers,* McGraw Hill, NY(1964).

84. D. W. Van Krevelen, in *Properties of Polymers*, Elsevier, Amsterdam, 1976.

85. J. D. Hoffman and J. Weeks, J. Chem. Phys., 37, 1723(1962).

86. J. D. Hoffman, SPE Trans., 4, 315(1964).

87. J. D. Hoffman, G. T. Davis and J. I. Lauritzen, in *Treatise on Solid State Chemistry:* "Crystalline and non-crystalline solids", J. B. Hannay, Eds., Vol. 3, Chap. 7, Plenum, NY,1976.

88. M. Avrami, J. Chem. Phys., 7, 1103(1939).

89. B. Wundelich, in *Macromolecular Physics*, Vol. 2, Academic Press, NY, 1976.

90. Y. P. Khanna and J. J. Taylor, Polym. Eng. Sci., 28, 1042(1988).

91. W. Dietz, Colloid and Polym. Sci., 259, 413(1981).

92. P. Cebe, Polym. Eng. Sci., 28, 1192(1988).

93. P. Archambault and R.E. Prud'homme, J. Polym. Sci., Polym. Phys. Eds., 18, 35(1980).

94. K. Nakamura, T. Watanebe, K. Katayama and T. Amano, J. Appl. Polym. Sci., 16, 1077(1972).

95. K. Nakamura, K. Katayama and T. Amano, J. Appl. Polym. Sci., 17, 1031(1973).

96. M. R. Kamal and E. Chu, Polym. Eng. Sci., 23, 27(1983).

97. C. Velisaris and J. Seferis, Polym. Eng. Sci., 26, 1574(1986).

98. P. J. Flory, J. Chem. Phys., 15, 397(1947).

99. K. Kobayishi and T. Nagasawa, J. Macromol. Sci.(B), 4, 331(1970).

100. J. W. Haas and B. Maxwell, J. Appl. Polym.Sci., 14, 2407(1970).

101. J. H. Southern and P. H. Porter, J. Appl. Polym. Sci., 14, 2305(1970).

102. A. Ziabicki, Colloid Polym. Sci., 252, 207(1974).

103. W. J. Dunning, Trans. Faraday Soc. 50, 1115(1954).

104. K. Katayama and M. Yoon, in *High Speed Fiber Spinning*, Wiley, NY, p. 207, 1985.

105. R. M. Patel, J. H. Bheda and J. E. Spruiell, J. Appl. Polym. Sci., 42, 1671(1991).

106. J. E. Spruiell and J. L. White, Polym. Eng. Sci., 15, 660(1975).

107. P. H. Hermans, in *Contributions to the Physics of Cellulose Fibers*, Elsevier, NY, 1946.

108. L. R. G. Treolar, in "Physics of Rubber Elasticity", 2nd ed., Oxford Univ. Press.

109. H. T. Jessop and F. C. Harris, in *Photoelasticity, Principles and Methods*, Cleaver-Hume, London, 1949.

110. T. Matsumoto and D. C. Bogue, J. Polym. Sci., Polym. Phys. Eds., 15, 1663(1977).

111. L. E. Abbot and J. L. White, Appl. Polym. Symp., 20, 247(1973).

112. J. L. White, K. C. Dharod and E. S. Clark, J. Appl. Sci., 18, 2539(1947).

113. H. P. Nadella, H. M. Hemson, J. E. Spruiell and J. L. White, J. Appl. Polym. Sci., 21, 3003(1977).

114. T. Kitao, S. Ohya, J. Furukawa and S. Yamashita, J. Appl. Sci., 11, 1091(1973).

115. P. G. Anderson and S. H. Carr, J. Mater. Sci., 10, 780(1975).

116. J. E. Spruiell and J. L. White, in "Fiber and Yarn Processing", J. L. White Ed., Appl. Polym. Symp., 27, 121(1975).

117. O. Ishizuka and K. Koyama, Sen-i-Gakkaishi, 32, T-43(1976).

118. J. Shimuzu, K. Toriumi and Y. Imai, Sen-i-Gakkaishi, 35, T-405(1979).

119. F. M. Lu and J. E. Spruiell, J. Appl. Polym. Sci., 34, 1541(1987).

120. Y. Lin, J. Zhou and J. E. Spruiell, in "Proceedings SPE ANTEC", 1991, Vol. 37, p. 1950.

121. F. M. Lu and J. E. Spruiell, J. Appl. Polym. Sci., 49, 623(1993).

122. S. E. Ross, J. Appl. P olym. Sci., 9, 2729(1965).

123. J. E. Spruiell, University of Tennessee, Private communication, August 1993.

124. F. M. Lu and J. E. Spruiell, J. Appl. Polym. Sci., 34, 1521(1987).

125. R. J. Samuels, in *Structured Polymer Properties*, John Wiley and Sons, New York(1974).

126. A. Keller and M. J. Machin, J. Macromol. Sci., (phys.), B1(1), 41(1967)

127. M. J. Hill and A. Keller, J. Macromol. Sci., 9, 225(1969).

128. F. M. Lu, University of Tennessee, Private Communication, Oct. 1993.

VITA

Satyashayee Misra was born in Berhampur in the state of Orissa, India on the 5th of December, 1969. He attended High School in Burla, Orissa. He joined the Indian Institute of Technology at Kharagpur in July 1987 from where he graduated with a Bachelor of Technology with Honors in Chemical Engineering in Summer 1991. He then joined the University of Tennessee, Knoxville in August 1993 where he pursued graduate studies in Polymer Engineering. After completing his Master of Science, he is currently working in eastern Europe and India.